

Diss. ETH No. 24549

# Spatial Wire Cutting

Integrated Design, Simulation and Force-adaptive  
Fabrication of Double Curved Formwork Components

A thesis submitted to attain the degree of  
DOCTOR OF SCIENCES of ETH ZURICH  
(Dr. sc. ETH Zurich)

presented by

Romana Rust

Dipl.-Ing., Graz University of Technology

born on 18.02.1984  
citizen of Austria

accepted on the recommendation of

Prof. Matthias Kohler  
Prof. Fabio Gramazio  
Prof. Dr. Mark Pauly

2017





# Abstract

The development and dissemination of computer-aided modelling tools in the last two decades have enabled architects to design with complex, often double curved, geometry. In order to convert these digital data sets into the physical reality, digital fabrication technology has become crucial and, in turn, has stimulated the field of architectural geometry. However, commonly used digital fabrication methods are still time- and material-inefficient in producing bespoke double curved surfaces, generating the need for alternative solutions.

This thesis develops around a multi-robotic hot-wire cutting technique, that allows to significantly expand the set of possible hot-wire cutting geometries. In contrast to standard computer-controlled hot-wire cutting processes, in which the cutting medium remains straight, this technique modulates the curvature of the hot-wire, which adopts itself against the resistance of the processed material. This allows to produce a particular family of double-curved surface geometries: sweep surfaces defined by the motion of an altering profile curve along two guide curves. While the technique's principle is simple, its implications comprise to momentarily react and adapt to occurring forces, which dynamic change determine the overall form being cut.

The aim of this thesis is to develop methods and techniques that allow to control this cutting technique and to foresee its outcome. Knowledge is acquired directly from the physical form-finding process and implemented in a respective digital model. The thesis investigates material- and fabrication process-related constraints, correlations between operating physical factors, such as heat input, cutting speeds, resulting cutting forces and wire shape. It develops and validates suitable design, simulation and fabrication techniques and examines possible architectural applications, such as the time-efficient production of formwork components at full architectural scale.

The work is built upon the hypothesis that the integration of digital design and simulation techniques with adaptive control strategies can not only

lead to efficient manufacturing procedures, but can also yield unique formal vocabularies in placing materiality as an a priori agent in the formulation of architectural building elements. As such, the thesis investigates topics that are generally relevant for digital fabrication processes with complex or non-linear behaviour and contributes to fabrication-aware design methods at large.

# Zusammenfassung

Die Entwicklung und Verbreitung von computergestützten Entwurfswerkzeugen in den letzten zwei Jahrzehnten haben es Architekten ermöglicht, komplexe, oft doppelt gekrümmte, Geometrien zu entwerfen. Infolge der Notwendigkeit, diese digitalen Daten in die physische Wirklichkeit zu überführen, haben auch digitale Fabrikationstechnologien an wesentlicher Bedeutung gewonnen und wiederum dazu beigetragen, das Forschungsfeld der architektonischen Geometrie zu fördern. Jedoch ist die Produktion von doppelt gekrümmten Flächen durch herkömmliche digitale Fabrikationsmethoden noch immer zeintensiv und mit grossem Materialverbrauch verbunden, warum gegenwärtig nach effektiveren Alternativlösungen geforscht wird.

Im Zentrum der vorliegenden Dissertation steht die Untersuchung einer speziellen robotischen Heissdraht-Schneidetechnik, die das Spektrum bekannter Schnittgeometrien massgeblich erweitert. Im Gegensatz zu herkömmlichen computergesteuerten Heissdraht-Schneideverfahren, bei denen das Schneidemittel geradlinig bleibt, steuert diese Technik die Krümmung des Heissdrahts, der sich dem Widerstand des bearbeiteten Materials anpasst. Dies erlaubt die Erzeugung von speziellen doppelt gekrümmten Flächen, die durch die Bewegung einer sich verändernden Profilkurve entlang zweier Leitkurven definiert werden kann. Obwohl der Prozess auf einem einfachen Prinzip beruht, erfordert er eine kontinuierliche Reaktion und Anpassung an die vorkommenden Kräfte, deren dynamische Veränderung die gesamte geschnittene Form bestimmen.

Das Ziel der Arbeit ist es, Methoden und Techniken zu entwickeln, die es erlauben, die Schneidetechnik zu kontrollieren und das Ergebnis vorherzusehen. Dabei werden Kenntnisse direkt vom physischen Formfindungsprozess erworben und in einem entsprechenden digitalen Modell implementiert. Es werden material- und prozessbezogene Bedingungen untersucht und Verhältnisse zwischen den vorkommenden physischen Faktoren, wie Wärmezufuhr, Schnittgeschwindigkeiten, resultierende Schnittkräfte und Krümmung

des Heissdrahtes, ermittelt. Zudem werden Entwurfs-, Simulations- und Fabrikationstechniken entwickelt und mögliche architektonische Anwendungen untersucht, wie etwa die Produktion von Schalungselementen im architektonischen Massstab.

Die Dissertation basiert auf der Hypothese, dass die Verknüpfung von digitalen Entwurfs- und Simulationstechniken mit adaptiver Kontrolle nicht nur zu effizienten Produktionsverfahren führt, sondern auch einzigartige Formsprachen hervorbringen kann, in der die Materialität die führende Kraft der Formgebung architektonischer Bauelemente einnimmt. Die Thesis trägt somit zu herstellungsbewussten Entwurfsmethoden bei und behandelt Themen, die im Allgemeinen für digitale Fabrikationsprozesse mit komplexem oder nichtlinearem Verhalten relevant sind.

# Acknowledgements

First of all, I would like to express my gratitude to my advisors Prof. Fabio Gramazio and Prof. Matthias Kohler. Thank you for giving me the opportunity to pursue the project *Spatial Wire Cutting*, for guiding my research and for your confidence. I am particularly grateful for your thought-provoking impulses and our numerous discussions, that encouraged and inspired me throughout the course of the research project.

I would also like to sincerely thank my co-advisor Prof. Dr. Mark Pauly for supporting me with his valuable suggestions and feedback on this dissertation. I am thankful to the ITA Institute of Technology in Architecture and the Department of Architecture at ETH Zurich for supporting the research.

I would like to acknowledge Ryan Luke Johns for his preparatory work in the feasibility study of *SWC* and Florian Rist, who gave valuable advice and help in the development and realisation of the custom cardan joint end-effector. Prof. Dr. Jan Willmann has been very supportive throughout the course of the research project. I'd like to thank him for his confidence and encouragement. Furthermore I thank Prof. Dr. Volker Helm for his support in various ways and my thesis reader Dr. Ammar Mirjan for his constructive feedback and insightful comments, which have pushed this dissertation that one step further.

David Jenny has been a great team partner in organizing and holding the elective course, the Swisspearl<sup>®</sup> Summerschool and the AAG workshop with. I thank him for covering my back and for making me laugh, even in the most stressful times. Furthermore, I'd like to thank all students from the workshops, they were so dedicated, eager and worked with great enthusiasm: I owe you these successful results.

I count myself lucky of having conducted this research in the inspiring environment of the ITA Institute. I would like to thank my colleagues for all discussions that sparked many ideas, particularly Diederik Veenendaal, Lukáš Kurilla, Kathrin Dörfler and Norman Hack. Kathrin, I am privileged

to call you both my work partner and dear friend. No matter which kind of problem I am stuck with, of professional or personal matter, I know I can always count on your understanding, support and encouragement. Norman, thank you for taking me out for running, which allowed to clear my mind and to shed new light on things. Thank you both for the funny actions apart from work, for all crazy dancing sessions and those, which will come.

I thank my dear friends, Anna and Marlene, and my Austrian and Guatemalan family for always standing behind me and for their support in various ways. I am grateful for my older sister Iris, who keeps looking after me and my parents Elisabeth and Andreas, the ones who raised me to be a fighter, be creative and to always seek new challenges. Thank you for believing in me.

Finally, my deep gratefulness belongs to you, Carlo and David. This PhD has brought us to Switzerland where we found a new home. Without your unconditional support I would have never been able to pursue this dissertation. Thank you for being incredibly understanding, for keeping me grounded and for being the reason of my strength.

# Contents

<b>Abstract</b>	<b>i</b>
<b>Zusammenfassung</b>	<b>iii</b>
<b>Acknowledgements</b>	<b>v</b>
<b>Contents</b>	<b>vii</b>
<b>1 Introduction</b>	<b>1</b>
1.1 Background and motivation . . . . .	1
1.2 Research goal . . . . .	4
1.3 Methodology . . . . .	5
1.3.1 Adaptive robotic control system . . . . .	6
1.3.2 Analysis and modelling of material behaviour . . . . .	6
1.3.3 Design and simulation framework . . . . .	7
1.3.4 Application and validation . . . . .	7
1.4 Structure of the thesis . . . . .	7
<b>2 Context</b>	<b>9</b>
2.1 Robotic hot-wire cutting . . . . .	9
2.1.1 Ruled surface based design and panelling . . . . .	11
2.1.2 The process of thermal plastic foam cutting . . . . .	13
2.1.3 Research and application of RHWC in architecture . . . . .	17
2.1.4 Feasibility study of <i>SWC</i> . . . . .	22
2.2 Digital fabrication in architecture . . . . .	23
2.3 Form-finding and optimal shapes . . . . .	24
2.4 Conclusion . . . . .	26
<b>3 Techniques for design and control</b>	<b>29</b>
3.1 Adaptive robotic control system . . . . .	30
3.1.1 Objective . . . . .	30
3.1.2 Experimental set-up . . . . .	31
3.1.3 Sensors and tooling . . . . .	32
3.1.4 The UR robot . . . . .	39
3.1.5 Control system . . . . .	40
3.1.6 The fabrication process . . . . .	49
3.1.7 Feedback and feedforward . . . . .	51
3.2 Analysis and modelling of material behaviour . . . . .	53
3.2.1 Process description . . . . .	54
3.2.2 Thermo-mechanical mechanisms . . . . .	57
3.2.3 Cutting force model . . . . .	60
3.2.4 Operating ranges and scope definition . . . . .	61
3.3 Design and simulation framework . . . . .	64
3.3.1 Wire shape calculation . . . . .	65

3.3.2	Physical wire shape . . . . .	66
3.3.3	Force distribution . . . . .	69
3.3.4	Simulation model . . . . .	70
3.3.5	Design tool . . . . .	74
3.4	Validation of developed techniques . . . . .	77
3.4.1	Comparative studies N°1 . . . . .	77
3.4.2	Comparative studies N°2 . . . . .	82
<b>4</b>	<b>Application and validation</b>	<b>91</b>
4.1	<i>SWC</i> elective course 2015 . . . . .	91
4.1.1	Group 1 - Sigmoid curve . . . . .	92
4.1.2	Group 2 - Movement patterns . . . . .	93
4.1.3	Group 3 - Subtle variation . . . . .	94
4.1.4	Groups 4 and 5 - Ruled surfaces . . . . .	96
4.1.5	Results . . . . .	96
4.2	Swisspearl® Summerschool 2015 . . . . .	97
4.2.1	Group 1 - Double cuts . . . . .	99
4.2.2	Group 2 - Flipping peaks and valleys . . . . .	100
4.2.3	Group 3 - Waves . . . . .	101
4.2.4	Group 4 - Subdivision . . . . .	102
4.2.5	Results . . . . .	103
<b>5</b>	<b>Conclusion and outlook</b>	<b>107</b>
5.1	Summary and discussion . . . . .	107
5.1.1	Adaptive robotic control system . . . . .	107
5.1.2	Analysis and modelling of material behaviour . . . . .	108
5.1.3	Design and simulation framework . . . . .	109
5.1.4	Application and validation . . . . .	110
5.2	Contributions . . . . .	111
5.2.1	Integrated design and fabrication techniques . . . . .	111
5.2.2	Formal peculiarity . . . . .	112
5.2.3	Material process driven design methods . . . . .	113
5.3	Future work . . . . .	114
5.3.1	Robotic setup and adaptive control . . . . .	114
5.3.2	Modelling of physical behaviour . . . . .	116
5.3.3	Surface classification, design tool and application . . . . .	117
	<b>List of Figures</b>	<b>119</b>
	<b>List of Tables</b>	<b>127</b>
	<b>List of Symbols</b>	<b>129</b>
	<b>Bibliography</b>	<b>131</b>
	<b>Appendix</b>	<b>140</b>
A	AAG Workshop 2016 . . . . .	142
B	Process data . . . . .	145
C	Project credits . . . . .	161



# 1 Introduction

## 1.1 Background and motivation

Over the last two decades, computation and information technology have profoundly altered contemporary architecture. Computer-aided modelling software has enabled architects to design digital models of buildings with complex, double curved geometries, afforded by underlying mathematical concepts and equations. These digital models allow to superimpose a multitude of information about structure, material, etc., enriching the explicit three-dimensional model with the implicit n-dimensional space of heterogeneous, divergent and hybrid information. While these advancements have seriously redesigned the role of geometry in architecture [1, 2], increasing accessibility and availability of digital fabrication technology have complemented the needs to convert these intangible digital representations into physical reality, creating a link between parametric and algorithmic design models and their materialisation. The thereby facilitated production of non-standard building structures and envelopes represents a technological shift, parting from the mechanical age with its standardization and mass-production into the information age with the serial reproduction of non-identical parts that differ through variation [3, p. 99].

Yet, besides the geometric flexibility and versatility that materialisation by digital means involves, it also entails a multitude of constraints imposed by the physical limitations that come along with certain machines and materials. Formulated as design drivers<sup>1</sup> however, these constraints allow to unfold the specific tectonics of this combination. This development has fertilized the field of architectural design and geometry exploration and has led to an

revived engagement with craft and material systems, their behaviours and procedural nature. These are inherently architectural topics<sup>2</sup>, which today, can be investigated from a different angle: sensor technologies in combination with computer controlled machines allow to comprise, react to, and learn from materials with complex or non-linear behaviour, even in real time. The resulting feedback-based fabrication processes allow for a synthesis of material processes and information technology. Although digital fabrication machinery existed for half a century, it is through availability and accessibility of control interfaces, together with the proliferation and adoption of CAD software, that these hybrid systems are only recently becoming explored within the field of architecture [4, p. 238]. Amongst others, one of its implication, compiled in the phenomenon of *digital materiality* [5], is the dissolving of the long-established separation between the architects' practice of designing and the practice of building [6, p. 50]: the physical manipulation of the material and the fabrication process itself become constitutive elements of the design process.

Albeit these technical advancements and preconditions, the realisation of general double-curved building elements, and concrete formwork in particular, is still a costly endeavour in practice. Therefore, on the agenda of various industry and research institutions is the investigation of economical and ecological techniques, such as flexible or reusable formwork typologies [7, 8, 9], or the avoidance of formwork altogether through 3D-concrete printing [10, 11]. In this context also digitally controlled cutting techniques have become popular in the fields of architecture, design and construction, since they facilitate a fast, low-cost and material-efficient fabrication of non-standard volumetric elements, offering an economic alternative to other commonly used fabrication techniques, such as CNC milling. These elements are applied e.g. as inlays for bespoke formwork components and are prevalingly created by the material subtraction process of thermal plastic foam cutting, in which a hot cutting medium, generally a wire or blade, is introduced to melt the synthetic material just in advance of contact. Yet, the range of possible geometries, due

to the straight cutting medium, is limited mostly to ruled surface elements. The research presented in this thesis allows to significantly expand the set of possible hot-wire cutting geometries with a particular hot-wire cutting technique, of which will be referred to *Spatial Wire Cutting (SWC)* throughout the thesis. The technique is based on the principle of escaping from the straight to a curved cutting medium, that additionally is altered in its curvature throughout the cutting process. This is performed by two six-axis robotic arms that are connected through a single hot-wire, which is attached to their end-effectors (see Fig. 1.1). In the cutting procedure, their coordinated spatial movement guides the hot-wire through the processed material (e.g. expanded polystyrene), which takes up the form of a curve being shaped through the material's resistance.

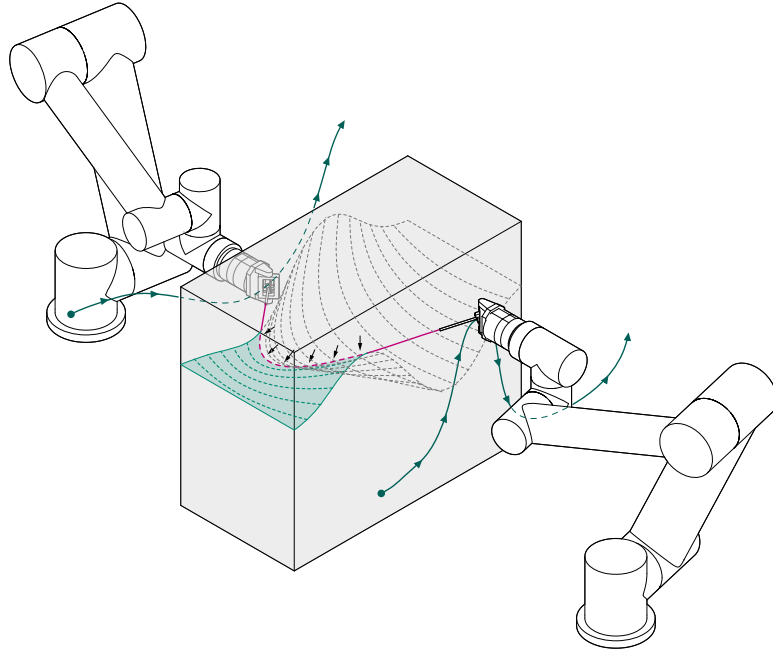


*Fig. 1.1: Illustration of the SWC cutting procedure: Two robotic arms are modulating the curvature of the hot-wire, which adopts itself against the resistance of the processed material [12]*

Contrary to other approaches, which are outlined in Chapter 2.1.2, the procedure operates in transition states between thermal cutting and thermo-mechanical cutting established through the interplay of velocity and heat. This generates gradual contacts along the hot-wire to the processed polystyrene

and subsequently gradual temperatures, as the hot-wire cools through contact. These gradual temperatures, in turn, create variable forces that act contrary to the moving direction onto the hot-wire, which adapts its form accordingly. Consequently, the technique exploits the non-linear relationship between temperature and wire curvature that allows to cut certain double-curved surfaces, in particular sweep surfaces, which can be described by the motion of a changing profile curve along two guide curves. Hence, the technique is not only a cutting, but also a form-finding technique that, in contrast to common form-finding methods, searches not for one optimized equilibrium state of a model, but for successive transitory equilibrium states.

## 1.2 Research goal

The aim of this research is to expand the geometric possibilities of hot-wire cutting in investigating *Spatial Wire Cutting*, a technique that is economically lean in terms of material use and time consumption. This thesis pursues the approach of acquiring knowledge from the physical form-finding process and implementing its digital counterpart. As such, methods and techniques are developed that allow to control the cutting technique and foresee its outcome. It investigates material- and process related constraints, correlations between operating physical factors, such as heat input, cutting speed, resulting cutting force and wire shape. The research targets the exploration of the procedures' specific geometry through a multitude of cutting samples and a computational simulation that serves both for analysis and designing of artefacts. Flexible controlling techniques are developed, since it is necessary to monitor occurring forces and to adapt estimated fabrication parameters accordingly. Ultimately, the goal is to examine the process' possible architectural applications, such as the production of formwork components at full architectural scale.

The thesis builds upon the hypothesis that the integration of digital design and simulation techniques with adaptive control strategies can not only lead

to efficient manufacturing procedures, but can also yield unique and differentiated formal vocabularies in placing materiality as an a priori agent in the formulation of architectural building elements. With this exemplary case, methods and techniques are developed that intend to optimize the relation between action and re-action, between material, machine and designed form, within both digital and physical domains. Thus, the thesis investigates topics that are generally relevant for digital fabrication processes with non-linear material behaviour and contributes to fabrication-aware design methods at large.

### 1.3 Methodology

The above outlined subject matter consequently requires a synthetic, multi-disciplinary approach that integrates both empirical physical robotic-based testing and digital simulation-based experimentation. To develop an in-depth understanding of the specific constraints and potentials of the procedure, a digital counterpart is developed, where information is gathered through the actual physical model itself.

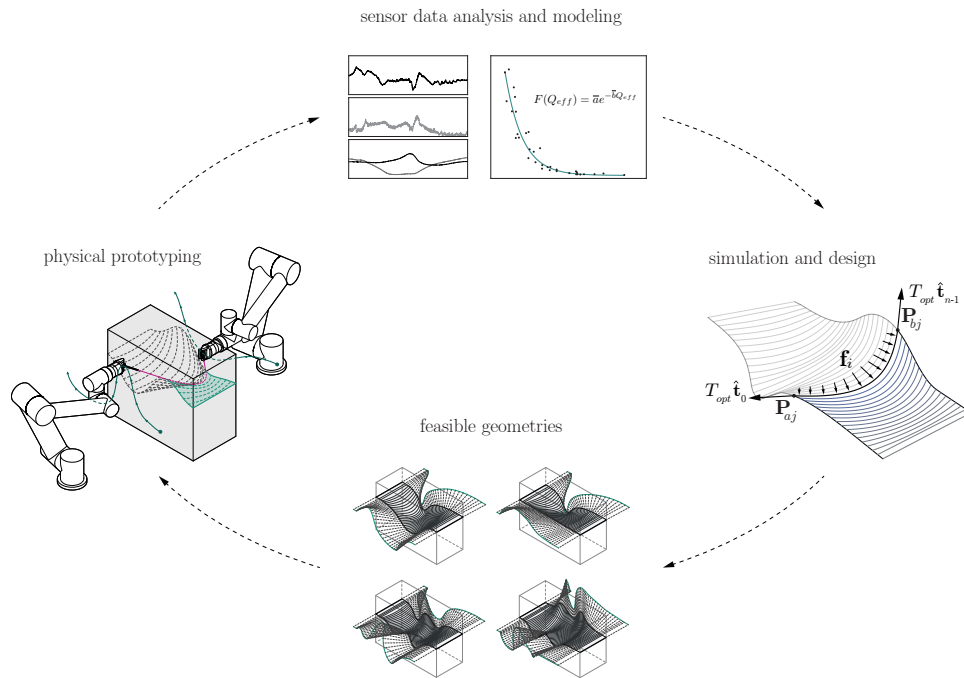


Fig. 1.2: Diagram visualizing the applied methodology

Throughout the thesis four research topics will serve as main, interconnected threads. Progress and advancement within each is mutually dependent and therefore they are mostly performed in parallel.

- *Machine*: the development of adaptive control techniques tailored for the robotic set-up, tools and sensor devices, that allow to efficiently control, but also to capture data from the process
- *Material*: the definition of physical fabrication parameters and constraints that are essential to the *SWC* procedure, the analysis of recorded data from the process and the modelling of the relationships between the fabrication parameters
- *Form*: the computational design and simulation of the procedure both to explore the formal capabilities and to predict the fabrication variables
- *Application*: the validation of the procedure in terms of precision and predictability and its applicability for architectural purposes

### **1.3.1 Adaptive robotic control system**

The project requires the implementation of control algorithms that process feedback information directly from the cutting procedure and suitable synchronisation strategies that allow to coordinate both of robots' movements. Multiple cutting tests are performed to calibrate the robotic control, while recording sensor data that, together with the actual physical artefact is validated and analysed.

### **1.3.2 Analysis and modelling of material behaviour**

Knowledge of occurring physical entities and their interplay are acquired empirically through repeated and systematic experiments that target the definition of relationships between heat input, speed, curve shape and material resistance in dependency to the curvature of the cut surface. Implemented

into a computational model, this lies out the basis for the design and simulation framework.

### **1.3.3 Design and simulation framework**

The procedure creates a specific set of double curved surfaces. In order to design within this constrained design space, it is necessary to integrate simulation capabilities into the design environment. Based on the observation of the physical process, the simulation model is employed to predict the resulting geometry for analysis and formal exploration and also to improve the control of the fabrication in emulating fabrication parameters.

### **1.3.4 Application and validation**

The relation and efficiency between the developed techniques, such as adaptive control and simulation, is continuously validated with physical artefacts. The predictability of the combined design and simulation framework and its applicability for architectural purposes is evaluated amongst others in workshops with students.

## **1.4 Structure of the thesis**

The thesis is structured into five chapters. Following this introduction, Chapter 2 covers the state of the art in robotic hot-wire cutting, provides an overview of the process of thermal plastic foam cutting, reviews previous work and displays it's application within the architectural domain. Further, the thesis is contextualised within the field of digital fabrication in architecture and gives an overview of precedents in analogue form-finding.

Chapter 3 represents the developed techniques, tools, methods, and acquired knowledge about the investigated process. It introduces the above mentioned topics of the adaptive robotic control system, the analysis and modelling of material behaviour, and the design and simulation framework. It outlines the

objectives, challenges and illustrates the results. The chapter is closed with comparative studies between physical artefact and digital counterpart that allow for a quantitative verification of the techniques regarding the process' predictability and repeatability.

Chapter 4 provides the implementation and validation of the developed techniques in regards to their applicability for architectural purposes. It illustrates workshop results with students, amongst others the production of formwork components for façade panels at an architectural scale, and addresses the topic of how the investigated process can be applied for design purposes.

Finally, Chapter 5 presents the overall conclusion. It begins with a summary and discussion on the development and results of the main topics of investigation. Further, it identifies the contributions, as well as limitations of the research and gives an outlook on future work.

## Notes

<sup>1</sup> Kilian introduced four types of constraints that can be used as design drivers: functional, topological, geometrical and quantitative constraints and argues that these play a key role in triggering design innovation [13, p. 90]. He further mentions constraints deriving from digital fabrication [13, p. 95].

<sup>2</sup> Semper is a famous example, who pushed for a reform of industrial design activities, advocating that form should be appropriate to the function, the material and the manufacturing process [14, pp. 7–9]. Another example is Frei Otto, who intensively explored analogue form finding methods with a palette of different materials [15].



## 2 Context

This chapter serves to embed the thesis in regards to architecture, fabrication and technology. It is divided into three subsections, of which the objective of the first one is to introduce the state of art in robotic hot-wire cutting in the fields of both architecture and mechanical engineering. This serves to display the application range of *Spatial Wire Cutting* and outlines the preceding research this project partly builds upon. However, since the technique differs strongly from the mentioned projects in this context in regards to fabrication control and geometry creation, the second subsection embeds the technique in the bigger picture of digital fabrication and refers to other digital fabrication processes dealing with non-linear material behaviour. The third part of this contextualisation reflects on form-finding within architecture, that allows to open a different perspective on the procedure. Finally, the chapter closes with a summary and conclusion.

### 2.1 Robotic hot-wire cutting

Albeit the manufacturing industry has advanced swiftly in recent decades, the realisation of non-standard, formally complex building structures and, in particular, formwork for concrete structures, is still involved with high building costs<sup>3</sup>. As a result, the investigation of economical and ecological techniques is on the research agenda of industry and academia. Topics are, for example, flexible or reusable formwork typologies, such as adaptive moulding [7, 8, 9], fabric formwork [16], dynamic slip-casting [17], combining formwork and reinforcement [18], or the avoidance of formwork altogether by developing additive manufacturing methods like 3D concrete printing [10, 11]. However,

one of today's commonly used way to produce generic double-curved concrete structures is CNC-milling. In this context also digitally controlled hot-wire cutting techniques, often performed with a robotic arm, have become popular in the fields of architecture, design and construction [19, 20, 21, 22], since they facilitate a fast, low-cost and material-efficient fabrication of non-standard volumetric elements.

In terms of production economy and for the fabrication of formwork elements at an architectural scale, the advantages of robotic hot-wire cutting (RHWC) over CNC-milling become most evident: Milling is a incremental material removal process, requiring significantly high machining steps and is therefore a very time- and waste-intensive fabrication routine. Tolerating a rougher surface could reduce machining hours, however, smooth surfaces may be required due to aesthetic and practical reasons for the formwork dismantling process. Hot-wire cutting produces smooth surfaces already through a single sweeping motion, and further on the cast product [22], while reaching the same surface quality with milling requires high machining hours. Additionally, the removed material through the milling process is waste, while in hot-wire cutting the negative part of the cut can be processed further entirely.

Yet, while the decrease of production time in RHWC is dramatic, the feasible geometric vocabulary is considerably limited in comparison to the geometric possibilities of milling. The consequences are that the application of CNC-milling is either limited to exclusive high-end building budgets, for detailing tasks and reusable formwork modules in the principle of standardization. Complex design geometries are post-rationalized and simplified, leading often to formal restrictions of planar surfaces and geometric derivatives.

This chapter provides an overview over the geometric limitations of robotic hot-wire cutting, exhibits different set-ups and visualizes its application range. Further, it gives a state of the art in the field of thermal foam cutting mechanics, on which this thesis builds upon.

### 2.1.1 Ruled surface based design and panelling

A ruled surface can be described as the surface swept by a moving straight line. This is the basic principle of standard hot-wire cutting, where the hot-wire, representing the straight line, is moving relative to the work-piece, resulting in a kerf. Ruled surfaces can be either single-curved (developable surfaces, like the cylinder, see Fig. 2.1) or double-curved (like the hyperbolic paraboloid, see Fig. 2.2) and there are multiple ways to physically produce ruled surfaces apart from wire cutting due to their simple and comprehensible principle of creation. A famous pioneer in the use of ruled surfaces for his designs was Antonio Gaudí, who's reference in this thesis is two-fold: Besides his vast experimentation with ruled surfaces and their intersections, which actually withdraw from simple comprehensibility, he also used physical computation methods with catenary chain models for form finding, which will be a topic in Section 2.3.

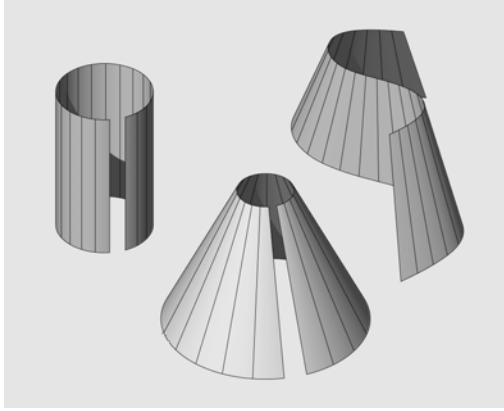


*Fig. 2.1: Developable ruled surfaces*



*Fig. 2.2: String surface model of a hyperbolic paraboloid [23]*

Gaudí used helicoids, hyperbolic paraboloids and hyperboloids of revolution for the design of the Sagrada Família [24, p. 25]. Through permutations of individual parameters of each of these surfaces and their combinations, he applied a rich formal and structural palette throughout the building, leaving a legacy to an incredible oeuvre designed in times without CAD modelling. Gaudí primarily worked with gypsum plaster for the creation of his models: For the model of the clerestory window, half of a hyperboloid of revolution is

formed by rotating a hyperbolic curve around a central pivot while the plaster sets during the rotation of the profile. Multiple thereby created surfaces are composed together by chipping off their edges, creating three-dimensional curves of intersection [25]. The actual full-size moulds for the window were constructed similarly.

Further famous architects that developed an architectural language of ruled surfaces are Félix Candela, Heinz Isler, Iannis Xenakis and Frei Otto. Ruled surface based design is still of interest to contemporary free-form architecture, due to the practicability of production.

While Gaudí developed his design based on physical ruled surfaces, quasi pre-processing the constraints of materialisation at large, in today's digital design process often free-forms are generated that, in the first instance, have not yet incorporated their means of production. Therefore, rationalization of designed geometries, such as panelling tasks<sup>4</sup>, have become an important research topic in the field of architectural geometry. For example, for the glass fiber reinforced concrete panels of the façade of the Cagliari Contemporary Arts Center by Zaha Hadid Architects, hot-wire cutting was intended to be used to produce the EPS foam moulds for the panels that have been approximated to ruled surfaces [26] (see Fig. 2.3). Likewise, in the project *Fondation Louis Vuitton* by Gehry Technologies (see Fig. 2.4) the curved enclosure of the building was post-processed and divided into 19 000 custom-shaped panels. Each mould for the glass-reinforced concrete was either hot-wire cut (for ruled and developable surfaces) or routed (for non-ruled surfaces) [27].

Although theoretically the definition of the ruled surface meets the standard hot-wire cutting procedure, it is important to note here that not all ruled surfaces can be produced by this technique. Apart from set-up specific limitations, tool size, possible intersections with the existing surface object, this is primarily due to its constrained operating time-frame in the relationship between temperature and speed, further explained in the next section. For example, half hyperboloids of revolution, like mentioned before, are critical to fabricate, because, if the lead angle becomes too flat, the two wire (exit)



Fig. 2.3: Cagliari Contemporary Arts Center, Zaha Hadid Architects, Cagliari, Italy, 2006 [28]



Fig. 2.4: Fondation Louis Vuitton, Gehry Technologies, Paris, France, 2014 [29]

ends experience a high difference in speed, causing high temperature on one end and melting the foam too much, while on the other end the foam would be hardly melted due to low temperature.

### 2.1.2 The process of thermal plastic foam cutting

Thermal plastic foam cutting is the material removal process, in which a heat source is introduced to melt a synthetic material while advancing, resulting in a kerf. This heat source, generally a hot-wire or hot-blade, is generated by passing an electrical current through a resistant material (Joule heating), metal alloys such as Nichrome, Kanthal or stainless steel. Commonly used plastic foams for foam cutting are polystyrene foams, because they are inexpensive, widely available, the low density (less than  $60 \text{ kg/m}^3$ ) and their physical properties make them ideal for the process. The kerf width and the surface finish of a cut are determined by the cutting speed, the electrical power input and the material properties of both the cutting medium and the plastic foam.

Thermal plastic foam cutting is a well-known technology for manifold applications. Apart from architectural purposes, outlined in Section 2.1.3, it is further employed for rapid prototyping purposes and in the production



*Fig. 2.5: Manual fabrication (left) and photo of the installation EPS grotto (right) from artist Kwangho Lee in collaboration with NAMELESS Architecture, 2013 [30]*

of models for the film industry, advertising, aero- and hydrodynamic testing and artwork (see Fig. 2.5). Many commercial CNC-cutters<sup>5</sup> are available and the open source community provides instructions and blue-prints for self-buildable CNC hot-wire cutters<sup>6</sup>. The following processes developed within the field of mechanical engineering are a selection of the current state in thermal plastic foam cutting and are mainly developed for rapid prototyping purposes. Here, approaches to overcome the geometric limitations of the process are either only, or combinations of

- layer based approaches, in which the desired geometry finish is linearly approximated by layers
- flexible tools that change the cutting shape
- hot cutting tools that mainly carve or sculpt the foam of the work piece; similarly to clay sculpting

Besides the following projects' different set-ups, they are mentioned since they investigate the physical factors of influence, on which this thesis builds upon.

#### **2.1.2.1 Variable Lamination Manufacturing (VLM-s)**

This patented and commercialized process has been developed at the Department of Mechanical Engineering at the Advanced Institute of Science and Technology in Korea (KAIST). The VLM-s rapid prototyping process

employs a four-axis synchronized automatic hot-wire cutter (with a taut hot-wire) to cut EPS foam sheets with variable thickness, which are consequently bonded together to form the finished object. The process includes also a material storing and -transport system [31].

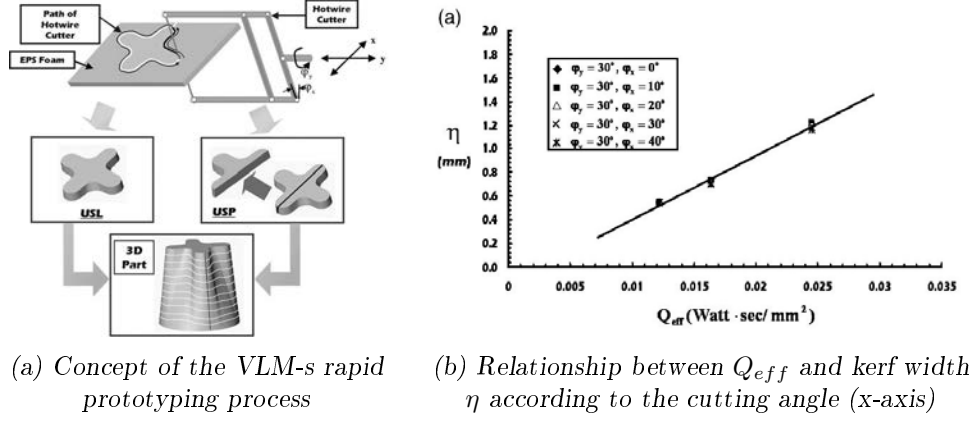


Fig. 2.6: Variable Lamination Manufacturing [32]

In the context of the research project, mainly to improve the dimensional accuracy and part quality, a number of experiments have been carried out to identify the relationships between the heat input, cutting speed and kerf width, and, for this project in particular, the cutting angle. The property effective heat input  $Q_{eff}$  was introduced and it was concluded, that, within the experimental range, the relationship between kerf width and the effective heat input is linear (see Fig. 2.6b) [32].

### 2.1.2.2 Freeform Thick Layered Object Manufacturing (FF-TLOM)

The FF-TLOM technology was developed at the Faculty of Industrial Design Engineering and Production, Delft University of Technology in the Netherlands. The proposed system combines the advantages of layer oriented manufacturing with the speciality of having a flexible cutting tool, a hot-blade. The research focuses on the decomposition of free-form CAD models into producible layers and also on the production process, investigating the influential parameters of plastic foam cutting with hot blades [33, 34, 35, 36, 37]. The prototypical cutting tool controls the shape of the blade through four actuators: two stepper motors, which rotate each of the blade's supports and

two linear slides to change the distance between the connection points (see Fig. 2.7a). The FF-TLOM technology is most suitable to the production of objects with slow changes in curvature, since rapidly changing curvature will require the blade to move transversal. For the fabrication, a six-axis industrial robot was applied to move the foam slab while the tool remained in a fixed position. The concept of the flexible blade is also central to the project BladeRunner, further explained in Section 2.1.3.2.



(a) Prototype of the cutting tool



(b) Example of a stacked foam model

Fig. 2.7: Freeform Thick Layered Object Manufacturing (FFTLOM) [36]

### 2.1.2.3 Freeform Automated Sculpting Technology (FAST)

Research into thermal foam cutting mechanics is also performed at the Department of Mechanical Engineering, University of Canterbury, New Zealand with implemented systems in publications refereed to as Freeform Automated Sculpting Technology (FAST) and also Robotic Foam Sculpting (RFS). The set-up consists of a six-axis industrial robot and hot-wire and hot-blade tools to sculpt blocks of polystyrene foam similarly to clay sculpting. On the basis of multiple experimental cutting tests with both hot-wire [38] and hot-blade settings, Brooks investigated empirically relationships between cutting force, wire temperature and kerf width, together with observations of the surface texture [39]. Furthermore, a force-feedback control system was implemented (using a loadcell and a thermo-couple) that modulated the electrical current to provide constant tool temperature for the purpose of maintaining both the surface characteristics and kerf width [40]. Quantitative measurements of the



surface roughness and form were investigated by Bain [41], who developed also the model of the relationship between the effective heat input and the cutting force in the steady state, to which this thesis will be referring to and will further be explained in Section 3.2.2.

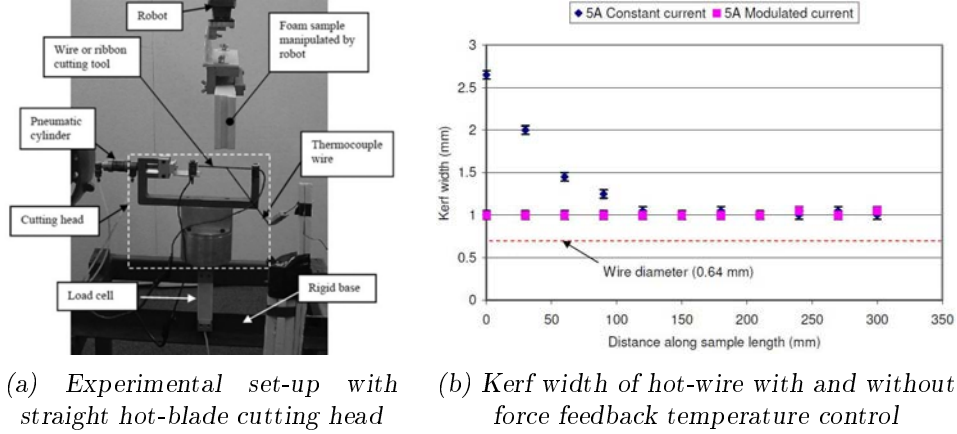


Fig. 2.8: Freeform Automated Sculpting Technology (FAST) [40]

### 2.1.3 Research and application of RHWC in architecture

In the course of the recent shift towards robotic technology in architecture and construction, robotic hot-wire cutting has become a topic within both academia and industry. Here, the general set-up for hot-wire cutting consists of one industrial robotic arm and a conventional end-effector, where the hot-wire is tightly fixed at two points of a custom clamping device. In the fabrication process, either the foam-block is moved relative to the hot tool or vice versa (see Figs. 2.9, 2.10) and the set-up can further be extended with a turn-table. In contrast to research projects from the field of mechanical engineering, the focus within the following projects is more on application scenarios and geometric possibilities of elements fabricated by the technique.

The method of cutting and associated operations and techniques has its historical precedent in stereotomy, the science or art of stone cutting. From the Renaissance on, stereotomy described the way of cutting solids into certain figures or sections with developable surfaces, for the purpose of building load-bearing structures such as arches, vaults and domes. The application of



Fig. 2.9: Set-up used for fabricating *Persicope* by Matter Design Studio [42]



Fig. 2.10: Set-up at RMIT Architectural Robotics Lab, workshop by Robots in Architecture [43]

RHWC in architecture can be clustered into three different research fields: First, the investigation of the volumetric possibilities and the assembly of cut elements for temporal building structures similar to stereotomy, second, the fabrication for formwork purposes and third, the combination of using both the thermal insulation properties of the foam as well as its form-giving capabilities for composite elements.

### 2.1.3.1 Temporal building structures

The *RDM vault* was a collaboration between the research group Hyperbody (TU Delft), Block Research Group (ETH Zurich) and ROK (Rippmann Oesterle Knauss GmbH) [44] exploring the joint approach of designing and fabricating vaulting structures (see Fig. 2.11), which consisted of the aggregation from several dissimilar hot-wire cut foam components, also topic of investigation in [20, 21]. Foam vaults have similarly been explored in the project *Light-Vault* [45] from Tongji University and Schwartz's *Automated FoamDome #1 and #2* [46]. In the installation *Persicope* by Matter Design Studio, the fast process of robotic hot-wire cutting allowed to build a 15m tall tower of foam within a two-week construction window, assembled by fabricated mass-customized masonry units [47, 22]. In comparison to the aforementioned vaults, in which the elements were three-dimensionally hold in place, these large units were stacked in layers building a volumetric tower.



Fig. 2.11: RDM vault, TU Delft, Netherlands, 2012 [44]

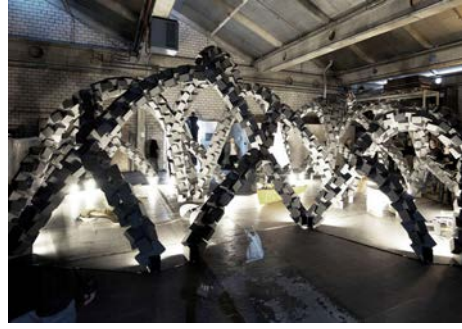


Fig. 2.12: The Catenary Pavilion, Gramazio Kohler Research, Langenthal, 2010

Another potential of joining robotically cut foam elements was investigated at the installation *The Catenary Pavilion* (see Fig. 2.12) from Gramazio Kohler Research (ETH Zurich) and further, in the elective course *The Interlocking*. Here, custom interlocking elements were fabricated and allowed for a constructive equilibrium during the assembly of the differentiated foam structures [48, pp. 224-237].

### 2.1.3.2 Casts and formwork

In the project *Opticut*, resulting from a research partnership between Aarhus School of Architecture, TU Delft's Hyperbody's Robotics Lab and the companies Odico Formwork Robotics and Hi-Con, the potentials of topology-optimised spatial structures were explored. The formwork was fabricated with RHWC and casted with concrete [49] (see Fig. 2.13). The research group of CEAU/FAUP at the University of Porto, Portugal developed different panels in concrete by applying several sweep cuts onto one single foam block to create a closed mould [50] and thus explicitly profiting from the positive and negative parts of a cut. Similarly, the Institute of Architecture and Media (TU Graz, Austria) investigated the cutting of formwork of a single block for column-like concrete structures and further explored pre-shaped hot-wire tools [51, 52]. A research workshop at the Massachusetts Institute of Technology by Clifford focused on robotic cutting with hot-knives (using

semi-circular and 'J'-shaped blades) to carve negative geometries from EPS foam and then used to mould a glass-fiber reinforced gypsum column [53].

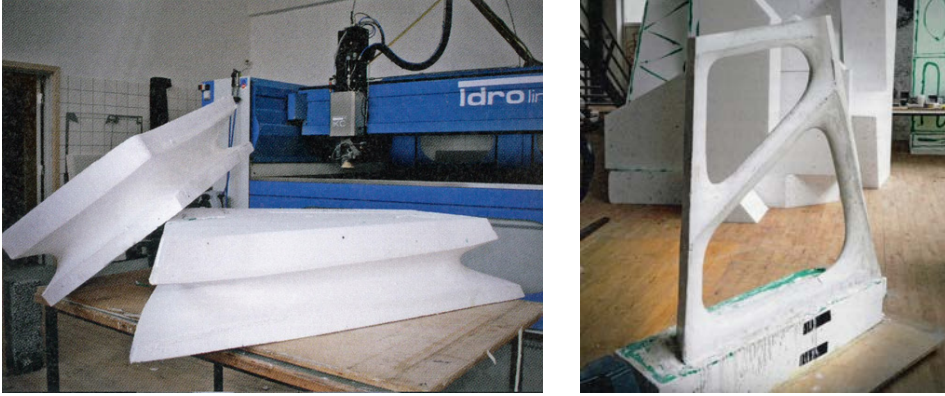


*Fig. 2.13: Project Opticut: Formwork (left) and casted prototype (right) [49]*



*Fig. 2.14: Robotic arm cutting large scale moulds at Odico Formworks Robotics [54]*

As apparent in the projects named above by Zaha Hadid Architects and Gehry Technologies (see Figs. 2.3, 2.4), architectural scale works in favour of RHC, since the limitation to ruled surfaces becomes less of an issue if a greater surface area allows for a satisfactory approximation. The aforementioned company Odico Formworks Robotics [55], founded in 2012, grew out of academic research at the Hyperbody TU Delft research group. Their focus is to apply the RHC technology also for larger industrial and architectural applications (see Fig. 2.14), such as the Kirk Kapital headquarters in Vejle designed by Danish-Icelandic artist Olafur Eliasson, which requires 4000 m<sup>2</sup> of formwork to be produced [56].

Within the field of architecture, one of the most recent and advanced projects, that expands the geometrical restrictions of RHWC is *BladeRunner* [57], supported the Danish National Advanced Technology Foundation. It presents a novel process for flexible hot-blade cutting for the production of concrete formwork: Two robotic arms are dynamically changing the shape of the blade, mounted on their flanges, while another robot is moving the foam block linearly through space, thus acting like a conveyer belt (see Fig. 2.15). The project expands the set of applicable surfaces to "surfaces swept out by continuously varying families of planar Euler elastica" [56, 58].



Fig. 2.15: Project *Bladerunner*: Tri-robot hot-blade cutting configuration (left) and fabricated prototype (right) [56]

Although the concept of the flexible blade is similar to the FF-TLOM project (see Section 2.1.2.2), there are some differences. For example, since the aim in the FF-TLOM project is to produce three-dimensional rapid prototype models and not concrete formwork, the segmentation problem of approximating a given surface is approached by finding appropriate *thick layers* whereas in the *Bladerunner* the surface is divided into patches swept by elastica or ruled patches. Further, the geometric problem to calculate the shape of the blade is approached differently: while the FF-TLOM group apply a numerical method to minimize the bending energy, the *BladeRunner* group apply the known analytic representation of the shapes, which allows for advantages in the post-processing of a given surface [59].

### 2.1.3.3 Composite elements

The project "Integrales Faserzement Verbund-Element (IFVE)" (engl. Integral Fibre-Cement Composite Element) [60] from the Chair of Architecture and Construction from Deplazes at ETH Zurich investigated the potential to utilize both the thermal insulation properties of the foam as well as its form-giving capabilities to develop composite elements. This façade system, supported by the project partners Swisspor Management AG and Eternit (Schweiz) AG, combines the advantages of a protecting material with insulating material [61].

### 2.1.4 Feasibility study of *SWC*

In the summer of 2012 Ryan Johns conducted a three-month preliminary study at the Chair of Gramazio Kohler Research, proofing in principle the feasibility of the *SWC* process [62]. The experimental set-up comprised two robotic arms, each equipped with a prototypical tool that allowed to measure the occurring force online (see Section 3.1.3.1).



Fig. 2.16: Cutting samples fabricated in the feasibility study

For one cutting iteration, the drawn path-curves from McNeel Rhinoceros 3D [63] were divided into a certain amount of positions and sent to the robotic arms. The implemented software allowed to modify the robots' speeds in the ongoing procedure according to the tools' measurements. This set-up allowed for multiple initial experiments, producing various surface samples and proved the potential of the *SWC* procedure (see Fig. 2.16).

However, the process of drawing path-curves and successive fabrication was mostly a trial- and error approach. It was concluded that in order to fully control and design with the procedure, more knowledge of physical factors was needed to foresee the outcome.

## 2.2 Digital fabrication in architecture

Today, the separation between design and building has dissolved, established by the technical continuity of computational design and its realisation by digital technologies [6, p. 50]. The recent shift towards digital fabrication technologies in architecture, has induced universities around the globe to set up research facilities with industrial robots. Following ETH Zurich in 2005, they have fostered promising architectural case studies and prototypes, exploring novel robotic construction processes that allow for the production of non-standard elements and structures. Additionally to the field of academic research this trend has been pursued by a number of start-up companies devoted entirely to architectural robotic fabrication processes, such as the aforementioned Odico Formwork Robotics, and further RoboFold, ROB Technologies, etc.

Central to projects within the field of digital fabrication in architecture, including some of the projects presented in the last section, is the development of tools to master the production. The purpose is not only to efficiently control the fabrication process, but its integration in a design environment to fully explore and deal with the fabrication-inherent constraints, that relate to certain machines, materials and processes. Further, this allows to combine the capacity for algorithmic design and robotic instruction code directly from within CAD environments [19], and to investigate the full potential of this combination<sup>7</sup>.

Although initially design-to-fabrication workflows within architectural research were linear and deterministic approaches, simply transporting digital information to the physical world, but not vice versa, recent projects are

emphasizing the potential of closed-loop feedback processes [64, 65, 66, 67]. Apart from obvious advantages, that the integration of feedback entails, such as increasing stability, decreasing tolerances, synchronization of parallel executing processes, etc., it further establishes an momentarily fusion between the digital and the physical world, between design and realisation, encompassing the potential to rephrase the goal in every iteration of exchange. For example, this can be utilized for incorporating human interaction in the process, to combine operational logics with intuitive actions [68, 69, 70] or, and therein this thesis is embedded, for complex and non-linear architectural materialization processes. Examples are projects such as *Procedural Landscapes* [71, 72], in which sand is formed through a feedback-driven process, or the research project *Smart Dynamic Casting* [17], in which feedback is applied for shaping concrete in its early hydration phase with a dynamically formable formwork. Investigations as such provide the ground to mature from predictable material processes inherited by the industrialisation, of which most of today's architectural production is still making use, and start to investigate materials with heterogeneous or non-linear behaviour, *adapt form and design to the variability of nature almost as aptly as artisanal manipulation once did* [3, p. 105], and even, with the potential of digital simulation and control, go beyond. Against this background, the thesis investigates topics that are generally relevant for digital fabrication processes with non-linear material behaviour and contributes to fabrication-aware design methods at large.

### 2.3 Form-finding and optimal shapes

*Spatial Wire Cutting* is a form-finding procedure, that searches not for one optimized equilibrium state of a model, but for successive transitory equilibrium states. The changing shape of the curve and the resulting swept surface, are explicitly dependent on forces that operate time- and material dependent. By controlling and inducing the respective forces, the resulting form is controlled. Contrary to the hereafter discussed analogue-, and other digital



form-finding methods<sup>8</sup>, the project's combination of physical manipulation and the integration with sensor technology in an adaptive manufacturing system extends the notion of form-finding, to a process that is neither merely analogue nor merely digital. Hence it enqueues alongside other emerging categories such as *Fabrication-Aware Form Finding* [73], as through digital fabrication this dichotomy is continuously fading.



Fig. 2.17: Minimal surface of revolution [74]

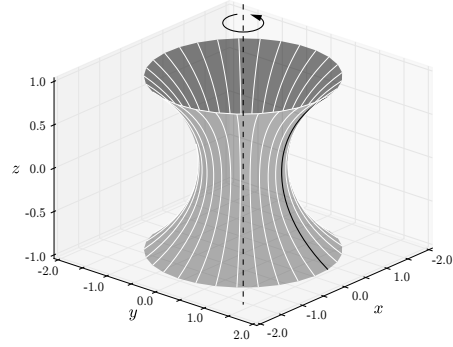


Fig. 2.18: Catenoid creation

Before the introduction of computers, architects and engineers used dynamic analogue physical models to compute optimal shapes and structural scenarios. The hanging chain suspended from its two ends, takes up in tension the shape that, when inverted is optimal for a compression structure [75, p. 118]. Its discovery has a long history: In 1675 Hooke studied the mathematical properties of the catenary curve and stated that he had discovered the optimal shape of an arch [76]. Around same time Leibnitz, Huyges and Johann Bernoulli discovered the algebraic description of the curve following a challenge of Bernoulli's brother Jacob and demonstrated that this shape was not, as Galileo had conjectured, a parabola but a catenary [77, p. 124]. Euler proved that the catenary is the curve which, when rotated about its directrix, gives a surface of minimum area<sup>9</sup>, the catenoid [78] (see Fig. 2.18). This surface results for example by the soap film between two bubble wands (see Fig. 2.17). Jacob Bernoulli first and Euler later are also responsible for the development of *elastica*, the theory on bendings or curvatures of beams caused by weight or other compression forces (as applied in the Bladerunner project, see 2.1.3.2) [79, 80] (as cited in [58]).

Gaudí was the virtuoso in the expression of the catenary principle [75, p. 119]. He applied it in arches, columns and extended it to the forth dimension in his funicular model based on strings and sand bags for the unfinished chapel Colònia Güell. Felix Candela, Pier Luigi Nervi, Heinz Isler, Iannis Xenakis and Frei Otto are a few of many architects that found surfaces through a variety of physical analogue modelling techniques. Frei Otto generalized the principles of form-finding based on physical models to a large group of physical phenomena beyond chains and strings. He and his team at the Institute for Lightweight Structures in Stuttgart experimented with multiple materials that process forces by transformation. As a crucial pre-condition, they used materials that have a certain flexibility and through material interaction would result in a geometry based on the complex behaviour of elasticity and variability [81]. Otto's material repertoire extends to sand, balloons, paper, wool-thread and water, soap film and -bubbles, glue, varnish, etc [15]. To digitalize these physical models, for example the pre-stressed cable net roofs of the Olympic Stadium in Munich, stereo-photogrammetry was applied. Based on these data, a computational validation and correction of the measured equilibrium form was calculated, using the *Force Density Method (FDM)*<sup>10</sup> [82, 83], one of today's most commonly used numerical form finding techniques. This method will also be used to approximate the shape of the hot-wire, further explained in Section 3.3.1.

## 2.4 Conclusion

Robotic hot-wire cutting (RHC) has manifold applications, as outlined in Chapter 2.1, but is geometrically limited to ruled surfaces. In the current state of art, approaches to overcome these limitations are either layer-based approaches, carving strategies or the use of flexible tools that change the cutting shape. Concerning the latter, the project BladeRunner (see Section 2.1.3.2) also exemplifies the relevance of a multidisciplinary integration of geometry processing with robotic fabrication for the purpose of architectural production. From an architectural and geometrical perspective, the project

has similarities to *Spatial Wire Cutting*: Both create a particular family of sweep surfaces, however the curve formed by the blade lies within a two-dimensional plane, whereas the *SWC* curve utilizes the full three-dimensional space. Since the profile curve and both guide curves, through which the sweep surface is created, are different, it can be argued that the Bladerunner's surface family does not coincide with the set of *SWC* surfaces. Additionally, the difference of *SWC* lies particularly in the interaction with the processed material.

For this reason *SWC* is an exception in the field of RHWC, because apart from Brooks [40] and Gallina [84, 85], that use force-feedback to maintain both the surface characteristics and the kerf width, hot-wire cutting is usually a linear and predictable fabrication method, in which the resulting geometry and the process parameters are predetermined. The discussed technique however, requires a different design- and fabrication approach: It is necessary to continuously adapt fabrication parameters in the procedure and to comprise the process' peculiar formal language. Therefore not only direct feedback is needed in the process itself, but also an indirect feedback, which is built up as empirical knowledge, implemented in a digital counterpart and which subsequently guides formal design decisions.

Thus, the discussed technique extends conventional hot-wire cutting geometry with a yet unexplored surface vocabulary that stems from the physical process, based on the interplay of material properties, speed, heat and force. Through the investigation of this unique process, this research develops methods and techniques, integrating digital design and simulation techniques with adaptive control strategies and thereby contributes to the domain of digital fabrication and fabrication-informed design methods at large.

## Notes

<sup>3</sup> Examples for high building costs due to non-standard formwork are: EPFL Learning Center [86], Meiso No Mori Municipal Funeral Hall [87] or Spencer Dock Bridge [88].

<sup>4</sup> *The approximation of a design surface by a set of panels that can be manufactured using a selected technology at a reasonable cost, while respecting the design intent and achieving the desired aesthetic quality of panel layout and surface smoothness.* [89]

<sup>5</sup> One commercial CNC-cutter is for example Hotwire Direct [90].

<sup>6</sup> Instructions for self-buildable CNC hot-wire cutters can be found at the websites [91] and [92].

<sup>7</sup> Many of the projects presented in Section 2.1 are simultaneously developing or working with tools such as PyRAPID [49], superMatterTools [19], KUKA|prc [93], Robots.IO [94], and HAL [95].

<sup>8</sup> Digital form-finding methods are for example: Dynamic relaxation [96], the Force Density Method [82, 83] or constraint solvers such as ShapeOp [97].

<sup>9</sup> A minimal surface is a surface that locally minimizes its area. This is equivalent to having a mean curvature of zero. Also, the helicoid, a ruled surface, is a minimal surface.

<sup>10</sup> The Force Density Method (FDM) *is commonly used in engineering to find the equilibrium shape of a structure consisting of a network of cables with different elasticity properties when stress is applied. While shape analysis of tensile structures is a geometrically non-linear problem, the FDM linearises the form-fitting equations analytically by using the force density ratio for each cable element,  $q = F/L$ , where  $F$  and  $L$  are the force and length of one cable element respectively.* [98]

### 3 Techniques for design and control

This chapter describes the process-specific developed methods, technology and acquired knowledge for the *Spatial Wire Cutting* process, implemented throughout the two and a half year lasting research project (see project credits in Appendix C). It followed a preliminary study (see Section 2.1.4), which proofed the technical feasibility of the *SWC* process. This chapter is structured into four sections, of which the first three discuss the core topics such of adaptive robotic control, modelling of material behaviour, computational design and simulation. The last one documents on the validation of the developed techniques, particularly on the predictability and reproducibility of the physical process by means of the simulation framework and the adaptive control software.

The complex and interconnected relation between the presented topics demanded an analytical as well as an empirical research method. Computational simulations concurrently supported and were informed by real world experiments. Physical artefacts and the capturing of sensor data from the fabrication process delivered comprehensive insights on a number of multi-layered interdependencies such as material behaviour, fabrication control, as well as resulting geometrical articulations. As such, calibration and parallel development in the topics was necessary, however started with implementing the robotic control, on which the others were based upon.

### 3.1 Adaptive robotic control system

This section describes the development of the adaptive control techniques tailored for the robotic set-up, as well as the tools and sensor devices, that allow to efficiently control, but also to capture data from the fabrication process. Parts of the below described prototypical control software and strategies have been developed within the scope of a collaborative master thesis [99] by Kathrin Dörfler and the author of this thesis [69, 100]. Within the framework of this thesis, the software has been developed further with a generic approach, which, apart from little set-up specific deviations, enables to write control sequences for various actuator- and sensor devices. Out of practicality it has been decided not to switch to far more advanced tools that have similar goals and are currently in intensive use in the field of robotics, such as ROS (Robot Operating System)<sup>11</sup>. For the purpose of keeping clarity and simplicity not all modules and processes are explained on the following pages, the focus is on those that are specific and relevant for the *SWC* procedure.

#### 3.1.1 Objective

The preliminary requirements for the development of the robotic control can be outlined as follows:

- The necessity to collect data from the physical process requires the identification of appropriate sensors and tools, which specifications have to be identified through physical experiments
- High frequency of data flows from sensors and actuators must be established, which requires the development of appropriate communication protocols and status control
- The partial unpredictability of the fabrication procedure requires an open control system that allows to adjust certain pre-estimated fabrication parameters online

- To guarantee at a proper surface quality a smooth movement of the robotic arms is requisite
- Appropriate synchronization methods for the two robots must be identified and tailored for the robotic set-up
- Interrupt channel and safety control have to be implemented to protect the sensors

### 3.1.2 Experimental set-up

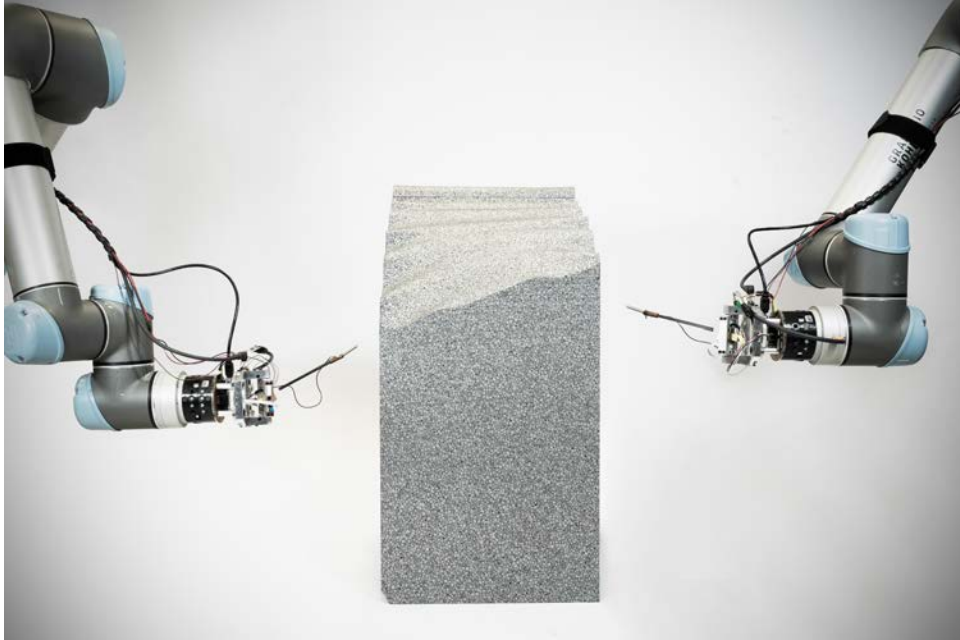


*Fig. 3.1: The experimental set-up*

The experimental set-up (see Fig. 3.1) was built upon the Robotic Model Laboratory (RML) of the Gramazio Kohler Research group, which provides a platform for scaled research on architectural robotic fabrication. It consists of two Universal Robots UR5 [92] (six-axis robotic arms with a payload of 5 kg and an operating range of 850 mm each), two customized end-effectors (further explained in Section 3.1.3) that are connected to a hot-wire (Kanthal A, 0.20 mm diameter), which is heated via programmable laboratory power supply. All software-based implementations are summarised in the control

system (see Section 3.1.5), of which the *Control Core*, a custom Python program, monitors and orchestrates all passing information (see Section 3.1.5.1). It is running on a laptop computer, to which the UR5 robots are connected over TCP/IP socket and each of the micro-controllers (Arduino Nano 3.0), controlling the sensors in the end-effectors, are connected over USB, as well as the laboratory power supply, continuously streaming data to the *Control Core*. In the cutting procedure, the robotic arms are moving the hot-wire through material blocks of graphite-enhanced expanded foam<sup>12</sup>, which is placed in between. The size of these blocks varied in the course of the development and ranged from 200 x 300 x 600 mm up to 800 x 600 x 1200 mm<sup>13</sup>.

### 3.1.3 Sensors and tooling

The necessity to collect data from the physical process in order to be able to adapt certain fabrication parameters online, requires the identification of appropriate sensors and the development of adequate tools, which measure certain physical quantities while not distorting the outcome. Experiments have been performed to determine the most necessary quantities and the specifications of the tool.

#### 3.1.3.1 Force measurement with linear potentiometer

As already mentioned in Section 2.1.4, in the preliminary study of *SWC* a prototypical end-effector was developed, and used during the beginning of this thesis, which allowed to investigate fundamental problems and requirements. It consisted of a milled PVC encasement which served as guidance for the internal spring. The spring extension was measured with a linear potentiometer attached to the encasement. As the wire was pulled or released, the slider shifted and the output voltage of the potentiometer was scaled (see Fig. 3.2). Together with the spring constant, the tension force was calculated on basis of Hooke's law.



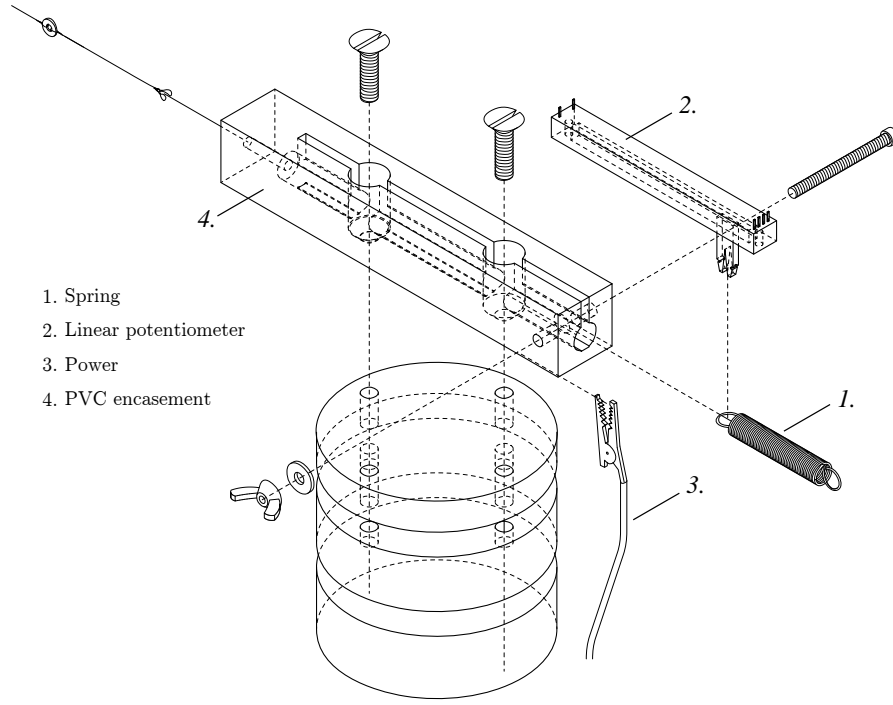


Fig. 3.2: Prototypical tool with linear potentiometer

This end-effector solved some problems encountered in early experiments: For example, the spring allows a tolerance in wire tension, which enables the hot-wire to be taught without breaking and therefore works as a damper. The alligator connector from the power supply is fixed to the bolt at the opposite end of the PVC encasement, passing the current successively through the bolt, to the spring, a flexible stranded cable and the hot-wire. As such, it does not interfere with the hot-wire and omits clipping the alligator connector directly to and weighing upon the hot-wire (see Fig. 3.2). Although this tool served well for early experiments, for the purpose of producing consistent and reliable measurements, it had major disadvantages:

- Force is required to move the slider of the linear potentiometer, and therefore force measurements below a certain value can not be measured
- The current flows through the spring, which is heated according to its respective electrical resistance and changes its spring constant. Therefore the spring extension cannot be reliably and consistently measured.
- Most importantly, the tool remains in a fixed position along the cut

and if the wire deflects from the axis of the tool, the spring is extended with deflected force and additionally melts the PVC encasement.

### 3.1.3.2 Force and torque sensor

The ATI Nano17 is a sensor that measures all six components of force and torque ( $F_x, F_y, F_z, T_x, T_y, T_z$ ) [101]. For temporary usage, a prototypical tool was developed (see Fig. 3.3) and several tests were carried out to further identify and concretise the requirements for the appropriate end-effector.

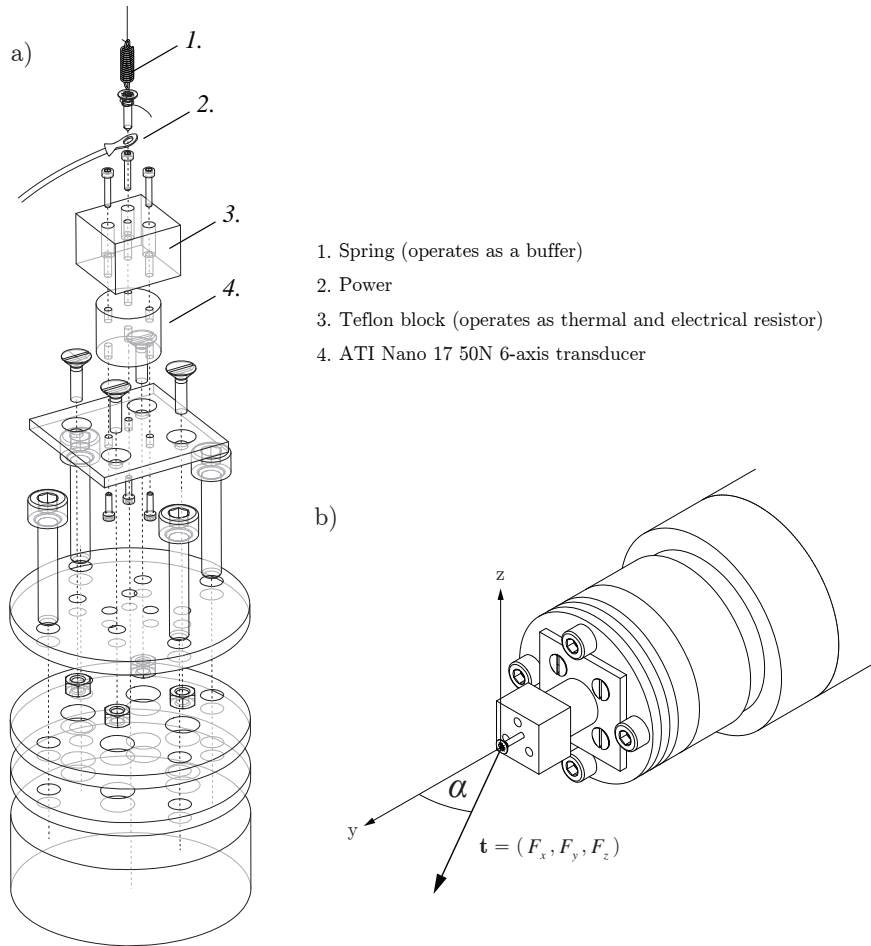


Fig. 3.3: a) Prototypical tool with the ATI Nano17 force/torque sensor and b) deflection  $\alpha$  from the tool's z-axis calculated with the sensor's measurements

The experiments were performed with the two UR5 robotic arms; one robot equipped with the ATI Nano17 tool and the other one with the linear potentiometer tool. The hot-wire was heated with constant current, moved with

constant velocity through the foam on parallel path curves and the measurements of both tools along the cut were logged. The purpose of these tests was, on the one hand, to show the differences between both force measurements and, on the other hand, to check the repeatability of the force measurements from the ATI Nano Tool to different heat inputs.

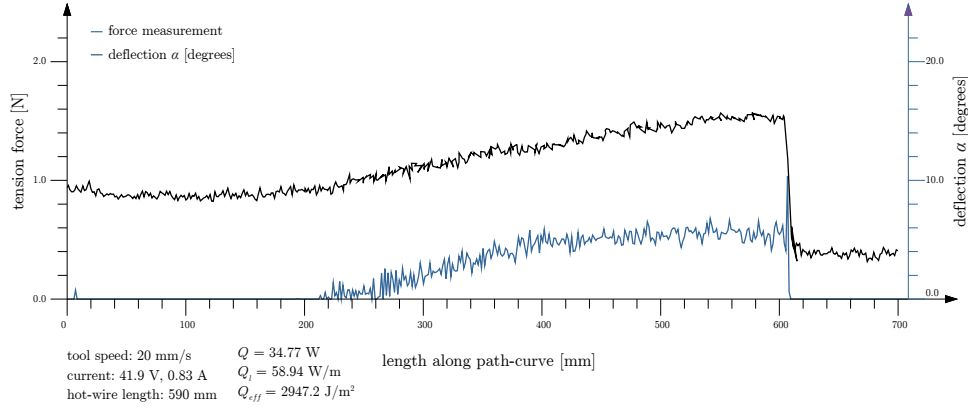


Fig. 3.4: Measured tension force and deflection  $\alpha$  along one cut

From the measured tension force vector  $\mathbf{t} = (F_x, F_y, F_z)$  its magnitude and deflection  $\alpha$  about the tools' z-axis were calculated (see Fig. 3.3). The graph in Figure 3.4 shows the force magnitudes and deflections along one cut, which is characteristic for foam cutting (see Section 3.2.2). The angular measurements resemble the force's profile curve, as with increasing force, the wire deflection from the mounting point increases as well. The hot-wire's exit from the foam is obvious in the falloff of the curve in both profile curves.

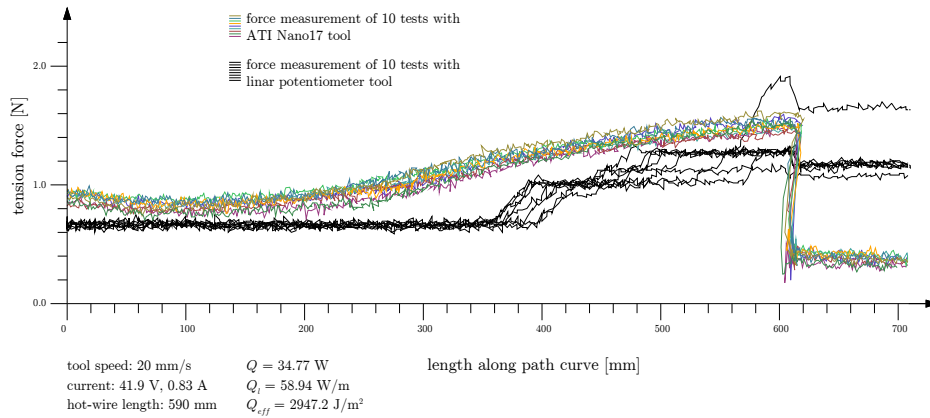


Fig. 3.5: Data plot from ten repeated cutting tests, linear potentiometer data in black, ATI Nano17 tool coloured

The graph in Figure 3.5 shows the force measurements of ten repeated cutting tests and, beside the force measurements of the ATI Nano17 sensor, shows the force calculated from the spring extension of the linear potentiometer tool. In this comparison it becomes clear that the ATI Nano17 sensor, with a much higher resolution, allows for a better investigation into the variation of the tension force. The standard deviation of the ten tests at various test points was within the acceptable range of 0.045 to 0.052 N.

### 3.1.3.3 The cardan-joint end-effector

On basis of the aforementioned prototypes and several cutting experiments, the requirements for the design of the end-effector could be characterized. It was concluded that, besides measuring the tension force, it is important to measure the deflection about the mounting point. This would allow to calculate the cutting force acting contrary to moving direction (see Section 3.2.3). Additionally, it is necessary, that the force measurement follows the deflection of the hot-wire in order to measure the tension in the force direction and that all sensory equipment should not disturb the outcome by its measurement. This end-effector was developed in cooperation with Florian Rist, who gave valuable advice and help in its realisation.

- For the purpose of measuring the tension force, a force sensor operating with foil strain gauge was used, that provides an appropriate resolution and accuracy (see Fig. 3.7, 5.).
- This sensor is placed in the center of a cardan joint (see Fig. 3.7, 6.a and 6.b), which follows the rotation of the hot-wire and therefore the force direction. The maximal rotation range in axis A is from -129.34 to +129.34 degrees, and in axis B from -61.07 to +61.07 degrees (see Fig. 3.6). Ball bearings are used to reduce the friction in the joint.
- The rotation of each of the axis of the joint is measured by magnetic rotary encoders, which don't need contact, but just a certain distance

to a magnet to sense its rotation and therefore the measurement does not interfere with the rotation.

- The light-weight carbon fibre stick (see Fig. 3.7, 4.) from the force sensor operates as a handle, additionally reducing the force needed to rotate the joint.
- The ceramic cylinder (see Fig. 3.7, 2.) operates as thermal and electric resistor and as a connector for the spring.
- The spring (see Fig. 3.7, 1.) operates as damper or buffer between the hot-wire and the handle, allowing for a smooth contraction and extension, omitting breaking the wire.
- The hot-wire is attached to the spring and the cable transmitting the current, which is fixed at the handle.
- The weight of the handle, ceramic cylinder, spring and cable of the current entry is equalized with a lead weight, fixed below the force sensor (see Fig. 3.7, 8.).
- For practical reasons it was decided to build a compact, space-saving tool, with a custom circuit board on which the small micro-controller Arduino Nano 3.0 is placed.

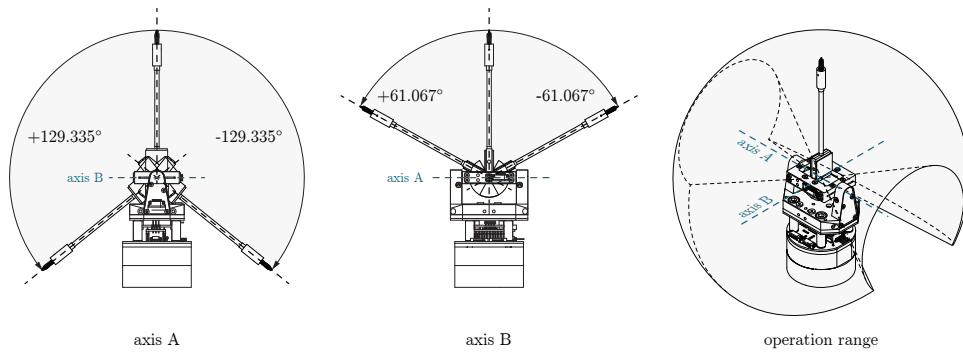


Fig. 3.6: Visualisation of the tool's operating ranges in axes A and B

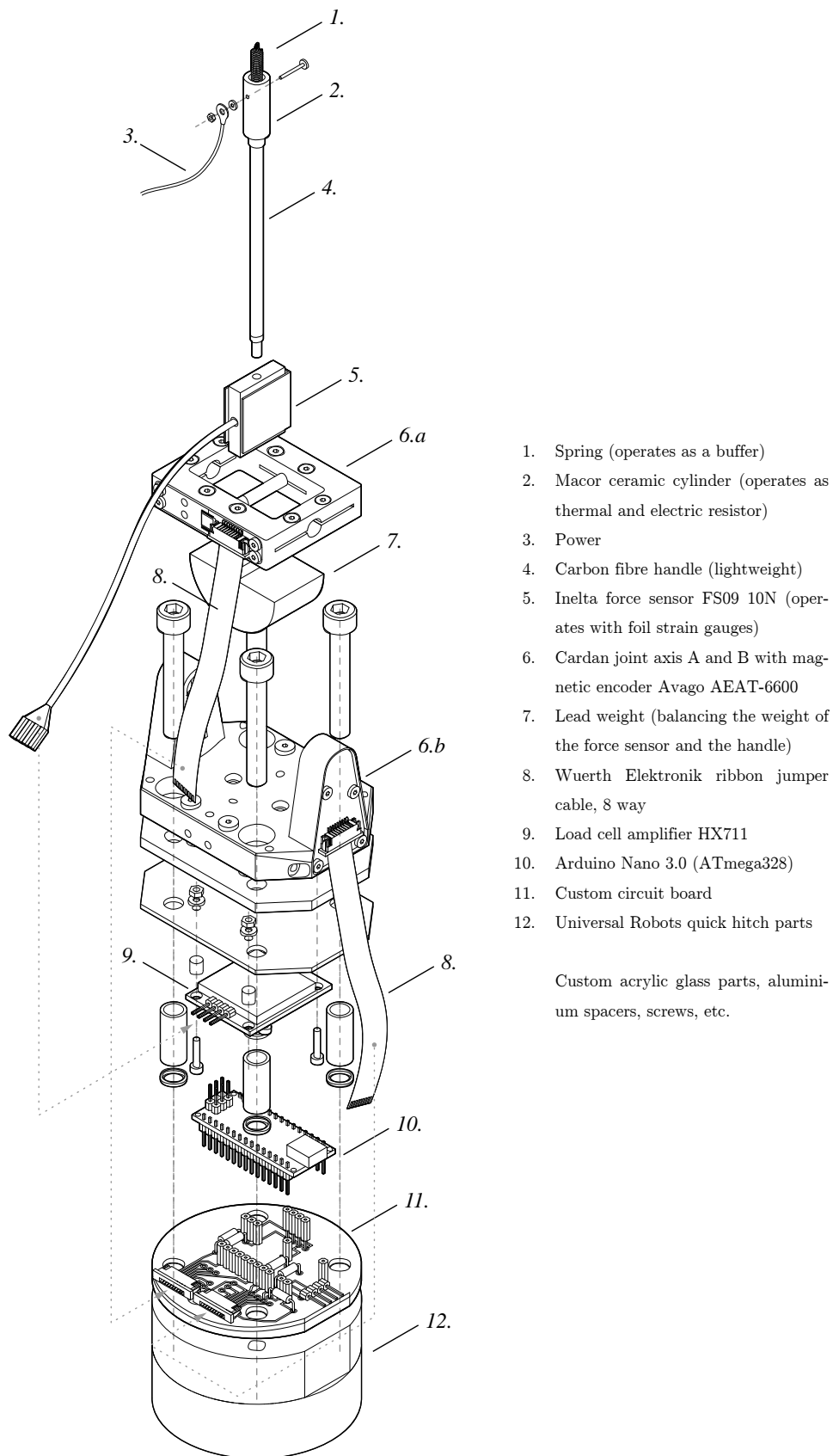


Fig. 3.7: Exploded view of the cardan-joint end-effector

### 3.1.4 The UR robot

The UR5 robot is programmed at the script level with a custom program written in the robot programming language *URScript*. The script is sent as pure text from the computer over TCP/IP socket to the URControl RuntimeMachine (RTMachine) that evaluates and executes the code in real-time. The RTMachine communicates with the robot with a frequency of 125 hz [102, p. 9]. To generate a robot trajectory, the *URScript* provides several move functions, of which `movej`(move linear in joint space) and primarily `movel`(move linear in tool space) are used.

```
movel(pose, a=1.2, v=0.3, t=0, r=0)
```

**pose** Target pose, consisting of a list of six floating numbers. The first three are Cartesian coordinates and the last three describe the tool orientation in axis-angle representation [103].

**a** tool acceleration [m/s<sup>2</sup>]

**v** tool speed [m/s]

**t** time [s]

**r** blend radius [m]

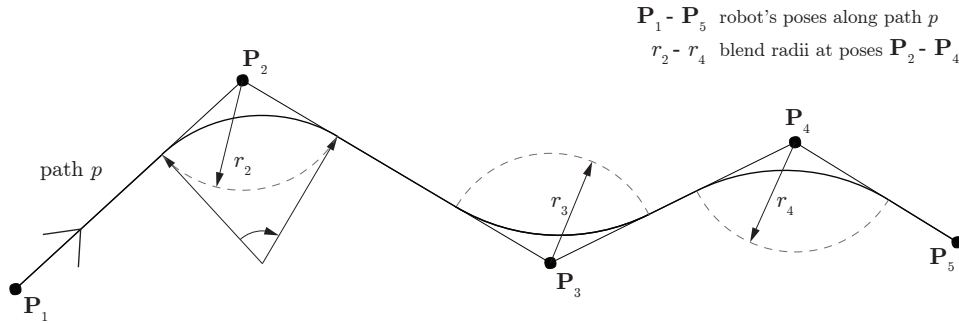


Fig. 3.8: Robot example path, specified through poses  $\mathbf{P}_{a1}$  to  $\mathbf{P}_{a5}$  and respective blend radii  $r_2$  to  $r_4$

To specify the type of the movement, it is possible to control the trapezoid speed profile of the move either with the speed  $v$  and acceleration  $a$  parameters, or to set the time for the move with the parameter  $t$ , which has priority over  $v$  and  $a$  settings. The blend radius can be set with the parameter  $r$  to avoid the robot stopping and to achieve a smooth movement from one to another pose, which is relevant for the *SWC* procedure to produce a proper

and smooth surface. Yet, if the robot starts to execute a path with pose  $\mathbf{P}_1$  (see Fig. 3.8), the URControl requires to *foresee* the next two poses ( $\mathbf{P}_2, \mathbf{P}_3$ ) in order to calculate the joint trajectories for the blend at  $\mathbf{P}_2$ . Therefore, to maintain adaptability features and to avoid sending all poses on a calculated path-curve at once, a buffer had to be implemented that stores just the next upcoming poses, which additionally requires appropriate messaging and status protocols between the *Control Core* (see Section 3.1.5.1) and the robot program (see Section 3.1.5.6) to allow for a piecewise sending of path information (see Fig. 3.15).

### 3.1.5 Control system

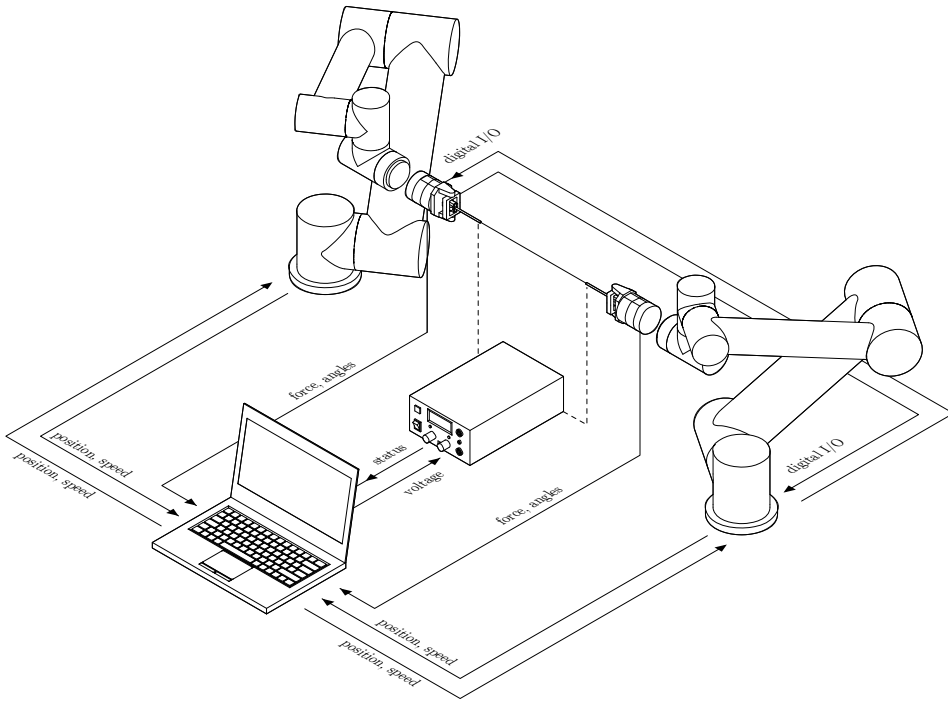


Fig. 3.9: The traffic within the SWC control system

The control system is the underlying system controlling the fabrication process, which is explained step by step in Section 3.1.6. It involves the set of software tools that manage the communication between the Python program *Control Core*, running on a laptop computer, the UR robots (further referred to as UR robots *a* and *b*), which are controlled by a custom *URScript* program, the Arduino micro-controllers in the end-effectors, which stream the



sensors' readings to the *Control Core*, the programmable laboratory power-supply and McNeel Rhinoceros 3D's Grasshopper [63, 104], also running on the laptop computer and which serves as graphical user interface (GUI) to the *Control Core*. As mentioned before, the *SWC* process requires adaptivity features, smooth robotic movements and high frequency of data flows from sensors and from/to actuators, wherefore appropriate communication protocols and status control were implemented. Furthermore, the system's structure was adapted and developed according to the experimental set-up and the functionality of the UR robot's programming language *URScript*. In the following, particular details of the control system are discussed.

<b>Control Core</b>	All communication streams converge here; it is the main control over the fabrication process.
<b>Message protocol</b>	All parties of the control system communicate with a uniform message protocol (except for the laboratory power supply that has its custom protocol <sup>14</sup> ).
<b>Status control</b>	The status control ensures a synchronisation of parallel executing processes on different devices.
<b>Robot buffer</b>	The implemented buffer together with the status control allow for a piecewise sending and execution of path information.
<b>Robot synchronisation</b>	Both UR robots <i>a</i> and <i>b</i> need to reach the specified poses on their respective path curves at the same time.
<b>Robot program</b>	The custom <i>URScript</i> program controlling each of the UR robots is constantly streaming its current position and speed, reading new commands from the <i>Control Core</i> , executing them and synchronizing the start of each move command to the other robot.

### 3.1.5.1 Control Core

The *Control Core* is a custom Python program, that monitors, manages and orchestrates the information passing between the different parties of the control system. The high frequency of information flows requires multiple processes to run in parallel. These processes are clustered into the following modules (see Fig. 3.10):

- Server** This module handles all communications over TCP/IP socket, such as the UR robots *a*, *b* and Grasshopper, which starts the fabrication process by transmitting the fabrication parameters in the beginning of the procedure and also allows to stop all processes immediately by sending the corresponding message. The **Server** module is further responsible for the piecewise sending of path information to the robots.
- Serial** This module handles all communications over USB connection, such as both Arduino micro-controllers *a*, *b* and the laboratory power supply.
- Fabrication** This module has global access to all information handled by the previously noted modules and is the main control over the fabrication procedure, further explained in Section 3.1.6.

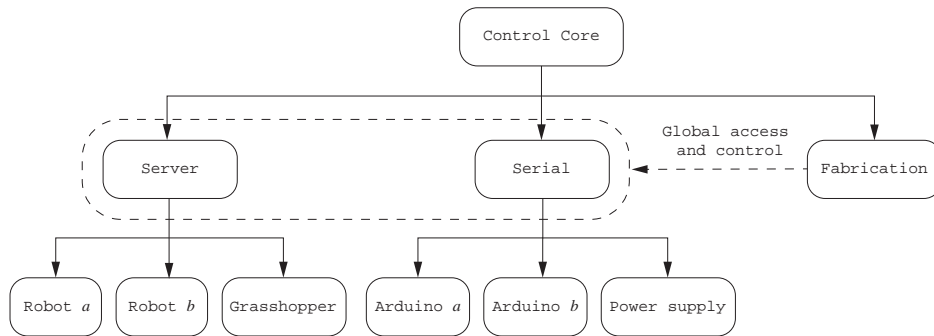


Fig. 3.10: Overview of the Control Core's structure

### 3.1.5.2 Message protocol

Throughout the procedure there are different message types passed around to different parties of the control system. With respect to generality and based on ROS's messaging system [105], a similar message protocol was implemented that allows for a common interface. Since the requirement is to have high frequency in data flow, it must be guaranteed, that all transmitted bytes are received and properly processed. They consist of

- `message_length`, which specifies the length of the message in bytes
- `message_identifier`, which classifies the message for the recipient
- the actual `message`, which will be converted according to the `message_identifier` into the correct data type and then passed on for further processing

**Example: the move message.** As mentioned before, in the *SWC* procedure the movement on a path is specified by several poses, each one consisting of a blend radius `r` and a speed value `v`, through which the robot controller calculates the joint trajectories. To track the robots current position along a path, the poses are numbered consecutively by a `WAYPOINT_ID`, which is also sent together with the pose settings. For example, a move `message` with message identifier `MSG_COMMAND` to the robot consists of

`message_length MSG_COMMAND WAYPOINT_ID pose v r.`

Other messages to the robot have self-explanatory message identifiers such as `MSG_STOP`, `MSG_QUIT`, `MSG_CURRENT_POSE_CARTESIAN` and so on.

### 3.1.5.3 Status control

According to the passed messages, the objects representing the different parties of the control system enter different states in the *Control Core*. While sensor devices may be in just two states (`READY` to receive data and `BUSY` processing a task), the robot can enter three different states:

---

READY_TO_PROGRAM	the robot's buffer is <i>empty</i> , it is ready to receive a move command, but not executing any command
READY_TO_RECEIVE	the robot's buffer is <i>not full</i> , it is ready to receive a move command and currently executing a move command
EXECUTING	the robot's buffer is <i>full</i> , it is <i>not</i> ready to receive a move command and currently executing a move command

The above mentioned states are changed by following message identifiers that are sent from the robot.

MSG_RECEIVED	the robot has received a move command and stored it in its buffer, but <i>not</i> executed the command yet
MSG_EXECUTED	the robot has definitely executed a move command

#### 3.1.5.4 Robot buffer

To enable path adaptability (for possible later improvements) and to avoid sending all poses on a calculated path-curve at once, a buffer was implemented. For example, a robotic move along a path  $p$  consisting of five poses (see Fig. 3.8) would be processed as follows: First, after connecting to the **Server** of the *Control Core*, the object representing the robot would enter the READY\_TO\_PROGRAM state (1a), its buffer is empty. Then, to fill the buffer, three poses have to be sent at once (2a). After receiving these poses with their identifiers, three times the message MSG\_RECEIVED together with each of the identifiers WAYPOINT\_ID of the poses would be sent back (2b). In parallel, the robot starts to execute the move to the first pose (4b) and if it has reached the pose, it would send an MSG\_EXECUTED together with the identifier to the *Control Core* (5b). This would tell the *Control Core* to send a new pose (5a), which is read in into the robot's free buffer entry (6b). As such, the timing of sending pose information is ruled by the robot that executes the poses. In the end, after having sent and executed all poses, the robot would enter the READY\_TO\_PROGRAM state again (9a).

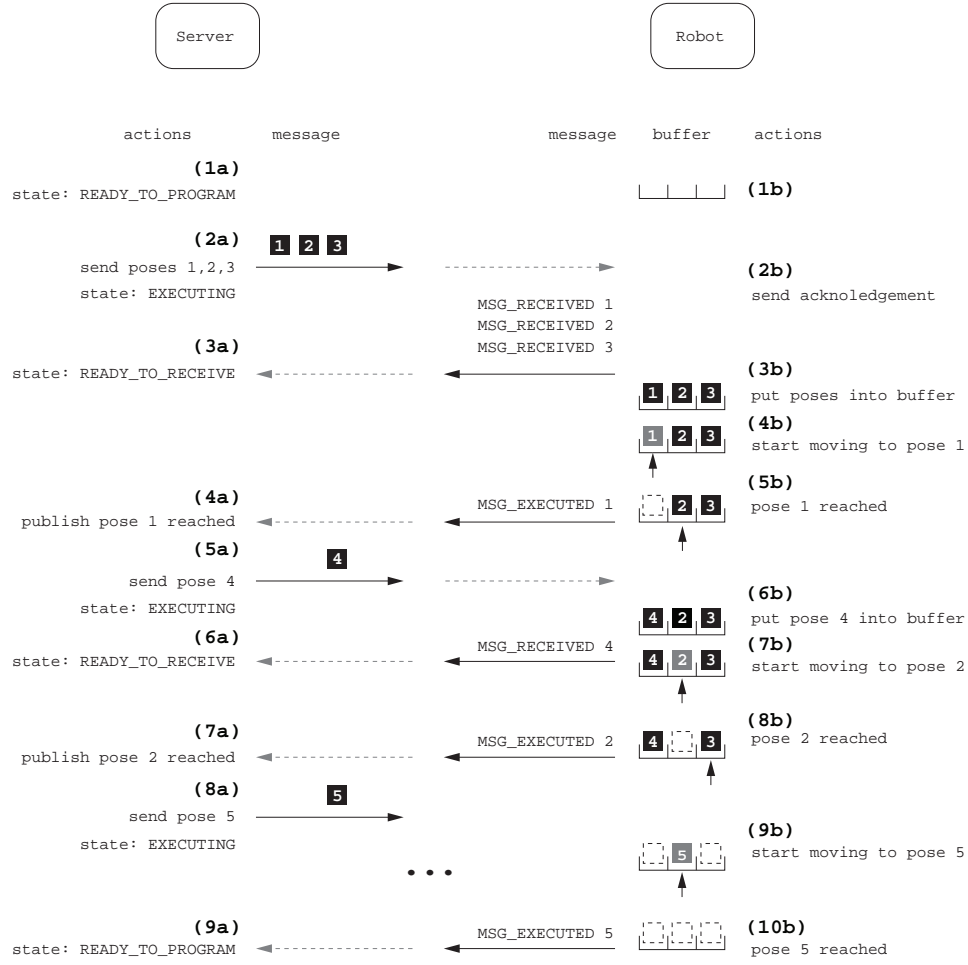


Fig. 3.11: Robot buffer explanation

### 3.1.5.5 Robot synchronisation

The UR robots  $a$  and  $b$  need to reach the specified poses on their respective path curves at the same time, while not stopping at the pose, keeping a smooth movement. The therefore required synchronisation was implemented in three parts:

- (1) Speed calculation
- (2) *Control Core* synchronisation
- (3) I/O synchronisation

(1) First the poses on the path curves must be calculated in such a way that the robots would reach the poses simultaneously. Therefore the speed parameters ( $v_a$ ,  $v_b$ ) between the poses are defined relatively to the distance ( $d_a$ ,  $d_b$ ) in between. For example, if the next pose of robot  $a$  is twice as

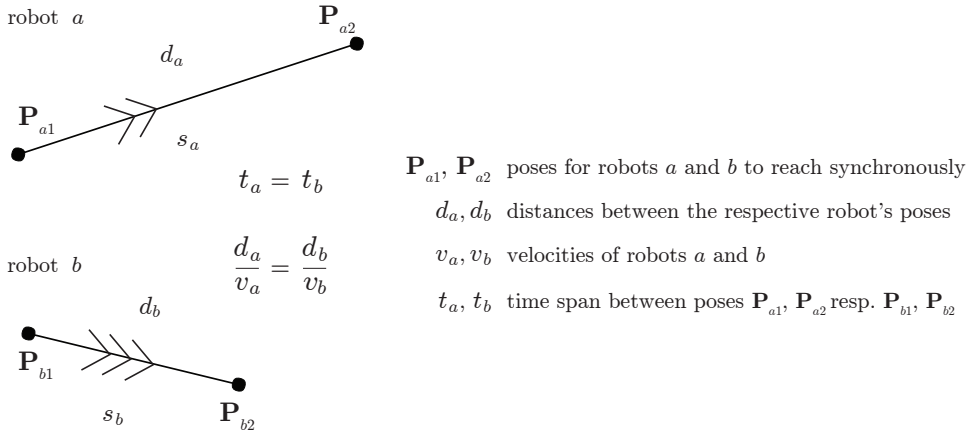


Fig. 3.12: Pose synchronisation with velocity calculation

far to the current pose as the distance of robot  $b$ , then also the speed must be twice as fast to guarantee a simultaneous movement (see Fig. 3.12). However, since the joint acceleration constraints are not taken into account for this calculation, additional synchronisation is necessary.

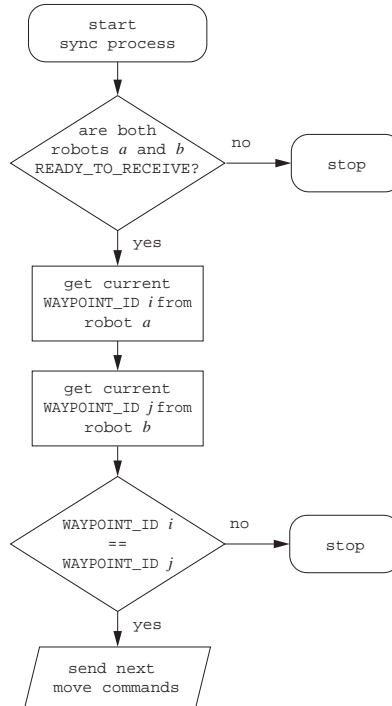


Fig. 3.13: This (pseudo-)synchronization process in the Control Core is called if one of the robots enters the *READY\_TO\_RECEIVE* state.

(2) In multi-robotic environments the position synchronization problem is commonly approached through a master-slave model [106, 107]. One robot would receive all commands from a controlling system, and would transmit

the information to the other robot wrapping the robot control towards outside as one system. However, it was decided upon controlling both robots directly from the *Control Core*, in which the time-stamp of sending to each robot a new move command is synchronised (see Fig. 3.13). Yet the reading of that command in the robot program and its execution depends on multiple circumstances, amongst others, the robot's task load and cycle time.

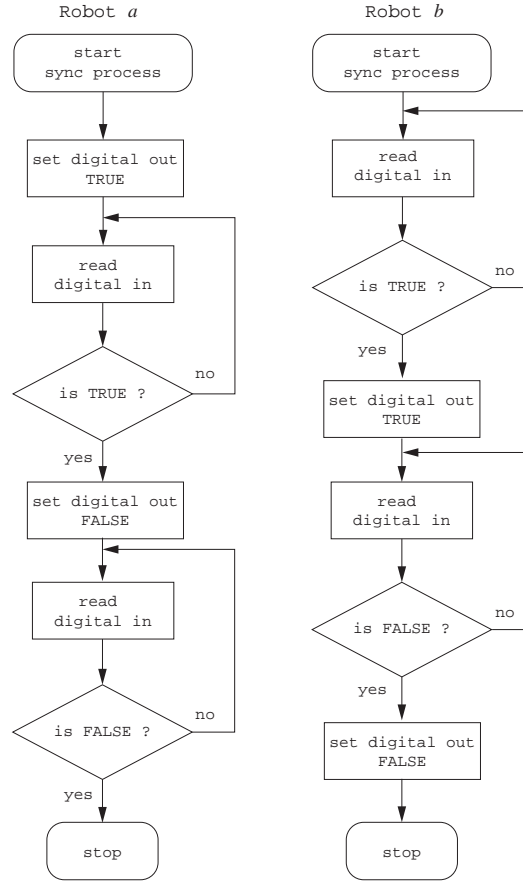


Fig. 3.14: Handshake over digital I/Os: Robot *a* = master, robot *b* = slave

(3) The buffer layout in the robot program makes it difficult to control when exactly the robot would start processing the move. Therefore, additionally to the mentioned synchronization approaches, a handshake between the robots *a* and *b* was implemented (see Fig. 3.14). The robots are connected to their digital I/Os and by switching the outputs to **TRUE** or **FALSE** and waiting until their inputs get **TRUE** or **FALSE**, they would signalize each other when to start the move. Secondary, this works as a safety loop. For example, if robot *a* would terminate the *URScript* out of any unforeseeable reason, robot *b* would

be stuck in the loop, not continuing the movement, and therefore saving the sensory equipment. The time spent on this handshake varies according to the robots' cycle time and takes up to maximal 48 milliseconds (= 4 cycle times).

### 3.1.5.6 Robot program

The program running on both UR robots consists of four sub-processes running in parallel (see Fig. 3.15). It was partially written in following the implementation of the ROS UR driver [108].

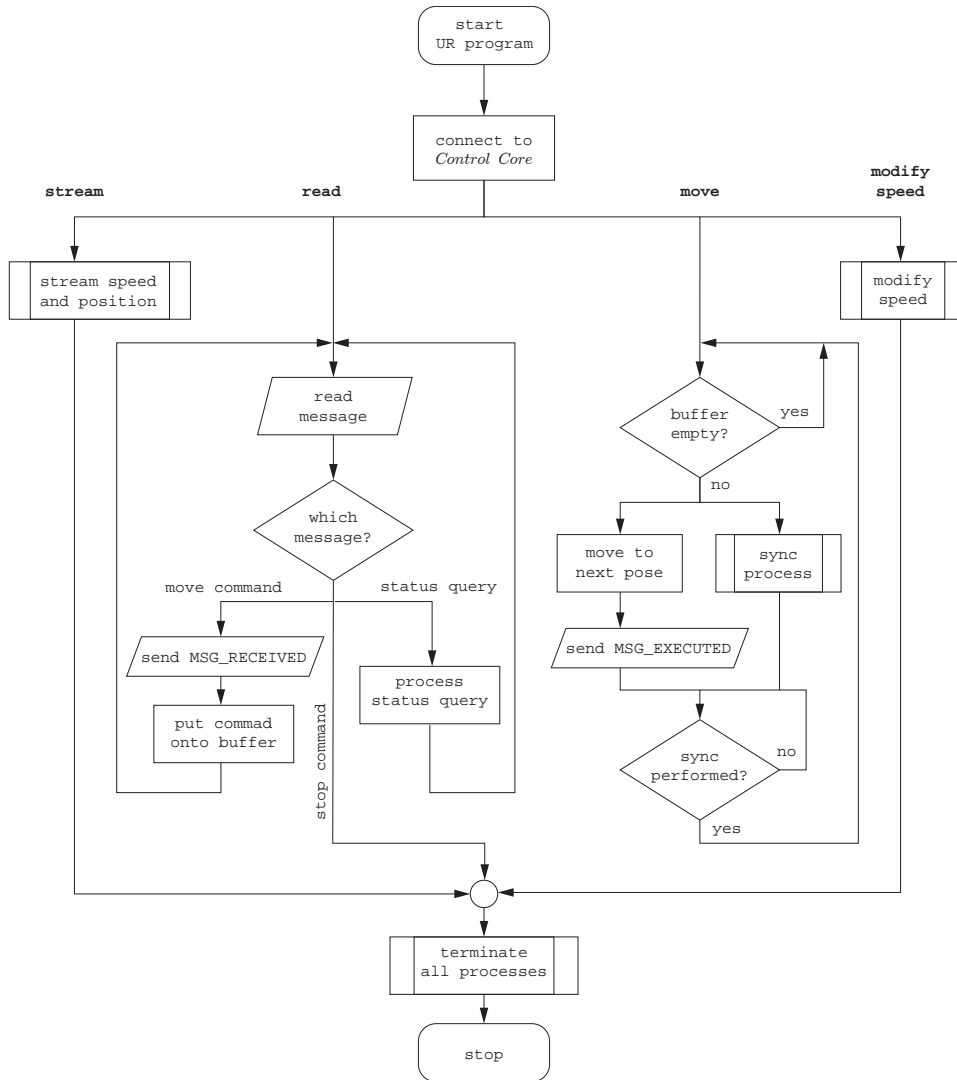


Fig. 3.15: UR program flowchart, focusing on the sub-processes **read** and **move**



---

<b>stream</b>	This sub-process streams the current position and speed to the <i>Control Core</i> .
<b>read</b>	This sub-process reads and processes the data from the <i>Control Core</i> and saves the move commands into a buffer.
<b>move</b>	This sub-process reads from the buffer, moves the robot and, before starting the move, synchronizes to the other robot. (see Fig. 3.14)
<b>modify speed</b>	This sub-process sets the global speed of the robot, which overwrites the speed settings in the move command. This is necessary in order to keep a constant tension force in the end-effectors.

### 3.1.6 The fabrication process

Designing and simulating of *SWC* surfaces is performed from within McNeel Rhinoceros 3D's Grasshopper, further described in Section 3.3. In order to cut one of the designed surfaces, the sequential steps are as follows: After the *Control Core* has been started, the *URScript* program is sent over TCP/IP socket to each of the robots, which move into their starting pose and connect as clients to the **Server** of the *Control Core* (see Section 3.1.5.1). The **Serial** module starts the communication to the programmable laboratory power supply and the Arduino micro controllers. Then the hot-wire is manually fixed at both robot end-effectors in a certain tension. The **Fabrication** module waits for the message from Grasshopper, containing all relevant information to fabricate. Amongst others, this includes, the sequential poses for each robot, the respective blend radii and pre-estimated speed parameters at each of these poses and the voltage, which is calculated according to the desired heat input, the length and a material constant of the hot-wire. The voltage is set by transmitting a custom protocol<sup>15</sup> to the laboratory power supply through the **Serial** module. When electric current passes through resistant material the Joule heating effect occurs and heats up the hot-wire,

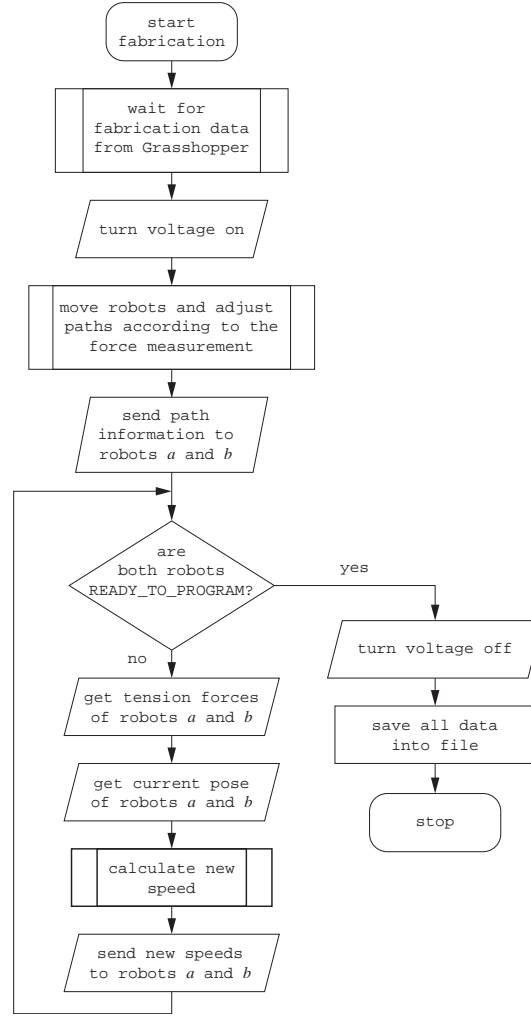


Fig. 3.16: Fabrication process flowchart

which slightly extents and experiences a loss of tension force. Since the wire is mounted manually and for the purpose of having comparable measurements in the experiments, a sub-routine was implemented that moves the robots either closer or farther until they reach the optimal tension force  $T_{opt}$  already in the initial positions, which, according to the experimental set-up and various tests was set to 2.0 N (see Section 3.2.4). According to this movement, all poses on the paths are updated. After this sub-routine the fabrication process starts and the move commands are sent piecewise to both of the robots. This step by step sending of path information is handled within the **Server** module (see Section 3.1.5.4). In parallel, the **Fabrication** module enters the loop of reading the force values, calculating new speeds accordingly and sending them to the robots (see Fig. 3.16). This loop is performed

until the robots have processed all poses and enter the `READY_TO_PROGRAM` state. All data that was transmitted within the procedure is stored with their respective time-stamps and saved into a file with a unique identifier, which is used for later analysis.

While the above description of the fabrication process did just change slightly over the course of the development, the way of how the new speeds were calculated according to the force measurements, indicated as sub-process in Figure 3.16, changed indeed and is described below.

### 3.1.7 Feedback and feedforward

To reach a proper surface quality and to efficiently control the procedure it is necessary that the hot-wire is kept under a certain tension all along the cutting procedure, which, as stated above, was set to  $T_{opt}$  (optimal tension force). Rather than adaptively changing the path-curves or the heat input, which was postponed to further development (see Section 3.2.4), it was decided to control this tension by moving faster or slower on the respective path-curves. This implies that the individual speed for each pose has to be calculated according to the occurring cutting force, as speed and force are related to each other: moving with higher speed results in higher cutting forces, following higher tension (reaction) forces at the wire ends and conversely. However, since the calculation of optimal speeds in respect to the tension force depends on multiple variables (see Section 3.2.1) and couldn't be calculated with absolute precision, it was decided to regulate this relation over feedback. A control loop feedback mechanism commonly used in industrial control systems is a proportional–integral–derivative controller (PID controller). This controller continuously calculates an error value as the difference between a desired set-point and a measured process variable and applies a correction to the control variable based on proportional, integral, and derivative terms, respectively. The set-point in this case is the force measured in the beginning of the procedure (initial force), the measured

process variable is the tension force and the control variable is the speed (see Fig. 3.17).

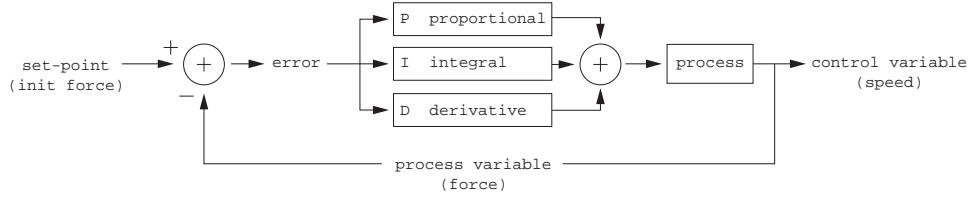


Fig. 3.17: Feedback control

However, the controller proved not to fit the application, despite various tests in alternating the proportional, integral and derivative coefficients. The output was oscillating (see Fig. 3.18) and caused deflections on the surface. The reason is that although the process variable should take about the set-point, the control variable, the speed, varies all along the process. Therefore, the controller would need different coefficients along one cutting procedure.

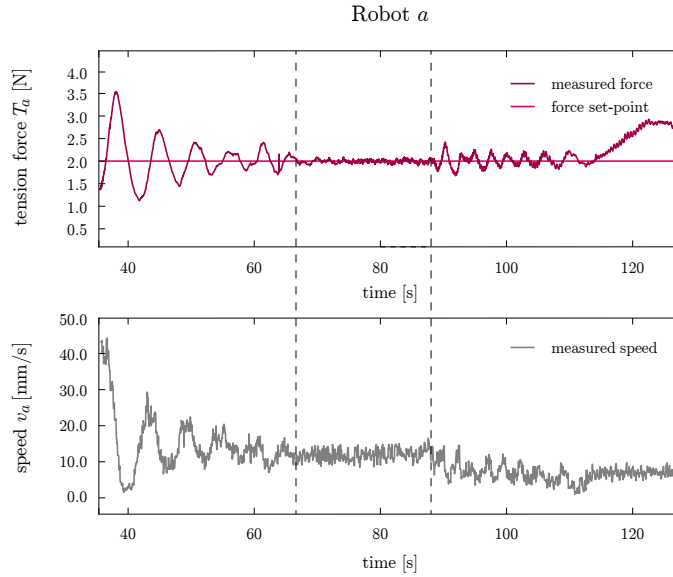


Fig. 3.18: Process data 151213\_03B15: In phases with constant speed, such as time stamp 66 to 88, the PID controller works fine, however the output is oscillating in phases in which the speed is decreasing

The logical consequence to reduce the oscillations was therefore to introduce a certain estimation of the optimal speed to reach the target tension force. Over the course of the development, the speed trajectories for the both robots could be more and more accurately calculated (see Section 3.3.4). These trajectories serve as input for the combined feedback-feedforward control (see

Fig. 3.19) to tare the speed according to the force measurement about this estimated speed. This combination was a big improvement to the adaptive control, see for example Figure 3.20, and its evaluation is further described in Section 3.4.2.

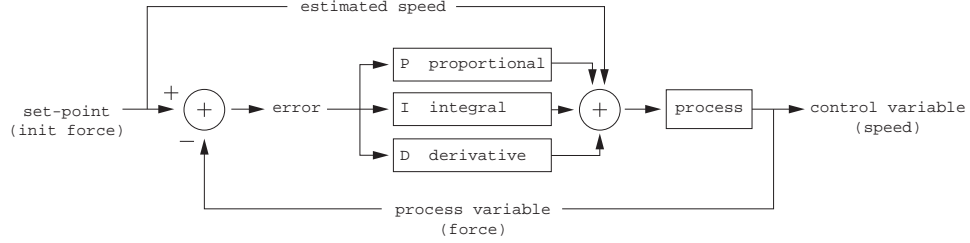


Fig. 3.19: Combined feedback and feedforward control

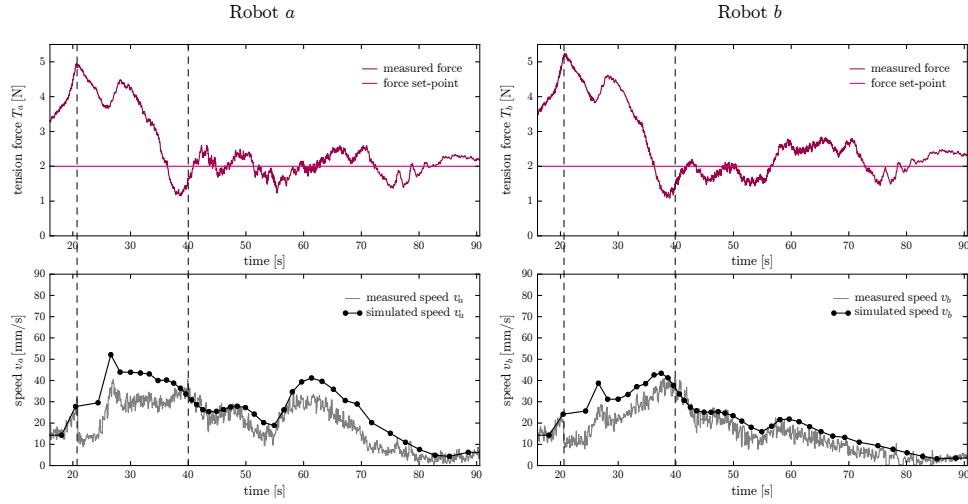


Fig. 3.20: Process data 160304\_B2140: The feedback-feedforward control starts approximately at time stamp 22. After a balancing phase, which approximately lasts till time stamp 40, the force measurements stay in a range of  $\pm 1$  N to the set-point and the speed measurements follow the simulated speed trajectory with no apparent oscillations.

## 3.2 Analysis and modelling of material behaviour

Computational modelling of the *Spatial Wire Cutting* process requires to considerate a large number of interacting variables. This chapter serves to identify them, define their operating range and the limits of the research's investigation. The knowledge of occurring physical entities and their interplay

was acquired empirically through repeated and systematic experiments. Although previous research (see Section 2.1.2) served as a good starting point, the *SWC* procedure has strong geometrical implications and therefore can only be understood with the complementary simulation. For this reason, the following documented estimation of process data, dependent on certain physical inputs, forms a basis for the design and simulation framework (see Section 3.3), which serves for further analysis.

### 3.2.1 Process description

In contrast to standard hot-wire cutting procedures, *Spatial Wire Cutting* operates in transition states between thermal cutting and thermo-mechanical cutting established through the interplay of velocity and heat, that generates gradual contacts along the hot-wire to the processed polystyrene and further gradual temperatures. This, in turn, creates variable forces that act contrary to the moving direction onto the hot-wire, which adapts its form accordingly. In order to control the process, it is requisite to understand how these forces, their magnitudes and directions, are induced and to comprehend the cutting mechanics. Initial cutting tests were performed to build a body of knowledge about the procedure and to characterize the interacting relationships between input parameters and process variables, as listed below.

Input parameters	Process variables
1. foam material	I. cutting speeds $v_i$
2. wire material	II. tension forces $T_a, T_b$
3. heat input $Q$	III. cutting forces $\mathbf{f}_i$
4. robotic path curves $\mathbf{P}_a, \mathbf{P}_b$	IV. engaged wire length $l_f$
	V. temperature gradient
	VI. kerf width
	VII. curve shape

#### 3.2.1.1 Input parameters

**1. Foam material.** The thermal behaviour of the thermoplastic foam influences the cutting process in virtually all aspects: It affects the amount

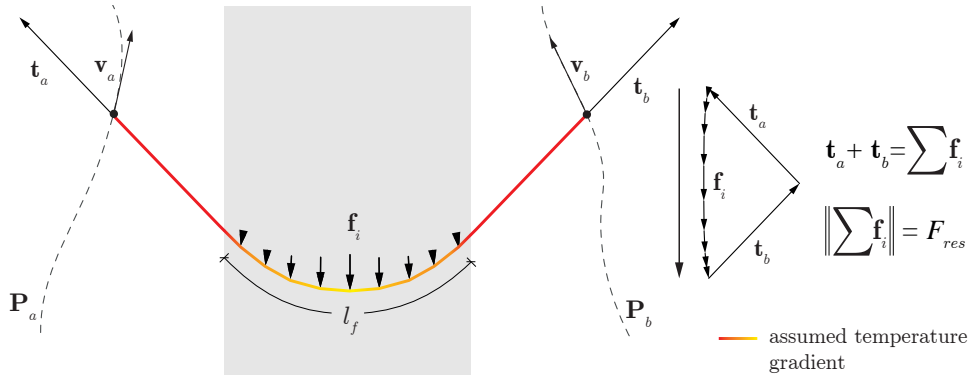


Fig. 3.21: Graphic of the hot-wire moving through in the foam block

of energy needed to melt it, the corresponding speed of the cutting medium that induces the cutting forces, etc. Additionally the dimensions of the foam block influence the engaged wire length  $l_f$ .

**2. Wire material.** The material, length  $l$  and diameter of the hot-wire determine its electrical resistance  $R$ . The wire material together with its temperature also influence the upper limit of the possible tension forces: too high forces will break the wire.

**3. Heat input.** The electric current  $I$  is defined by the voltage input  $U$  and the wire's resistance  $R$  through Ohm's law ( $I = \frac{U}{R}$ ). Joule heating is the process when electric current passes through a resistant material and releases heat. The heat input  $Q$  depends on the supplied current  $I$  and the electric resistance  $R$  of the hot-wire. It is defined by Joule's first law:  $Q = I^2 R$ .  $Q_l$  is the heat input per unit length of hot-wire and is calculated through  $Q_l = \frac{Q}{l}$ . The heat input is directly related to the overall temperature of the wire.

**4. Robotic path curves.** Amongst other variables, the path curves ( $\mathbf{P}_a$ ,  $\mathbf{P}_b$ ) mainly define the resulting geometry of the cut, as well as the curve shape, the direction of tension and cutting forces and the force distribution (see Section 3.3.3).

### 3.2.1.2 Process variables

**I. Cutting speeds.** The cutting speed is referring to the speed with which the wire moves through the foam. In *SWC* different segments along the wire can experience different cutting speeds  $v_i$  (more precisely: cutting velocities  $\mathbf{v}_i$ ) and are dependent on the velocities at the wire ends ( $\mathbf{v}_a, \mathbf{v}_b$ ) controlled by the robots and the wire's shape (see Fig. 3.21). The cutting speeds directly relate to the foam material, the temperature, the path curves, the tension and cutting forces and, amongst others, are constrained to the robotic joint acceleration limits.

**II. Tension forces.** The tension forces  $T_a$  and  $T_b$  at the respective wire ends are directly measured with the end-effector and are used as feedback signal for the adaptive robotic control. Together with the measured deflection from the mounting point ( $\alpha_a, \beta_a$ , resp.  $\alpha_b, \beta_b$ ), the tension force *vectors*  $\mathbf{t}_a$  and  $\mathbf{t}_b$  can be calculated, which have the same direction as the respective tangent at the wire's endpoints. The tension force vectors are the reaction forces to the acting cutting forces. With both tension force vectors the resulting cutting force  $F_{res}$  is calculated (see Fig. 3.22).

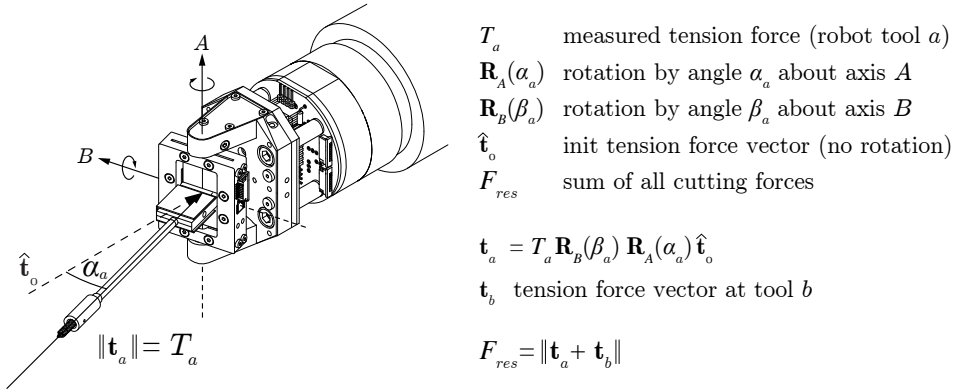


Fig. 3.22: Calculation of the tension force vector  $\mathbf{t}_a$  from the tool's measurements and calculation of the resulting cutting force  $F_{res}$  from tension force vectors  $\mathbf{t}_a$  and  $\mathbf{t}_b$  (from robot tool  $b$ )

**III. Cutting forces.** The resulting cutting force  $F_{res}$  is the magnitude of the sum of all cutting forces  $\mathbf{f}_i$  that act contrary to the moving direction of the hot-wire and can be calculated through the measured tension force



vectors (see Fig. 3.21). The cutting forces strongly depend on the foam material, the temperature gradient, the wire's shape, the path curves, the engaged wire length and the cutting velocities.

**IV. Engaged wire length.** The engaged wire length  $l_f$  is the amount of wire that is actually in the foam. As apparent in Figure 3.21, the wire is curved inside the foam, while it is straight outside. The engaged wire length depends therefore on the current curve shape and the path curves. With increasing engaged wire length, temperature decrease is assumed, which affects speed and force variables.

**V. Temperature gradient.** The electric energy is dissipated as thermal energy. A inverse relation is expected with the cutting forces. Since the *SWC* procedure operates between thermal and thermo-mechanical cutting, the hot-wire experiences differences in temperature, not only along the cut, but also along the engaged wire in the foam. Higher temperature is assumed at the exit zone of the wire from the foam [32] (see Fig. 3.21).

**VI. Kerf width.** The kerf width is dependent on the foam material, the speed and the heat input.

**VII. Curve shape.** The shape of the hot-wire curve as a multi-dimensional variable is dependent on all forces, respectively their directions and magnitudes, that acted upon the hot-wire from the beginning of the procedure to the current time stamp. Therefore the shape, and subsequently the cut surface, is dependent on all previously noted parameters and variables.

### 3.2.2 Thermo-mechanical mechanisms

Cutting tests performed with constant heat input and constant cutting speed revealed the characteristic cutting force profile curve [39, p. 123]. This profile exhibits the transient nature of hot-wire cutting and three different cutting stages (see Fig. 3.23): Shortly after entering the foam the wire is in an over-heated stage (stage 1), vaporising the foam ahead while advancing. Then it

cools and comes into a transitional phase (stage 2) until it enters the equilibrium stage (stage 3), or steady state *in which the thermal energy generated in the wire is balanced by the heat transferred from the wire into the surroundings* [39, p. 90]. Cutting force and the wire temperature are therefore approximately inversely related.

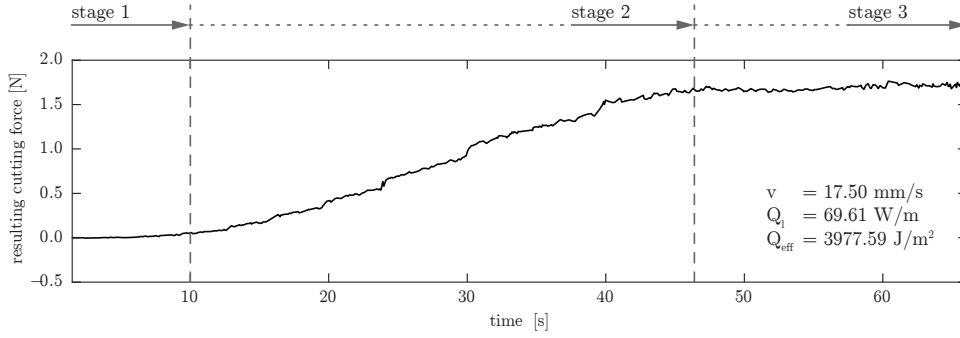


Fig. 3.23: Process data 150803\_D179F: Characteristic cutting force and cutting stages

According to Brooks [39, p. 19], this transient phenomenon also describes the thermo-mechanical mechanisms present in thermal plastic foam cutting, which can be separated into three main cutting modes and transitions between them (see Fig. 3.24):

- thermal cutting**      The foam is melted or vaporised ahead of the advancing heat source, there is no physical contact between wire and foam (see also Fig. 3.23, stage 1)
- thermo-mechanical**      The cutting element comes into contact with the foam and thus cuts via a combination of melting and shearing (see also Fig. 3.23, stage 3)
- mechanical cutting**      The temperature of the cutting element in relation to its velocity is too low

These cutting modes affect the kerf width and surface finish of the cut. While mechanical cutting results in ripped surfaces, purely thermal cut surfaces have a hard skin of relatively high density. The best surface finish however, can be achieved by low, but non-zero cutting forces, by thermo-mechanical

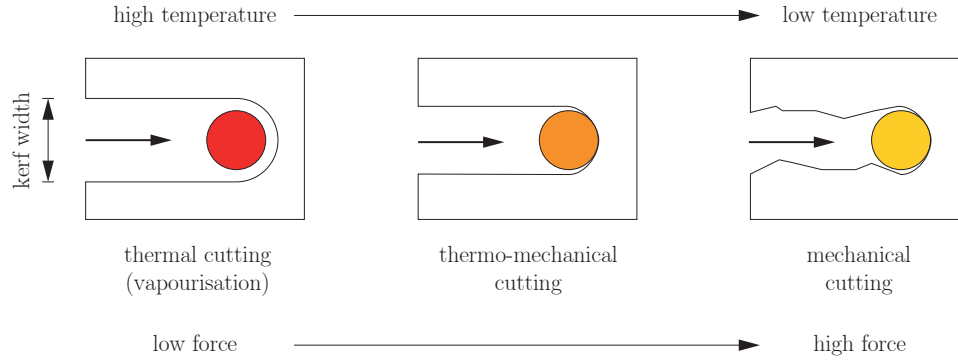


Fig. 3.24: Relationship between tool temperature and cutting force, cp. Brooks figure 1.18. [39]

cutting, being *the result of the wire dragging molten material into the recessed cell boundaries, smearing and smoothing the surface during the cut* [41, p. 12].

### 3.2.2.1 Effective heat input

The area specific effective heat input  $Q_{eff}$  was developed by Ahn et al. [31] and is a property that is calculated by dividing the normalized heat input  $Q_l$  by the speed  $v$  and has units  $J/m^2$ . Physically this value represents the amount of electrical or thermal energy used to create a unit area of cut surface. It is a very useful parameter as it allows a wide range of cutting data to be presented on a single graph. Ahn et al. [31] used  $Q_{eff}$  to observe how the kerf width changes with energy input (see Section 2.1.2.1), Brooks [39, p. 113] and Bain [41, p. 176] plotted the steady state cutting forces on a secondary axis to the effective heat input and observed that this relation follows an exponential trend, is related to the engaged wire length  $l_f$  and can be modelled for different foam materials and cutting tools. For the purpose of finding the material- and set-up specific coefficients for the exponential cutting force model, analogue tests have been performed and are illustrated below.

### 3.2.3 Cutting force model

The experimental set-up (see Section 3.1.2) was used to measure and log the tension force and the angles of cuts with various speed settings, heat inputs and engaged wire lengths (resp. foam block widths) while the robotic arms moved on parallel path curves, mainly inducing perpendicular forces on the wire. Each individual combination (see Table 3.1) produced a characteristic cutting force profile.

engaged wire length $l_f$ [mm]	voltage $V$ [V]	cutting speed $v = v_i$ [mm/s]
400, 500	43.5, 45.0, 46.5, 48.0, 49.5, 51.0, 52.5, 54.0, 55.5, 57.0, 58.5, 60.0, 61.5	12.5, 15.0, 17.5, 20.0, 22.5, 25.0, 27.5

Table 3.1: Input parameter values for developing the cutting force model

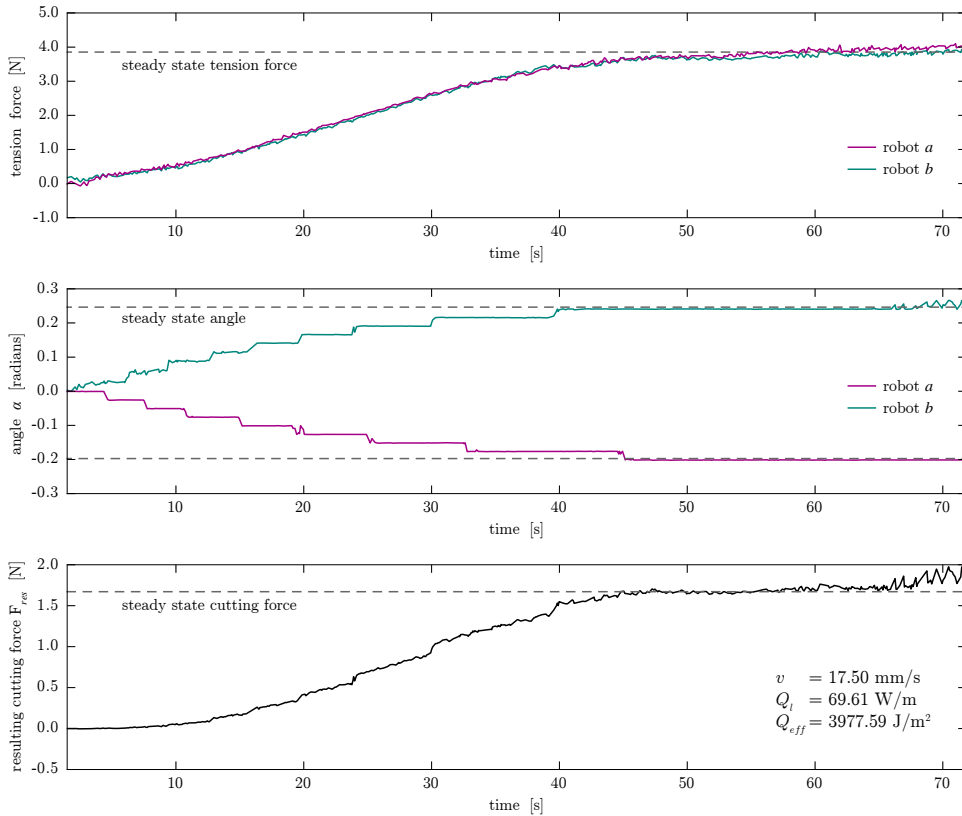


Fig. 3.25: Process data 150803\_D179F: From recorded tension forces and angles  $\alpha$ , the resulting cutting forces  $F_{res}$  were calculated and registered in the steady state

Through computing the histogram of the process data, the steady state for tension forces, angles and cutting forces was calculated (see Fig. 3.25, for an

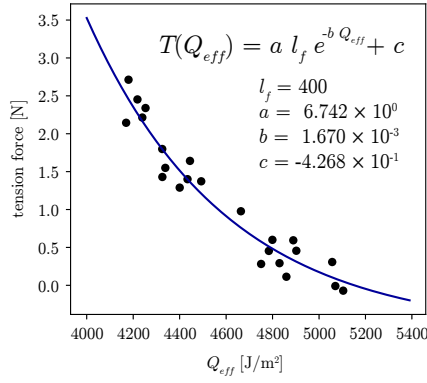


Fig. 3.26: Model of relation between  $Q_{eff}$  and the tension force  $T$  in the steady state for an engaged wire length of 400 mm.

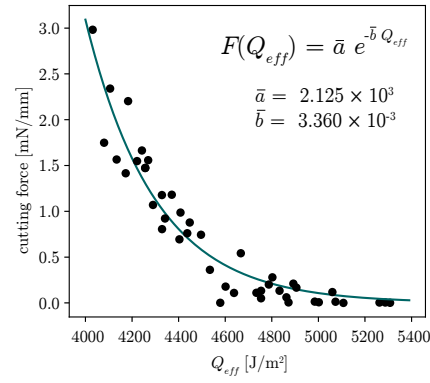


Fig. 3.27: Model of relation between  $Q_{eff}$  and the cutting force  $F$  in the steady state per unit of engaged wire length

overview of results see Appendix B.1). Figure 3.26 shows the steady state tension force  $T$  for an engaged wire length of 400 mm and Figure 3.27 shows the steady state cutting force  $F$  per unit of engaged wire length plotted against the effective heat input for several cutting tests, clearly indicating an exponential decay of force with increasing  $Q_{eff}$ . Model fitting was used to find the coefficients  $(\bar{a}, \bar{b})$  and to fit the data into an exponential model, which allowed to estimate the occurring cutting force according to given  $Q_{eff}$  settings.

$$F(Q_{eff}) = \bar{a} e^{-\bar{b} Q_{eff}} \quad (3.1)$$

or, splitting  $Q_{eff}$  into speed  $v$  and heat input  $Q_l$ , such as

$$F(v, Q_l) = \bar{a} e^{-\bar{b} \frac{Q_l}{v}} \quad (3.2)$$

### 3.2.4 Operating ranges and scope definition

On basis of the described tests, it was concluded that for the experimental set-up, in respect to the chosen hot-wire and foam material, the optimal effective heat input  $Q_{eff}$  ranges from 4400 to 6000 J/m². The lower limit is defined by the tension force of 3.4 N which still provides a buffer until the wire breaks. The upper limit is defined by the cutting force, which can be low, but not zero. This  $Q_{eff}$  range subsequently specifies the cutting speed

range (12 to 25 mm/s) (for cutting speeds of wire segments in the foam) and heat input per unit length of hot-wire  $Q_l$  (66 to 110 W/m). The optimal tension force  $T_{opt}$  was set to 2.0 N, since a certain minimal tension in the wire has to be kept throughout the cutting process. This is necessary to achieve a corresponding surface quality and, ultimately, to efficiently control the procedure (see Fig. 3.29).

The tests also served to define several process constraints and the limits of the research's investigation in respect to available resources.

- The temperature of the wire can be controlled by both the cutting speed and the heat input. However, for further tests it was decided to keep the heat input constant, just modulate the cutting speed and postpone the investigation of this relation for further development.
- The tension of the wire can be controlled by the robots' speeds, the heat input and the path curves. For further tests it was decided to adaptively control the speed, but postpone the investigation into adaptively changing path-curves or heat input for further development.
- The path curves are divided into the same amount of positions (poses) (see Section 3.3.5). The robots are synchronized at these positions, which may not produce the optimal tension at both wire ends and subsequently the optimal speed trajectory, however, facilitated control of the geometry was assumed (see Fig. 3.28).
- Thermo-mechanical cutting produces small kerf widths (in these tests  $< 2$  mm), therefore the kerf width is not considered in further calculations.
- Rather than keeping a constant sum of cutting forces, a constant tension force is targeted, which may produce different surface qualities on one cut, however the differences are negligible.
- The most beneficial variable to capture would be the temperature along the wire in the foam, but with the experimental set-up and devices it

was not measurable. However, the electric resistance of the wire is related to the temperature and is logged.

- The joint acceleration limits are not taken into account for speed calculations. This is postponed for further development.
- In the cutting procedure, the wire experiences slight expansion or contraction through temperature changes. However, this was considered not relevant for the investigation.



*Fig. 3.28: Cutting example with inadequate relation between left and right path-positions in the beginning: high force on left (top in picture) side controls the speed, while the wire at the right (bottom in picture) side melts the foam, since it is moving too slow. Additionally oscillation errors occur (see Section 3.4.1)*



*Fig. 3.29: Cutting tests, in which the tension was not at a constant level, leading the material to melt. The resulting surface pattern clearly exhibits the wire's traces, however is hardly controllable*



*Fig. 3.30: Cutting example in which through joint acceleration limits the tension force could not successfully be targeted resulting into melted material*

### 3.3 Design and simulation framework

Building upon the simplified physical behaviour, as described in the previous Section 3.2, this sub-chapter describes the design and simulation framework, which was successively developed to provide an interface for the design of *SWC* surfaces, produced with the adaptive robotic control. The main inputs for the fabrication procedure (see Section 3.1.6), are the path curves for the robotic arms (along with the robot's speed trajectories and the heat input of the wire), respectively their positions along that curves, that have to be reached at the same moment in time (see Fig. 3.31). The non-transparent relationship between these path-positions and the resulting physical cut surface is resolved by the developed simulation framework, that anticipates the wire's deformation within the material (see Fig. 3.32). As such, it is not only employed to virtually represent but also to provide information about the design's feasibility. The generated surfaces belong to a particular vocabulary of double-curved surfaces: sweep surfaces, which can be defined by the motion of a changing profile curve along two guide curves. In order to design with this constrained geometrical vocabulary, design and simulation were integrated. Additionally to the geometry, the simulation emulates fabrication variables, such as robots' speeds. With advancing development this estimation of variables was employed to improve the fabrication control.

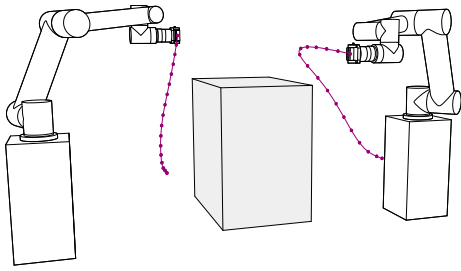


Fig. 3.31: Path curves, synchronized positions on the curves and foam block [12]

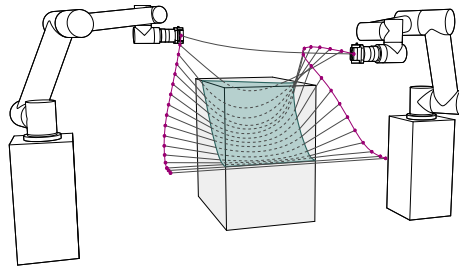


Fig. 3.32: Simulated hot-wire curves and lofted surface thereof [12]

Over the course of development different simulation strategies have been explored, for example, approximating the wire curve with particle/spring simulation or applying the library ShapeOp<sup>16</sup>. These strategies were not



continued, since the non-linear *Force Density Method*, as explained hereafter, proved to fit the requirements best. Generally, the development of the simulation can be divided into two stages, first without, and later with the integration of the force distribution equation 3.7. Without the equation, the forces were assumed with equal magnitudes. The simulation strategy, which was pursued and elaborated, is described on the following pages and starts with the investigation of one individual wire shape.

### 3.3.1 Wire shape calculation

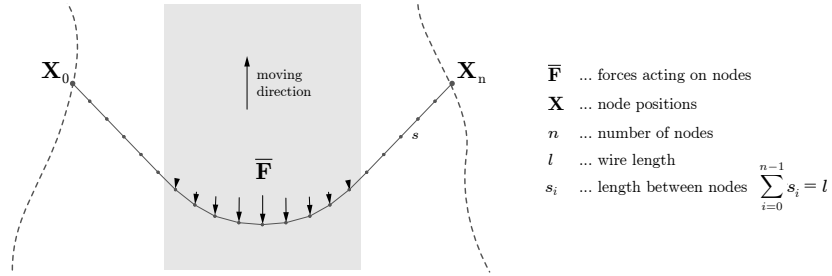


Fig. 3.33: Computational wire representation

Computationally the shape of the wire with length  $l$  is represented with discrete  $n$  nodes (node index  $i$ ) and  $n-1$  segments, with constant segment length  $s$  ( $= s_i$ ) between the nodes (see Fig. 3.33) [109]. Since in the *SWC* process the form of the wire and the acting forces on it are mutually depended, generating transitory equilibrium states along the cutting trajectory, the *Force Density Method* [82, 83] is applied to approximate its form: The two end-points of the wire are set to fixed nodes  $n_f$  with known positions  $\mathbf{X}_f$ . With the known connectivity matrix  $\mathbf{C}$  ( $= [\mathbf{C}_u, \mathbf{C}_f]$ ) and according to applied forces  $\bar{\mathbf{F}}$  [ $n \times 3$ ], we search for a vector  $\mathbf{q}$  of force densities, so that the length between each individual node matches the segment length  $s$ , equivalent to finding the unknown positions  $\mathbf{X}_u$  of the free nodes  $n_u$  [109]. An iterative approach is applied to find the target force densities [110]. We estimate a starting vector  $\mathbf{q}_0$  (diagonal matrix  $\mathbf{Q}_0$ ) and solve the equation in 3.5 for the

unknown positions  $\mathbf{X}_{u0}$  [109]

$$\mathbf{D}_u = \mathbf{C}_u^T \mathbf{Q}_0 \mathbf{C}_u \quad (3.3)$$

$$\mathbf{D}_f = \mathbf{C}_f^T \mathbf{Q}_0 \mathbf{C}_f \quad (3.4)$$

$$\mathbf{D}_u \mathbf{X}_{u0} = \bar{\mathbf{F}}_u - \mathbf{D}_f \mathbf{X}_f \quad (3.5)$$

$$\mathbf{q}_{k+1} = \mathbf{Q}_k \mathbf{S}^{-1} \mathbf{p}_k \quad (3.6)$$

Then we calculate the edge length vector  $\mathbf{p}_k$  according to  $\mathbf{X}_0$  ( $= [\mathbf{X}_{u0}, \mathbf{X}_f]$ ) and estimate the next force density vector  $\mathbf{q}_{k+1}$  with 3.6, which is again inserted into equations 3.3 and 3.4 as diagonal matrix  $\mathbf{Q}_{k+1}$ . We solve the linear system in 3.5 to calculate the new coordinates  $\mathbf{X}_{k+1}$ . This procedure is continued until the sum of all edge lengths matches the wire length  $l$  up to a certain tolerance [109].

This form-finding approach delivered quick results and proved to meet the requirements for an interactive design and simulation tool, however transferred the problem of calculating the wire shape towards calculating the forces that shape the wire. Therefore, experiments have been performed to analyse the actual physical shape of the wire and investigate how the forces  $\bar{\mathbf{F}}$  have to be distributed so that calculated and physical shape match.

### 3.3.2 Physical wire shape

With the experimental set-up and sensor equipment, it is not possible to track the process inside the foam block, especially not the deformation of the wire. The only indication of its form are the tension force vectors, as the tangents at the end points of the wire and the sum of which are the sum of all forces acting on the wire.

A series of cutting tests have been performed with different foam block widths, different heat inputs (see Table 3.2) and different path curves, generating different wire shapes. The purpose of these tests was

- to analyse the physical shape of the wire and its deformation, and investigate how the input of the shape calculation in 3.3.1 relates to the physical shape,
- to develop a method for estimating the forces (see Section 3.3.3) and
- to test the developed simulation model in comparing process- and simulated data (see Section 3.4.1).

In the cutting procedure, force-feedback control (see Section 3.1.7) was used, to keep the optimal tension force  $T_{opt}$  and adjust the speeds accordingly. This setting was chosen to constrain the range of investigation specifically to the selected tension force. Within the process the *Control Core* logged the robots' positions together with the respective measurements from both of the end-effectors (angles and forces). The robots' path curves were designed in such a way that all positions lay in the same horizontal plane but have different distances to each other, constraining also the force directions to lay in one plane. After the cut, to uncover the wire's shape from the cut surface, it was illuminated from two sloped angles and the distortion of the taken pictures was reversed (see Fig. 3.34).

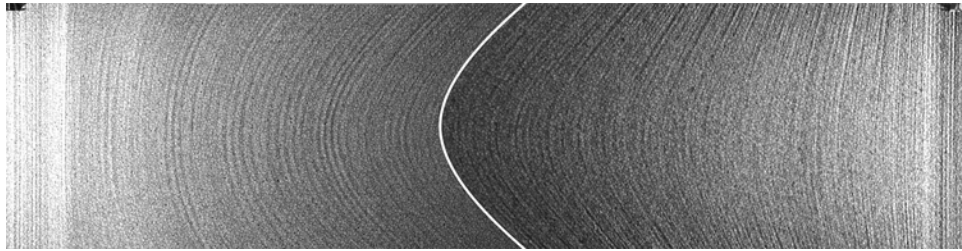


*Fig. 3.34: Photos from the cut surface. The wire's traces cannot be scanned, however are visible with inclined light incidence*

In the experiments symmetric and asymmetric path curves were used to produce different wire deformations and to generate different phases that are of interest to the analysis, due to expected distinctive differences in the force distribution:

- a) Entry phase: the wire starts straight but the wire's endpoints are continuously moving towards each other, expecting higher forces at

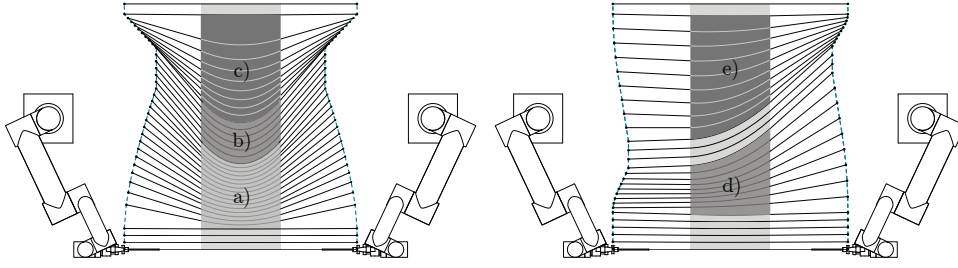


Fig. 3.35: Topview of symmetric and asymmetric path curves with phases a) to e)

outer zones, than in the center.

- b) Steady phase: the wire keeps its shape and the endpoints of the wire are moving parallel to each other, expecting little differences in the force distribution along the wire.
- c) Exit phase: the endpoints of the wire move off each other, expecting higher forces in the center than in the outer zones.
- d), e) Phases with asymmetric force distribution along the wire, expecting higher forces on one side than the other.

foam block widths [mm]	heat inputs $Q_l$ [W/m]	deflection $\alpha$ in the steady phase [radians]
300, 400, 500	50, 58, 67, 76, 85	0.30, 0.48, 0.58, 0.68, 0.78, 0.86

Table 3.2: Input parameter values for the symmetric path curves

### 3.3.2.1 Force magnitudes and shape comparison

For the purpose of finding a first estimation of forces, the recorded tension force vectors with their respective recorded positions and the surface's picture were visualised. On several positions along the path curves the force magnitude distributions for the nodes in foam were estimated by a graph (see Fig. 3.36, 1.) and adjusted until they fulfilled the tension force vector (see Fig. 3.36, 3.) and the wire pattern visible on the surface (see Fig. 3.36, 2.).

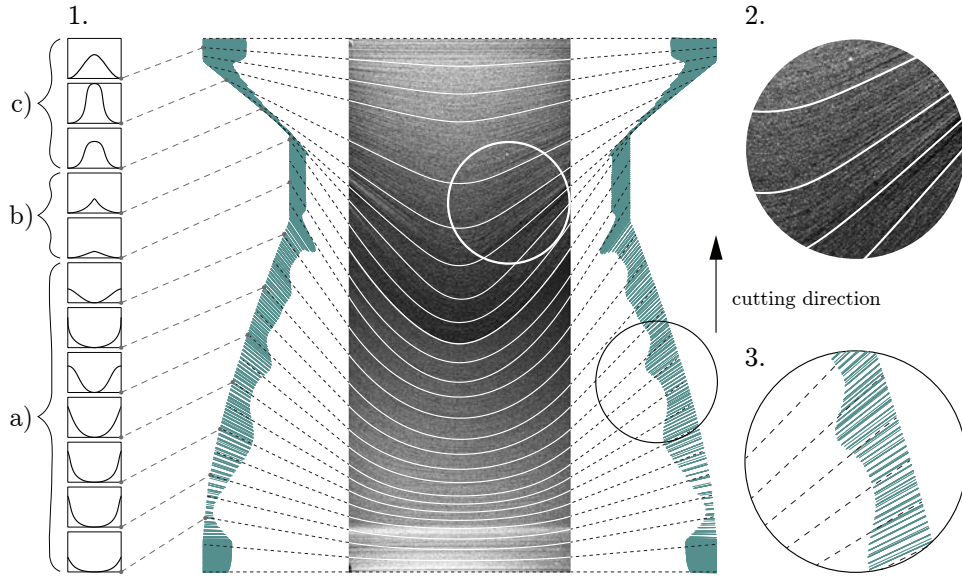


Fig. 3.36: 1. Defined mapping curves for the force distribution, 2. overlay of wire shape and surface picture, 3. overlay of recorded tension force vector and wire shape

As expected, the modelled forces exhibited a transition along the cut, which is connected to the different speeds along the wire: In the entry phase a) the wire segments at the exit zones of the foam have to move faster than in the center, resulting in higher forces, while in phase b) little differences in the force distribution are visible and in the exit phase c) the reversed picture to the entry phase is visible, where the wire segments at the exit zones move slower than in the center, resulting in lower forces at the exit zones than in the center. Low forces can also be recognized on the physical cut surface, e.g. in the detail picture of Figure 3.36, 2.: low or zero force means thermal cutting, melting more material and producing more rills.

On basis of this observations, the following force distribution equation was developed, which calculates the forces acting on the wire at one moment in time.

### 3.3.3 Force distribution

The wire, represented by  $n$  nodes, is experiencing different forces on every node  $i$ , which is in the foam. Nodes outside of the foam have zero vectors. The force  $\mathbf{f}_i$ , which is inversely related to the temperature, acting on one node

$i$ , is dependent on the actual shape of the wire, respectively the tangent  $\hat{\mathbf{t}}_i$  (tangent at node  $i$ ), the force direction  $\hat{\mathbf{f}}_i$ , the speed  $v_i$  and the heat input  $Q_l$  and is estimated as follows [109]

$$\mathbf{f}_i = F(v_i, Q_l) s_i \left\| \hat{\mathbf{t}}_i \times \hat{\mathbf{f}}_i \right\| \hat{\mathbf{f}}_i \quad (3.7)$$

where  $F(v_i, Q_l)$  is the force [N/mm] acting perpendicular to the engaged wire length according to equation 3.2,  $s_i$  the segment length, and  $\left\| \hat{\mathbf{t}}_i \times \hat{\mathbf{f}}_i \right\|$  a ratio between 0 and 1 depending on the angle between  $\hat{\mathbf{f}}_i$  and the node tangent  $\hat{\mathbf{t}}_i$ .

Since higher temperature is assumed at the exit zones of the wire from the foam [32, p. 1449], an linear falloff of the force magnitudes is estimated at arbitrary 30 mm before the exit of the hot-wire<sup>17</sup>. Thus, all  $\mathbf{f}_i$  acting on nodes, which match this assumption, are additionally scaled.

Since the target tension force in the endpoints of the wire with tangents  $\hat{\mathbf{t}}_0$  and  $\hat{\mathbf{t}}_{n-1}$  is constrained to the optimal tension force  $T_{opt}$ , the resultant cutting force  $F_{res}$ , which is the magnitude of the sum of all force vectors from equation 3.7 should comply [109]

$$F_{res} = \left\| \sum_{i=0}^{n-1} \mathbf{f}_i \right\| = T_{opt} \left\| \hat{\mathbf{t}}_0 + \hat{\mathbf{t}}_{n-1} \right\| \quad (3.8)$$

As such, with given wire shape, and force directions, it is possible to calculate the necessary speeds  $v_i$ , so that the wire experiences  $T_{opt}$  at both of the wire ends. The evaluation and validation of this force distribution is summed up in Section 3.4.1.

### 3.3.4 Simulation model

The dynamic system of the moving wire through the foam has boundary conditions such as path-positions  $\mathbf{P}_a$ ,  $\mathbf{P}_b$  (for robots  $a$ ,  $b$ ), size and position of the foam block as a volume, and a defined heat input  $Q_l$  [109]. The forces  $\mathbf{F}$  (= matrix of all  $\mathbf{f}_i$ ) from the force distribution equation 3.7 are the forces

that act at a certain moment  $t$  on the wire. The shape however, depends on the dynamic forces, thus the transient behaviour of the wire. The total forces  $\bar{\mathbf{F}}$  (see Section 3.3.1) we need to compute the shape, originate from all forces that have occurred since the entry of the wire into the foam at  $t_0$  to the current time-stamp  $t_j$  and are therefore numerically integrated over time [109]. We use a combination of the explicit Euler method with the trapezoidal rule and the predictor – corrector method (Heun’s method) for the integration. With constant  $Q_l$ , the forces  $\mathbf{F}$  are a function of the shape  $\mathbf{X}$  and the speeds  $\mathbf{v}$ ,  $\mathbf{F} = \mathbf{F}(\mathbf{v}, \mathbf{X})$  (cp. 3.7) acting at time  $t_j$ . We denote the step size with  $h_j$  and initial forces with  $\bar{\mathbf{F}}_0 = \mathbf{F}(t_0, \mathbf{X}_0)$ . Starting from the current forces  $\bar{\mathbf{F}}_j$ , in the predictor step the next forces  $\tilde{\mathbf{F}}_{j+1}$  are estimated with the Euler method [109],

$$\tilde{\mathbf{F}}_{j+1} = \bar{\mathbf{F}}_j + h_j \mathbf{F}(\mathbf{v}_j, \mathbf{X}_j) \quad (3.9)$$

which are used to calculate the shape  $\tilde{\mathbf{X}}_{j+1}$ , as described in Section 3.3.1. This initial guess is improved in the corrector step by using the trapezoidal rule,

$$\bar{\mathbf{F}}_{j+1} = \bar{\mathbf{F}}_j + \frac{1}{2} h_j (\mathbf{F}(\mathbf{v}_j, \mathbf{X}_j) + \mathbf{F}(\tilde{\mathbf{v}}_{j+1}, \tilde{\mathbf{X}}_{j+1})) \quad (3.10)$$

and with the forces  $\bar{\mathbf{F}}_{j+1}$  the shape  $\mathbf{X}_{j+1}$  is calculated. In each iteration step we estimate the speed  $\tilde{v}_{ij+1}$  for one node  $i$  through  $r\tilde{d}_{ij+1}$  ( $r$  factor, distances  $\tilde{d}_{ij+1} = \|\mathbf{X}_{ij} - \tilde{\mathbf{X}}_{ij+1}\|$ ,  $\mathbf{X}_{ij}$  position of node  $i$  at iteration step  $j$ ). We apply the secant method to find the factor  $r$  and the root to the non-linear equation 3.11. As such, the sum of  $\mathbf{F}(\tilde{\mathbf{v}}_{j+1}, \tilde{\mathbf{X}}_{j+1})$  acting in the moment  $t_{j+1}$  satisfy equation 3.8 [109].

$$g(r) = \left\| \sum_{i=0}^{n-1} F(r\tilde{d}_{ij+1}, Q_l) s_i \left\| \hat{\mathbf{t}}_i \times \hat{\mathbf{f}}_i \right\| \hat{\mathbf{f}}_i \right\| - T_{opt} \|\hat{\mathbf{t}}_0 + \hat{\mathbf{t}}_{n-1}\| = 0 \quad (3.11)$$

We calculate the step size  $h_j$  based on the solution  $r$  ( $h_j = d_{ij}/v_{ij}$ ), as the

time between two iteration steps. Then we downscale  $\bar{\mathbf{F}}_{j+1}$ , so that equation 3.8 is satisfied and multiply the forces by  $h_j$ . This is necessary since the relation to the new force vectors  $h_{j+1}\mathbf{F}(\mathbf{v}_{j+1}, \mathbf{X}_{j+1})$  in the next iteration step wouldn't correspond otherwise [109].

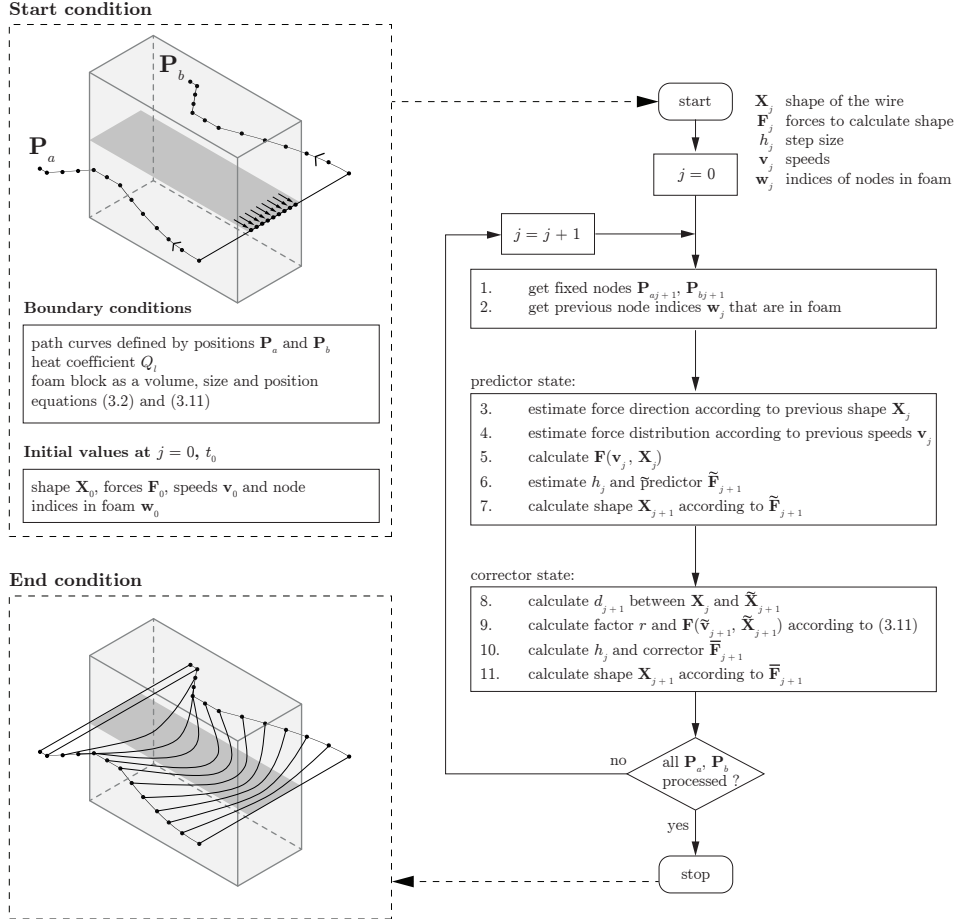


Fig. 3.37: Schematic of the simulation algorithm for one iteration step [109]

The inputs for the simulation are defined in the computational design tool-kit in McNeel's Rhinoceros 3D Grasshopper, but the described calculation, due to performance issues, is performed in Python running outside of Grasshopper utilizing libraries NumPy and SciPy<sup>18</sup>. Results from the simulation are again visualized in Grasshopper and include:

- node positions  $\mathbf{X}_{ij}$  of the discretized wire, from which NURBS curves are created. Additionally, the wire's deflection about the mounting points, resp. the estimated angles for the cardan joint end-effector are calculated (see Fig. 3.38, 1.).



- force vectors  $\mathbf{f}_{ij}$  for each of the node positions. The force magnitudes can be displayed in color for analysing the surface (see Fig. 3.38, 2.).
- speed values  $v_{ij}$  for each of the node positions, therefore also for the outer nodes, representing the robots' end-effector speeds ( $\mathbf{v}_a$ ,  $\mathbf{v}_b$  = estimated speed trajectories) The speed values can also be displayed in color for analysing the surface (see Fig. 3.38).

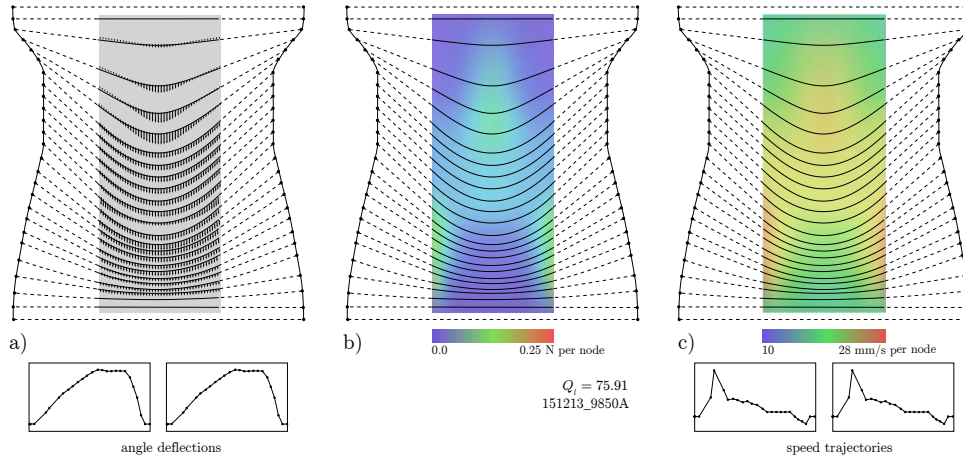


Fig. 3.38: Results from the simulation a) NURBS curves, force vectors at nodes and estimated deflection angles below, b) force magnitude color mapping onto the surface, c) speed value color mapping and speed trajectories below

#### 3.3.4.1 Force magnitude analysis

The force magnitude colouring, as result from the simulation, contributes to an understanding of what happens inside the foam block. It can be applied to reflect on critical phases (e.g. too big difference in high and low forces) and to make further assumptions about the procedure's scope. The Figure in 3.39 shows the results of five simulations, where each had the same boundary conditions except for the heat input. The forces are almost equally calculated, while the speed values increase with increasing heat input  $Q_l$ . Therefore, it can be recognised that within this experimental range, different  $Q_l$  settings may not change the wire shape drastically, which is also visible in the constant angular measurements as in Figures 3.44 and 3.45. Exceptions are path curves with high curvature in their speed trajectory: high heat input

will require higher speed to keep  $T_{opt}$ , which may lead to joint acceleration problems.

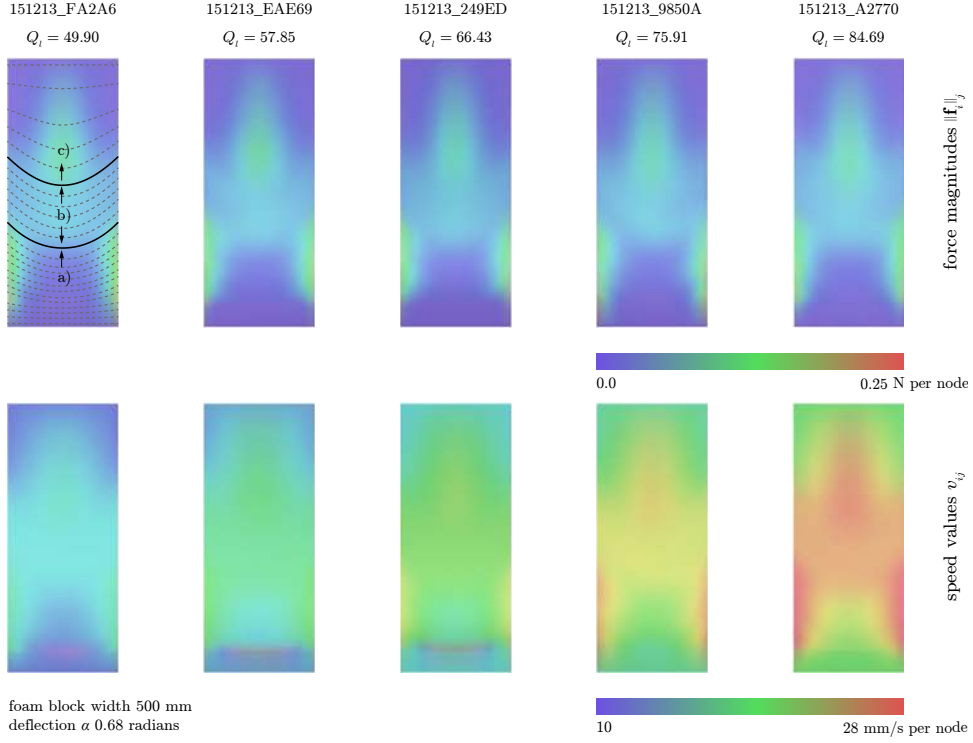


Fig. 3.39: Force magnitudes and speed values of the nodes mapped to color value and displayed on the surface

### 3.3.5 Design tool

Although the simulation generates results from given path-curves and step by step helps to develop an understanding about the process, designing those path-curves is counter-intuitive, especially if they are not planar. Not only different path-curves change the result, but different distributions of the synchronized positions on the curves change it. For example, all positions have to have less or equal distance than the first two positions, since the wire cannot extend. Another geometrical constraint is in the entry phase: if the robots approach each other too fast, the wire will not move in the center of the foam block, as indicated in the preliminary simulation with overlapping path curves (see Fig. 3.40). If the relation of the distance between two positions of the path curves differs too much, high force differences on

the opposite exit faces of the block occur, melting material on one side and exhibiting low temperature on the other.

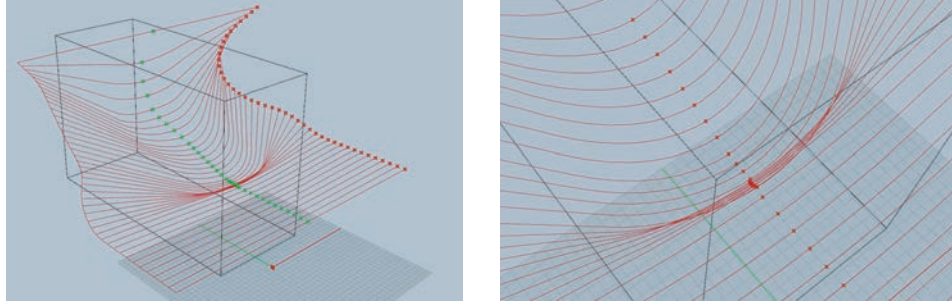


Fig. 3.40: Preliminary simulation: overlapping curves in the entry phase

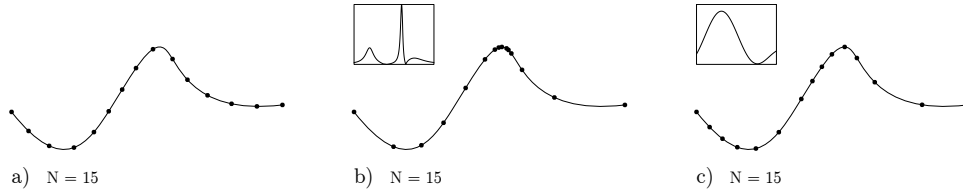


Fig. 3.41: Curve division a) by length, b) by curvature, or c) by arbitrary mapping

Therefore, the initial simulation set-up was altered to facilitate designing the *SWC* surfaces: Instead of modelling the path curves, edge curves on surfaces of the foam block are designed, which are discretized into an equal number of points, which distribution can additionally be chosen (see Fig. 3.41). Further, a function is created (a planar curve), that defines the additional length of wire to the distance between the points  $\mathbf{P}_{aj}$  and  $\mathbf{P}_{bj}$  (see Fig. 3.42, a.). In contrast to the simulation described in 3.3.4, this simulation calculates the forces for nodes that are constantly in the foam, and the fixed nodes are the defined positions on the edge curves. Since the length of the curve from one iteration step to the other changes, the nodes and their forces have to be redistributed. After all node positions have been calculated and NURBS curves have been created, a surface is lofted through the curves (see Fig. 3.42, b.). To generate the path-positions  $\mathbf{P}_a$  and  $\mathbf{P}_b$ , a minimum distance to the foam block is defined (keeping space for the tool handle) and the simulated curves are tangentially extended in such a way that all curves have the same length (see Fig. 3.42, c)).

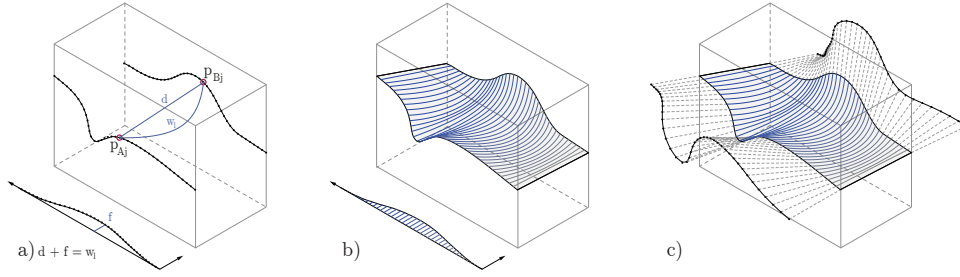


Fig. 3.42: a) Edge curves, distribution of positions and wire length extension function, b) simulated curves and lofted surface thereof, c) tangential extension of curve to calculate path curves [109]

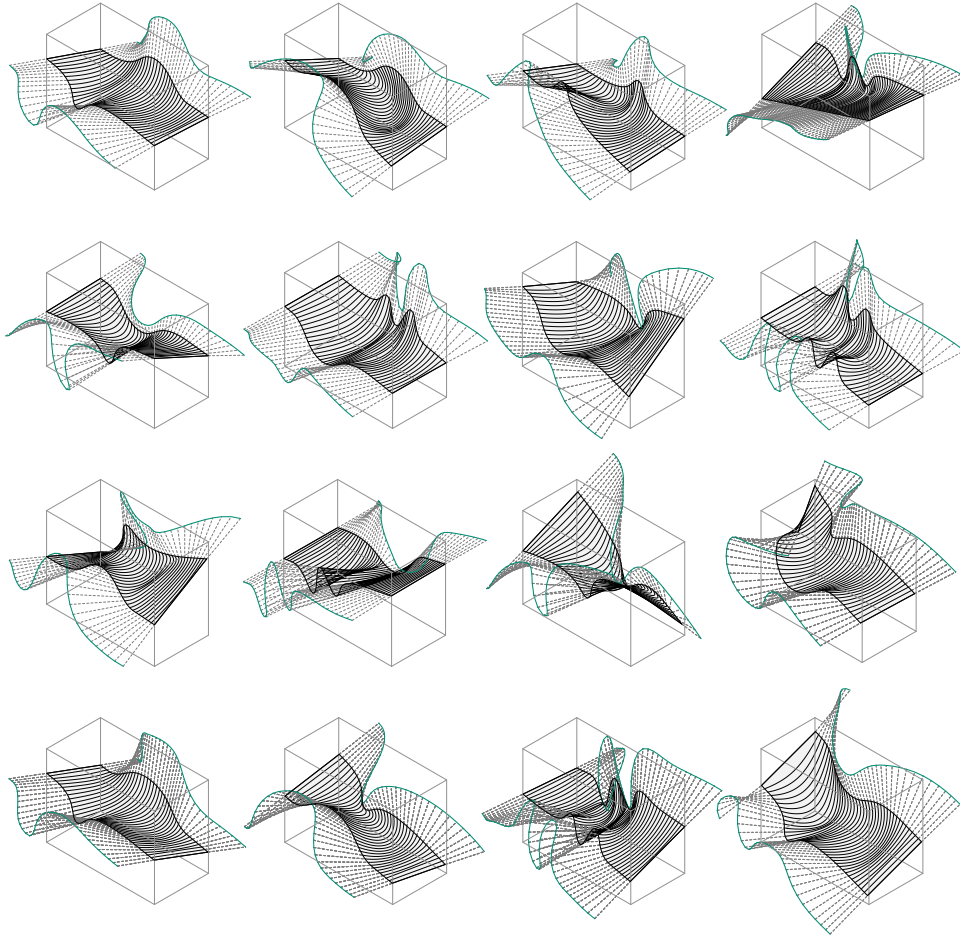


Fig. 3.43: Multiple simulated surfaces, with randomly created edge-curve pairs as inputs (curves differing in amplitude, frequency, rotation)

This simulation set-up allows to explore the geometrical solution range (see Fig. 3.43) and solved some issues encountered in the early design set-ups, for example in the elective course *Spatial Wire Cutting* (see Section 4.1). The function that defines the additional length allows to design smooth transitions for different phases and thereby omits erroneous results in the first place.

This design- and simulation framework was further empirically tested and validated in the Summerschool 2015 (see Section 4.2), a two-week design and building workshop with students, the two-day AAG Workshop 2016 (see Appendix A) and applied to design six surfaces for the comparative studies (see Section 3.4.2). These studies served to validate the overall integration of the design and simulation framework with the combined feedforward-feedback control and the repeatability of the process.

### 3.4 Validation of developed techniques

This section focuses on the evaluation and validation of the developed techniques documented in the previous sections in regards to the predictability and reproducibility of the physical process by means of the simulation framework and the adaptive control software. Over the course of development two series of cutting studies have been conducted that focused on the comparison between computationally calculated process data and the actual measurements from the physical process. The first comparative studies (see Section 3.4.1) served to validate the developed force distribution equation and the second comparative studies (see Section 3.4.2) focused on analysing the deviation between simulated surface and physical artefact. In the following they are described and discussed.

#### 3.4.1 Comparative studies N°1

Following the analysis of the physical wire shape (see Section 3.3.2) and the subsequent development of the force-distribution equation (see Section 3.3.3), the carried out tests with varying boundary conditions, such as path-curves and heat-inputs (see Table 3.2), have also been used to validate the force-distribution equation 3.7 and the simulation framework. The calculated wire curves and simulated process variables were compared to the measured data from its respective physical counterpart in phases a) to e) (see Fig. 3.35). The phases were selected for investigation due to expected distinctive

differences in the force distribution. The experiments have been performed with feedback-control only.

### 3.4.1.1 Process data comparison

The estimated speed trajectories and estimated cardan joint angles from the simulation (see Fig. 3.38), were overlaid in a graph to the measured speeds and the tools' measured angles (resp. just angles  $\alpha_a$  and  $\alpha_b$ , since angles  $\beta_a, \beta_b$  stayed constant) at their respective positions along the path (see Fig. 3.44).

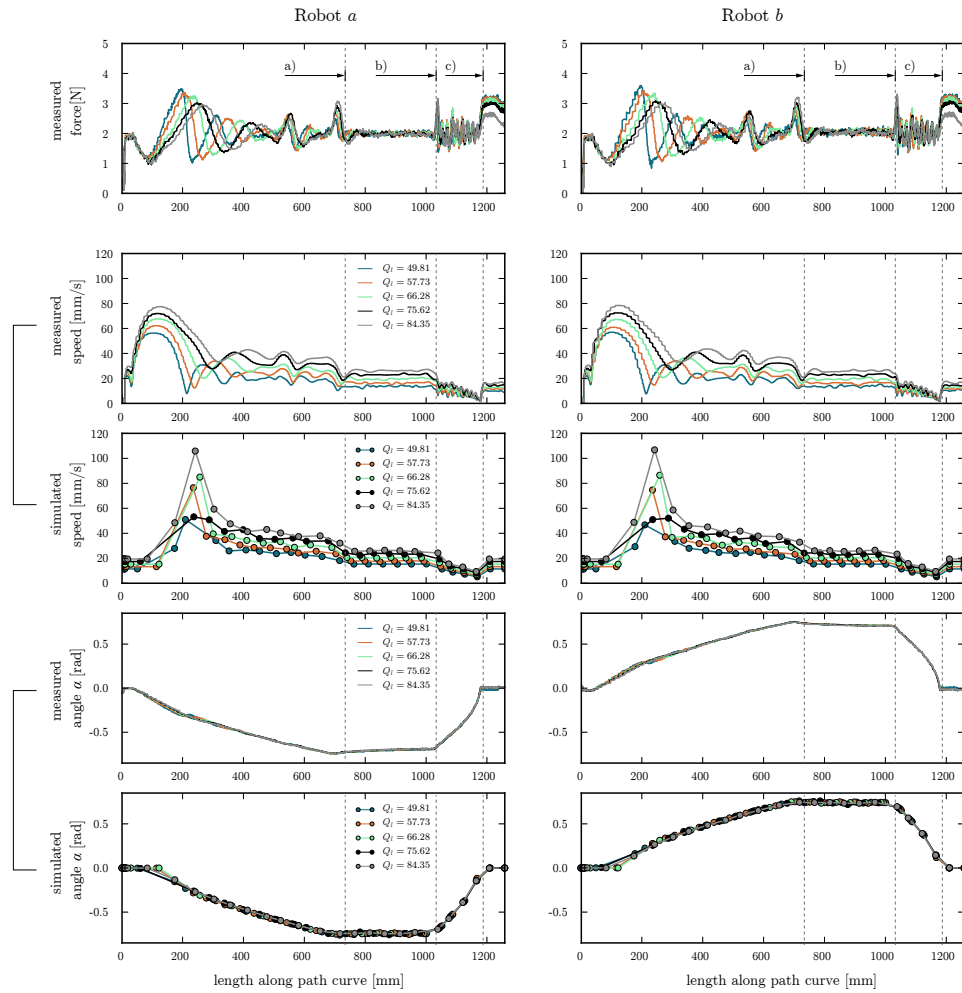


Fig. 3.44: Measured and simulated (dotted) process data (speed and deflection angle) from five cutting tests with different heat inputs  $Q_l$ , but the same symmetric path curves. Phases a), b) and c) are indicated

However, since the measured data was oscillating in the entry phase a) (see Fig. 3.44) and as well in phase d) (see Fig. 3.45) due to the force-feedback

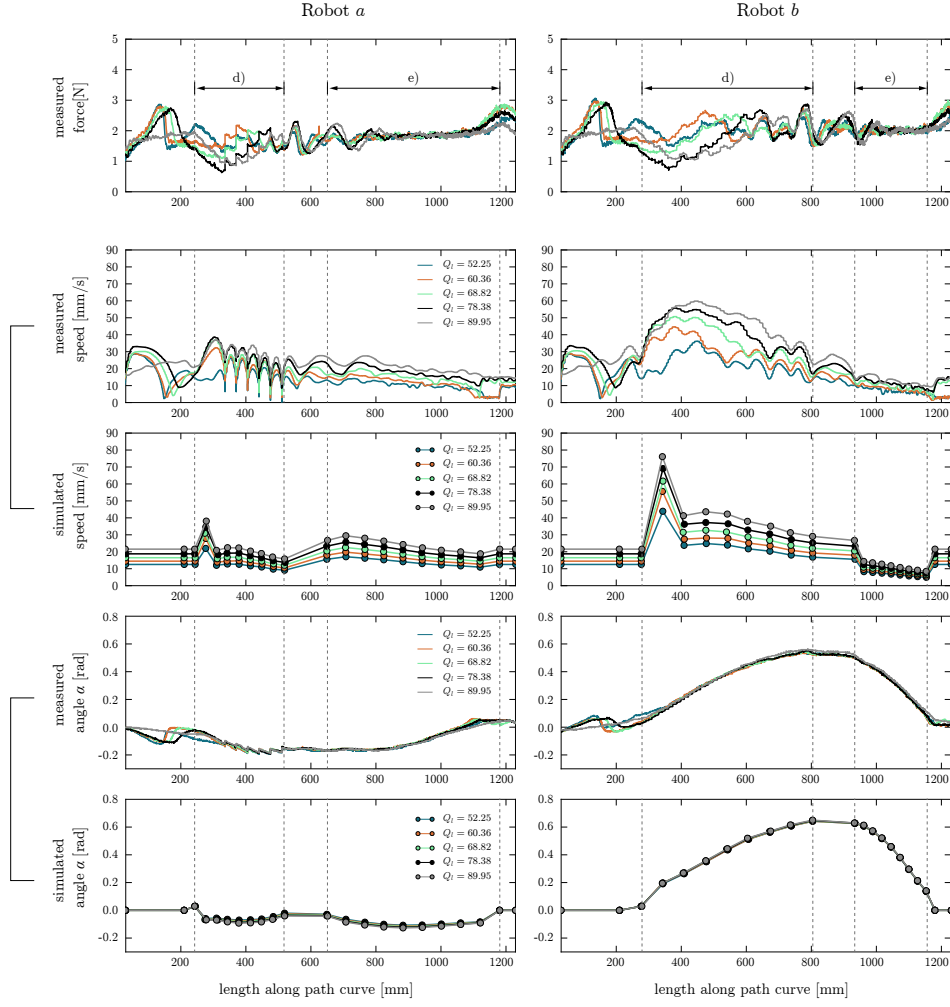


Fig. 3.45: Measured and simulated process data (speed and deflection angle) from five cutting tests with different heat input  $Q_l$ , but the same asymmetric path curves. Phases d) and e) are indicated

control (problem formulated in 3.1.7), the phases used for the quantitative comparison were just b), c) and e). For the symmetric tests the simulated angle  $\alpha$  ( $\alpha_a = \alpha_b$  for symmetric curves) in phases b) and c) had a normalized root-mean-square deviation (NRMSD)<sup>19</sup> of just 0.062. The estimated speed trajectory also produced very good results and a similar NRMSD of 0.076 in the cutting tests (see Fig. 3.44 and Table B.3). For the asymmetric tests in phase e) the speed estimation was similar successful (average NRMSD for  $v_a$  0.095, NRMSD for  $v_b$  0.058), however the angular comparison exhibited a deviation of 0.351 for angle  $\alpha_a$  and 0.189 for angle  $\alpha_b$  (see Fig. 3.45 and Table B.4). Further results are documented in Appendix B.2.



### 3.4.1.2 Shape comparison

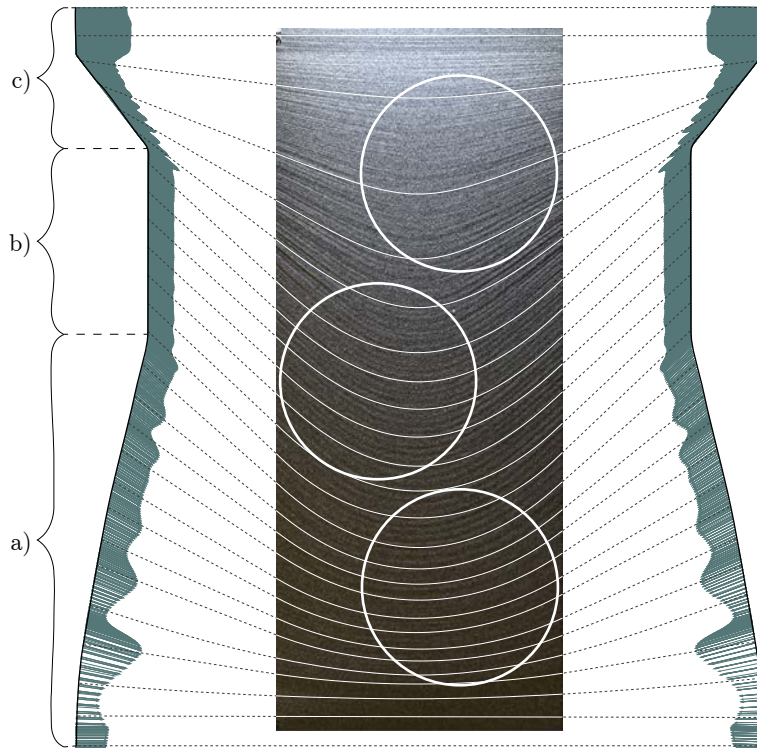


Fig. 3.46: Overlay of simulated curves and picture, measured tension force vector at its respective position for process data 151213\_FA2A6 and path-curves

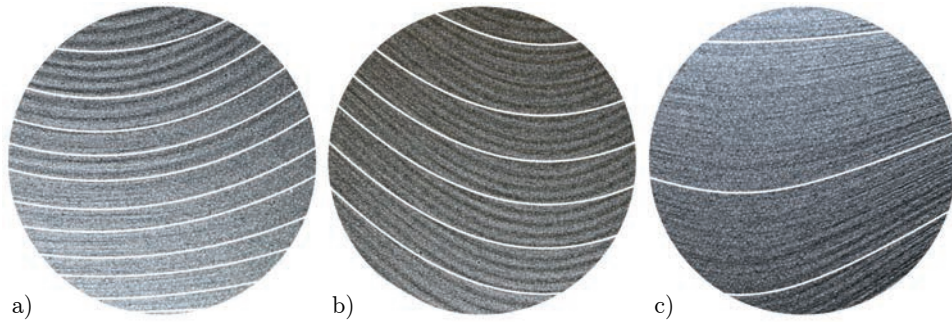


Fig. 3.47: Details from the overlay between simulated curves and surface picture, from a) entry, b) steady and c) exit phases, see Figure 3.46

Additionally to the process data, to compare the shape of the physical wire with the simulated curve shape, the taken pictures were overlaid with the simulated curves. This comparison was just performed visually (see Fig. 3.46)<sup>20</sup>. As apparent in the detail pictures a) and c) of the symmetric path-curves (see Fig. 3.47), the curves in the entry and exit phases resemble to the shadows from the surface, however phase b) has deviances.



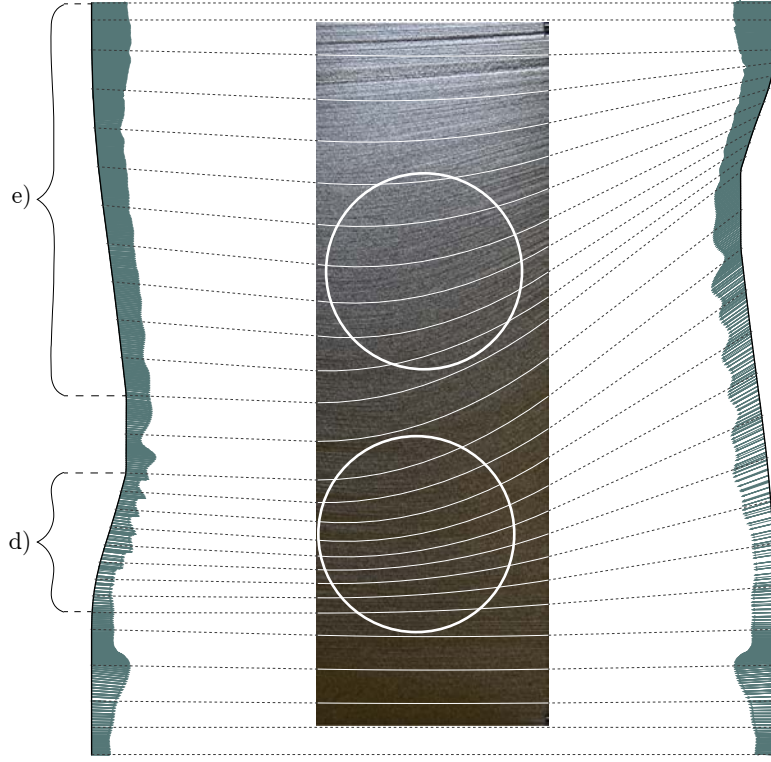


Fig. 3.48: Overlay of simulated curves and picture, measured tension force vector at its respective position for process data 151214\_8BAF4 and path-curves

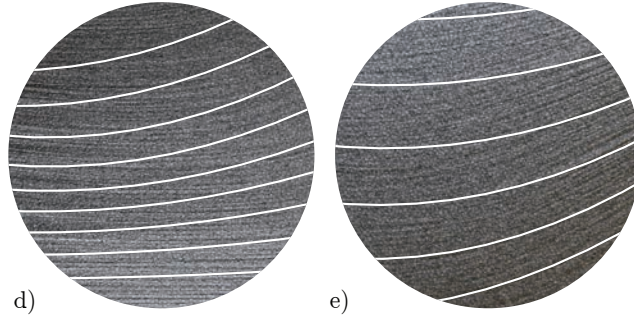


Fig. 3.49: Details from the overlay between simulated curves and surface picture, from phases d) and e) with asymmetric force distribution, see Figure 3.48

The shape comparison for the asymmetric curves was not successful, as clear aberrations are visible in the detail pictures (see Fig. 3.49) and follows the aforementioned insufficient NRMSD for angles  $\alpha_a$  and  $\alpha_b$  in the process data comparison. The reason for this may as well be the oscillation problem since it affects the shape of the curve as well. More comparisons of both symmetric and asymmetric tests can be found in the Appendix B.2.2.

### 3.4.1.3 Results

Summing up, the results of the comparative studies N°1 proved physical coherency for the force distribution equation 3.7 and therefore also a good estimation for the robot's speeds trajectories. However, the force-feedback controller was again proven not to fit the application as it caused oscillations in phases a) and d). But with the successful enhanced speed estimation, the feedback-feedforward control (see Section 3.1.7) could be improved to finally integrate the acquired knowledge of material behaviour in the process control and close the loop between simulation and fabrication which is evaluated next.

### 3.4.2 Comparative studies N°2

To evaluate the predictability and reproducibility of the physical process by means of the simulation framework and the adaptive control software, six different sample surfaces have been designed, simulated, two times fabricated and 3D-scanned, sizing 900 mm in length and 400 mm in width. The generated data allowed for quantitative comparisons between simulated surface, estimated process variables, physical artefact and acquired data during the process.

The edge curves and the wire length extension function (see Fig. 3.50), as input for the simulation, were designed in such a way to provide variability between moving directions and varying force distributions (see Figs. 3.51, 3.52) to generate double-curved surfaces. As mentioned in Section 4.1.2, double-curvature (negative Gaussian curvature, see Figure 3.54) can be achieved, if one wire end changes its moving direction contrary to the other, or, change the general moving direction radically. This causes the wire curve to leave the two-dimensional residing plane and to utilize its three-dimensional behaviour. Therefore, the designed edge-curves feature high- and low curvature peaks in positive and negative amplitudes with differing frequency.

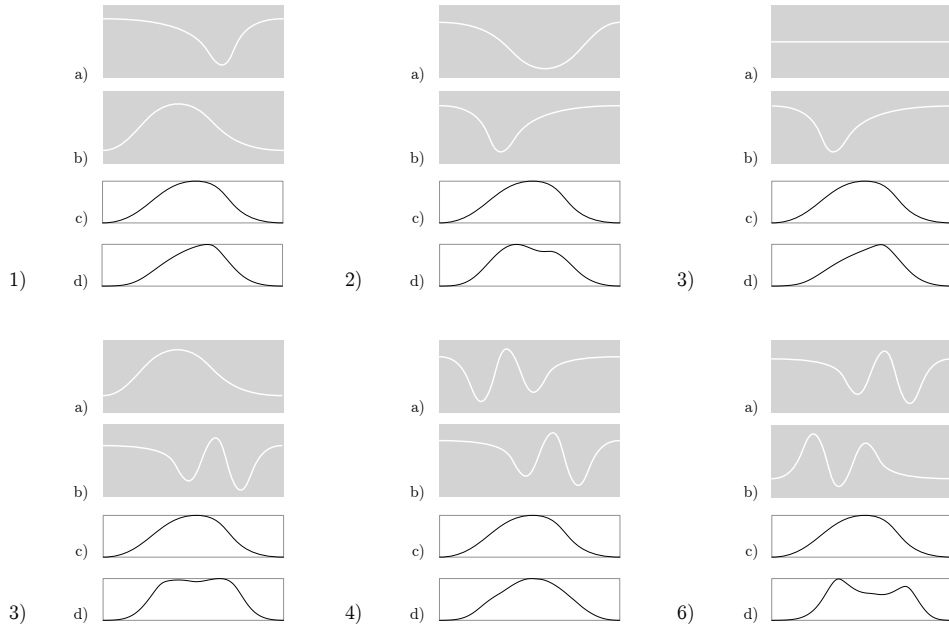


Fig. 3.50: Input curves for the six simulated surfaces: a), b) edge-curves, c) wire length extension curve and d) resulting engaged wire length

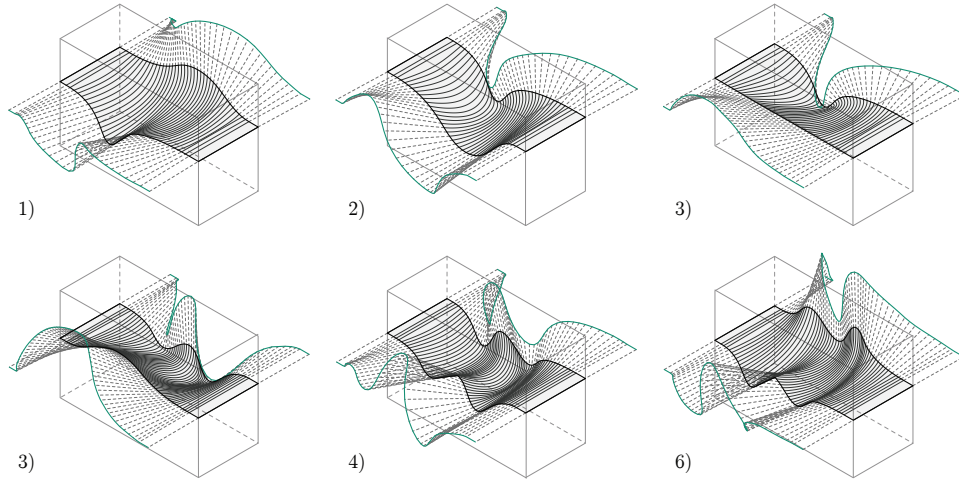


Fig. 3.51: Six simulated surfaces with varying edge-curves as inputs, see Figure 3.50 and generated path-curves thereof

The estimated speed trajectories for the robots, calculated in the simulation, served as input for the fabrication procedure, which used the combined feedback-feedforward control (see Section 3.1.7) to tare the speed according to the force measurement about the estimated speed trajectory. The *Control Core* logged the measured robots' speeds and angular and force measurements from both of the cardan joint end-effectors. To investigate the process

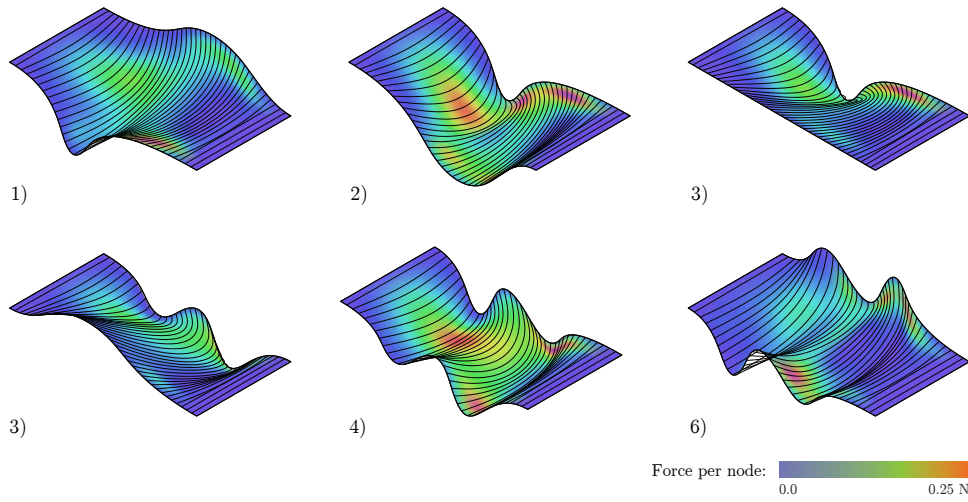


Fig. 3.52: Force magnitudes of the calculated nodes mapped as color values and visualized on the simulated surfaces

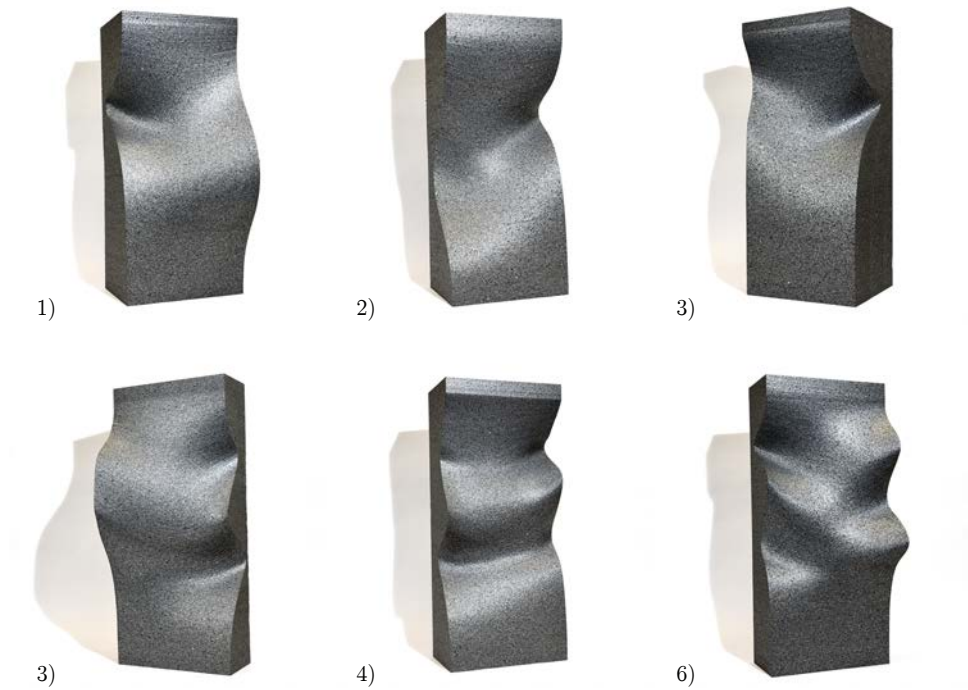


Fig. 3.53: Photos from the fabricated objects, 400 x 900 mm (width x length)

in the phase where the wire has already cooled, 200 mm of foam were cut before the actual start of the path curves without feedback control (see Section 3.2.2). After fabrication (see Fig. 3.53), all twelve surfaces were scanned with a Leica Nova MS50 Camera [111] and per surface an average of one million scan points was registered. From these point clouds, meshes were constructed<sup>21</sup>.

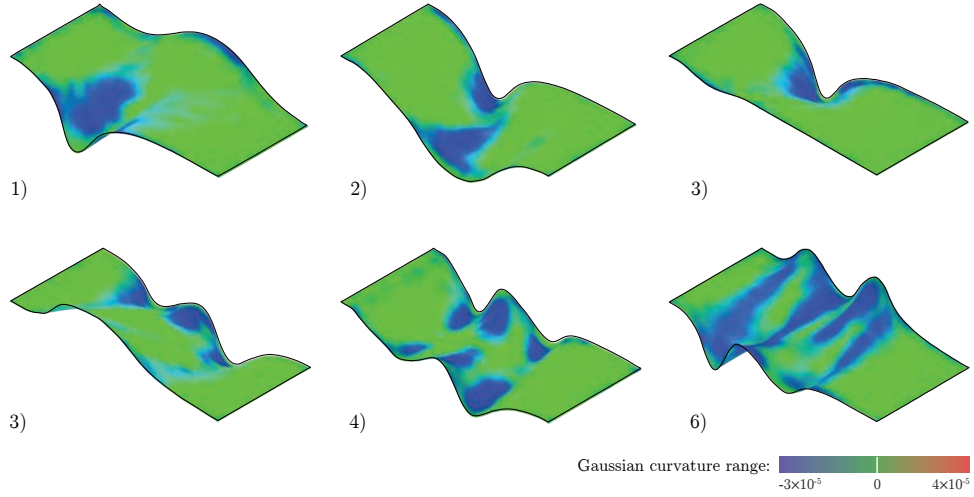


Fig. 3.54: Gaussian curvature analysis on the reconstructed meshes from the 3D-scanned point clouds

#### 3.4.2.1 Predictability of the *SWC* process

To validate the simulation framework, the estimated angles and speed trajectories from the simulation were compared with the measured speeds and angles of the twelve surface cuts (see for example Fig. 3.55). The normalized root-mean-square deviation (NRMSD) of speeds  $v_a$ ,  $v_b$  ranged between 0.23 and 0.09, of angles  $\alpha_a$ ,  $\beta_a$ ,  $\alpha_b$ ,  $\beta_b$  between 0.03 and 0.12 and proved a good estimation of process variables (see Table 3.3).

surface id	datafile id	$v_a$	$v_b$	$\alpha_a$	$\beta_a$	$\alpha_b$	$\beta_b$
1.	160304_17295	0.23	0.15	0.08	0.07	0.06	0.08
	160304_B2140	0.23	0.15	0.08	0.07	0.06	0.08
2.	160304_7C529	0.16	0.16	0.08	0.08	0.07	0.06
	160313_5017B	0.16	0.17	0.05	0.08	0.08	0.04
3.	160304_C9874	0.17	0.11	0.06	0.06	0.09	0.11
	160304_C2CEF	0.19	0.11	0.06	0.06	0.09	0.11
4.	160304_4C58B	0.10	0.15	0.06	0.05	0.11	0.05
	160304_680DB	0.10	0.15	0.06	0.05	0.11	0.05
5.	160305_314D1	0.12	0.09	0.08	0.08	0.12	0.04
	160313_03E5B	0.12	0.09	0.05	0.08	0.09	0.04
6.	160306_CEE87	0.14	0.12	0.03	0.07	0.12	0.03
	160306_BC582	0.14	0.13	0.03	0.07	0.12	0.03
<b>average NRMSD 1.-6.</b>		0.16	0.13	0.06	0.07	0.09	0.06

Table 3.3: NRMSD of speeds  $v_a$ ,  $v_b$  and angles  $\alpha_a$ ,  $\beta_a$ ,  $\alpha_b$ ,  $\beta_b$

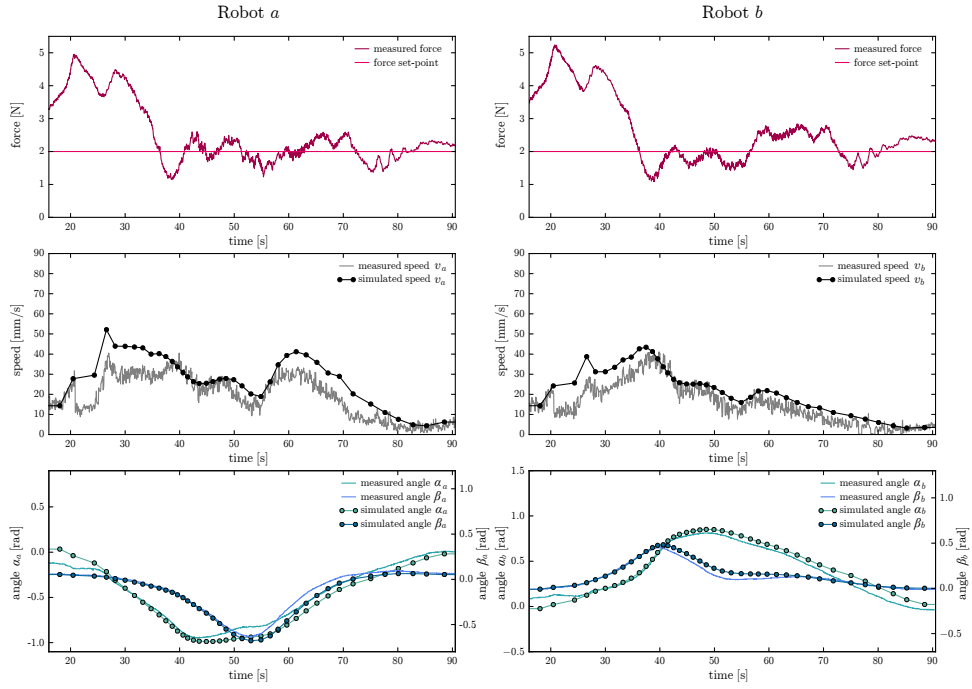


Fig. 3.55: Process data comparison of 160304\_B2140, surface 1)

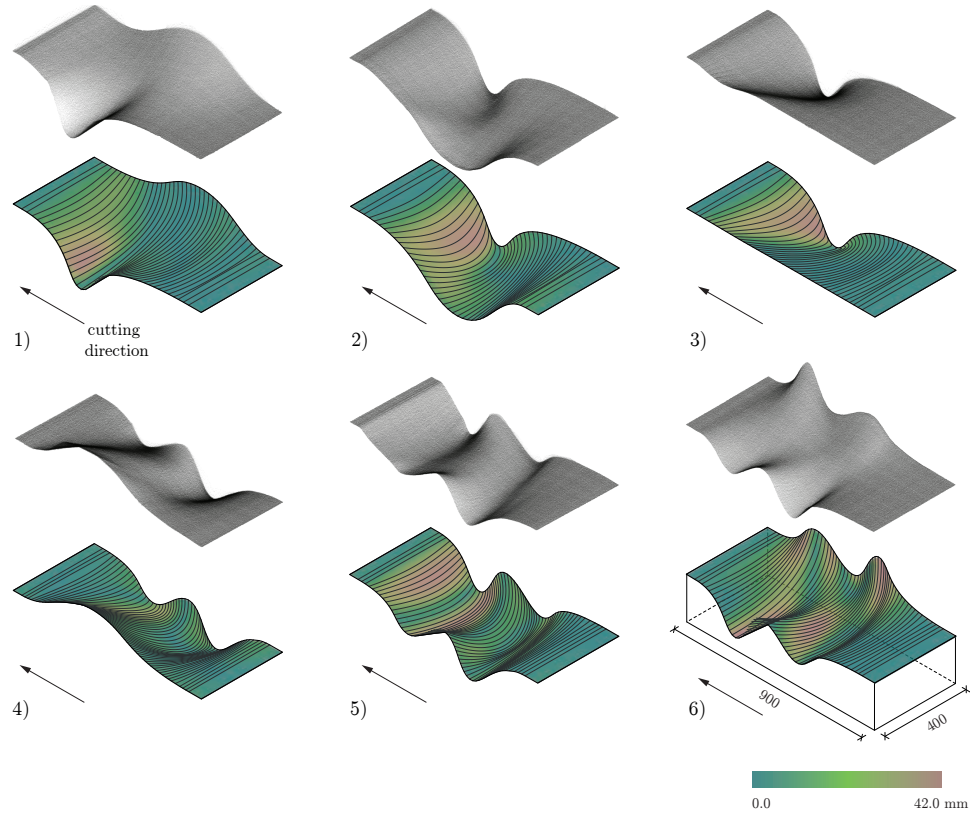


Fig. 3.56: Point cloud data from the scanning process and simulated surfaces with fabrication deviance mapping. The colours on the surfaces indicate the closest distance to the reconstructed mesh from the point cloud

The reconstructed meshes from the scanned surface were compared to the simulated surface and the offset distance was calculated (see Fig. 3.56). The maximum distance was 42 mm, which is high in terms of building tolerances. Areas of high deviation could be identified where the path curves show high curvature and increase at later moments in the procedure since small deviations along the path accumulate.

### 3.4.2.2 Repeatability of the *SWC* process

To validate the feedforward-feedback control and check the repeatability of the process, the process data of two cutting iterations with identical input parameters were compared to one another and exhibited almost no difference (see Fig. 3.57). Also the reconstructed meshes from both cutting iterations exhibited a maximal distance of just 6 mm to each other (surface example 1) drops out) and the histogram displays 94 percent<sup>22</sup> below 2 mm of the measured points (see Fig. 3.58). This proves that the integration of feedforward and feedback control makes the process very stable and repeatable, reducing additionally the oscillations.

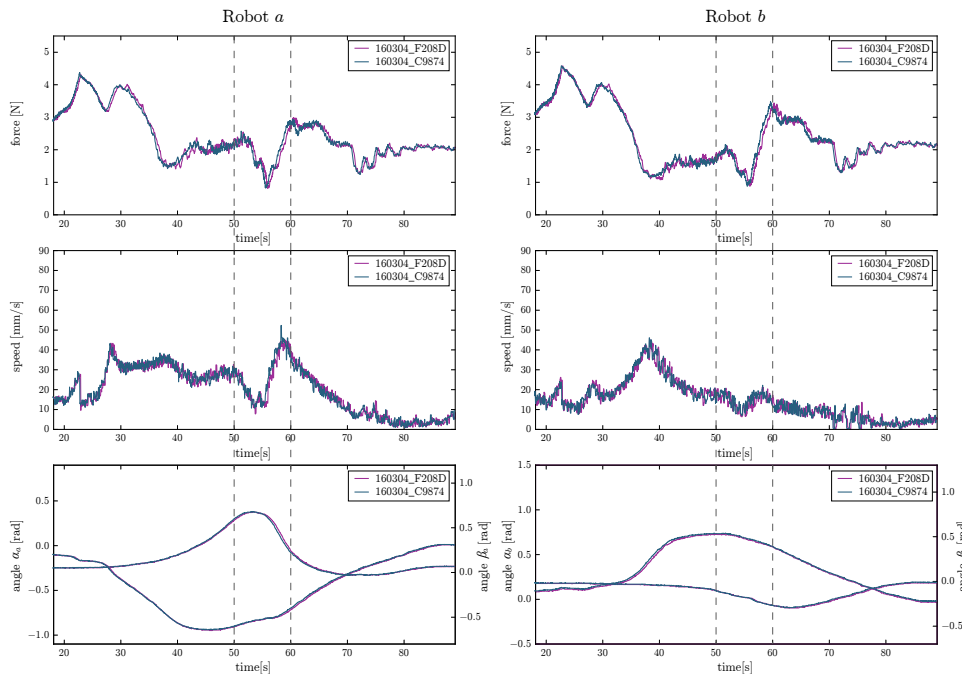


Fig. 3.57: Process data comparison of 160304\_F208D and 160304\_C9874, surface 2). More comparisons can be found in Appendix B.3.2

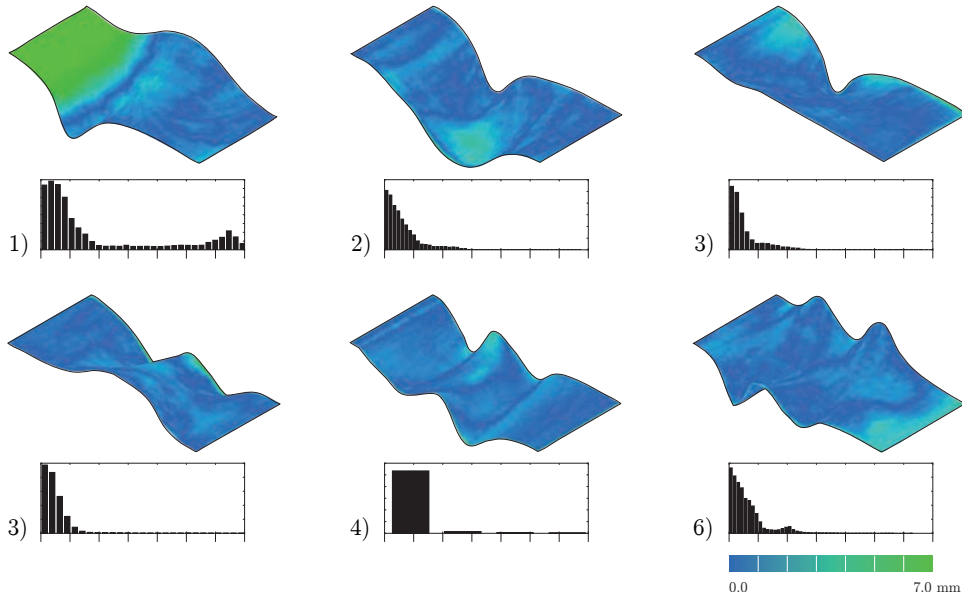


Fig. 3.58: Comparison between two cuts of the reconstructed meshes from the point clouds. Distances mapped to color and visualized on the surface. Below: histogram of the distances

Generally it can be noticed, that the optimal tension force  $T_{opt}$  can efficiently be reached where path-curves show less curvature (for example, peak between timestamps 50 - 60 (see Fig. 3.57)), implicating less speed change. The value of 2.0 N is very sensible, for example, if the wire is taut between the robots with tension force  $T_{opt}$  and one robot distances from the other in the wire direction of just 1.3 mm, this already leads to a difference of 0.6 N<sup>23</sup>. Therefore, force measurements between 1.0 to 3.0 N are optimal.

### 3.4.2.3 Results

Generally, the results of the second comparative studies were successful. The improved estimation of process variables through the simulation framework and the efficient adaptive control are clearly visible in the surface quality of all six cuts (see Fig. 3.59).

The simulated geometry however, had a high deviation from the actual object and therefore cannot predict the resulting physical surface with absolute precision. However, the comparison in this case is only for a single element. Considering these tolerances in context with the overall assembly in respect



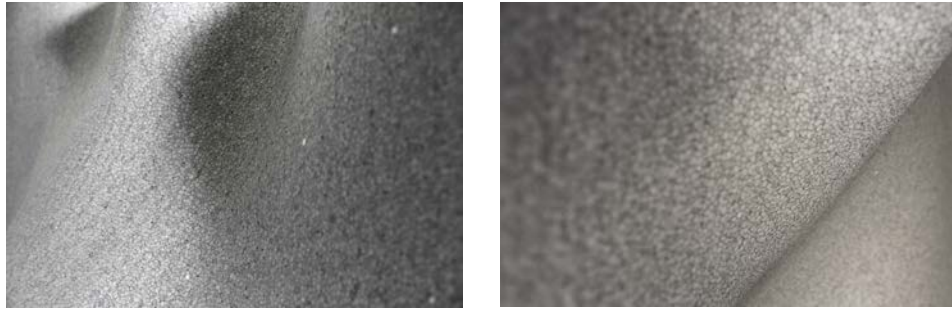


Fig. 3.59: Surface details of cut objects

to scale and relation between the elements, certain tolerances become acceptable. For example, in the case of façade systems (documented in Chapter 4), the deviations on the surface become less of an issue, if continuity at the edges between adjacent panels can be guaranteed. Although not accurate, the curvature of the surface in general is anticipated through the simulation framework and therefore it can be employed to digitally investigate and explore the geometrical particularities of the *SWC* process.

Strategies to reduce the deviances between digitally simulated surface and physically fabricated artefact should involve approaches from multiple directions: The fabrication control could be extended to adaptively adjust the path curves and prevent the accumulation of deviations, but also the design and simulation framework could continuously learn from the process and adapt to the physically fabricated artefact. The reduction of deviances is also one of the main challenges for future development and strategies therefor are explained in more detail in Section 5.3.

## Notes

<sup>11</sup> Robot Operating System (ROS) is a collection of software frameworks for robot software development. Unfortunately, currently just Ubuntu Linux is listed as "Supported" while other variants such as Fedora Linux, Mac OS X, and Microsoft Windows are designated "Experimental" [112]. For architectural purposes, the fabrication control needs to be interlinked with CAD Environment. However, McNeel Rhinoceros 3D, which is widely-used amongst architectural computational design, is not available for Linux. Thus to fully utilize ROS' potential, a second Linux computer or a Linux virtual

machine would be required and additionally a ROS node for linking Grasshopper to ROS would have to be implemented.

- <sup>12</sup> The expanded foam used throughout the research project was swissporLAMBDA Vento, a graphite-enhanced expanded polystyrene with a density of 15 kg/m<sup>3</sup> [113]. This material was chosen, as its cut surface was reflective, allowing for an increased visibility of curvature on the surface.
- <sup>13</sup> The foam block size is notated in the order of *width*, *height*, *length*; where *width* refers to the space between the two robotic arms and *length* along the cut
- <sup>14</sup> Programming guide for the programmable laboratory power supply can be found at [114].
- <sup>15</sup> The protocol can be found in the programming guide for the programmable laboratory power supply: [114].
- <sup>16</sup> ShapeOp is a library for static and dynamic geometry processing [115].
- <sup>17</sup> The estimation of the linear temperature falloff of the hot-wire was empirically evaluated. However, a correct temperature gradient of the wire should be on the agenda for future investigations.
- <sup>18</sup> NumPy is an extension to Python, adding support for multi-dimensional arrays and matrices, along with various mathematical functions on them. SciPy contains modules for optimization, linear algebra, integration, interpolation and other tasks commonly in science and engineering [116].
- <sup>19</sup> RMSD represents the sample standard deviation of the differences between the simulated values and measured values. NRMSD is the normalized RMSD according to the range of the measured data (= maximum – minimum value).
- <sup>20</sup> Canny Edge Detection [117] could eventually be used to find edges and compare with the simulated curves.
- <sup>21</sup> From the point clouds meshes were constructed using Meshlab [118] and its implementation of the Poisson Surface Reconstruction algorithm [119].
- <sup>22</sup> Surface examples 2) - 6) exhibit 94 - 96 % of data below 2 mm and surface 1) drops out with 70 %.
- <sup>23</sup> In the beginning, the wire was taut between the robots, their distance from each other was 1155 mm and the force sensor measured 1.05 N. After a movement of 1.3 mm away from each other (= 2.6 mm in total) allowed by the springs at the end-effectors, the measured force was 1.69 N.

## 4 Application and validation

This chapter provides the implementation and validation of the developed techniques documented in Chapter 3 in regards to their applicability for architectural purposes. It is structured into two sections, documenting first on results from an elective course and second from a summer school workshop, in which architectural students were participating. Based on a design task, the central focus in these experiments was to investigate particular design strategies, for individual- as well as for the assembly of multiple elements, reveal certain cutting characteristics and geometrical particularities of the *Spatial Wire Cutting* process. In the applied experimental methodology the specific design solution was empirically and iteratively developed using a combination of both the design- and simulation framework and the fabricated physical prototypes. Moreover, this chapter displays the application of the *SWC* technology for the production of formwork components for façade panels at an architectural scale.

### 4.1 *SWC* elective course 2015

In the spring semester of 2015, the preliminary design- and simulation framework and adaptive control software (using the feedback-control) were applied and validated in an elective course named *Spatial Wire Cutting* with ten architecture students at ETH Zurich [120]. The used foam block size varied depending on the student's projects and ranged from 300x300x300 to 600x400x300 mm. The design task in this course was to explore the typology and characteristics of individual cut elements and subsequently develop a

logic for their assembly as a façade system. The course was intended as pre-study to the following summer school workshop, as documented next. While three student teams developed projects that took advantage of the *SWC* procedure, following the bottom-up principle, the other two teams focused on the assembly of panels with ruled surfaces.

#### 4.1.1 Group 1 - Sigmoid curve

This group generated path-curves, through which the movement of the wire resembles a cross. The wire moves in different directions on the opposite exit faces of the block, which results into contrary force directions around the centre point of the wire's movement (see Fig. 4.1). As a consequence, the wire is shaped into a slight sigmoid curve. Through varying the angle, the depth and the path-curves for each element (see Fig. 4.2), the group produced an assembly of elements that featured a tension between single- and double curved surfaces, resembling a chequerboard (see Fig. 4.3). While casting the element might be difficult, the project however visualized a cutting characteristic apart from producing surfaces through entering on one side of a foam block and exiting on the opposite: The cut surfaces demonstrate a singularity in the form of self-intersections<sup>24</sup>.

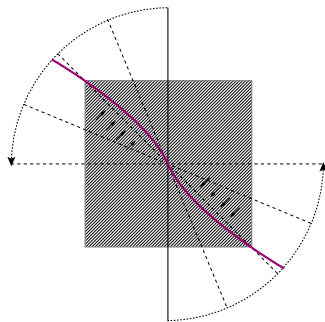


Fig. 4.1: Crossed cutting movement, resulting into a slight sigmoid curve



Fig. 4.2: Variation possibilities on one element: angle, depth and path-curves

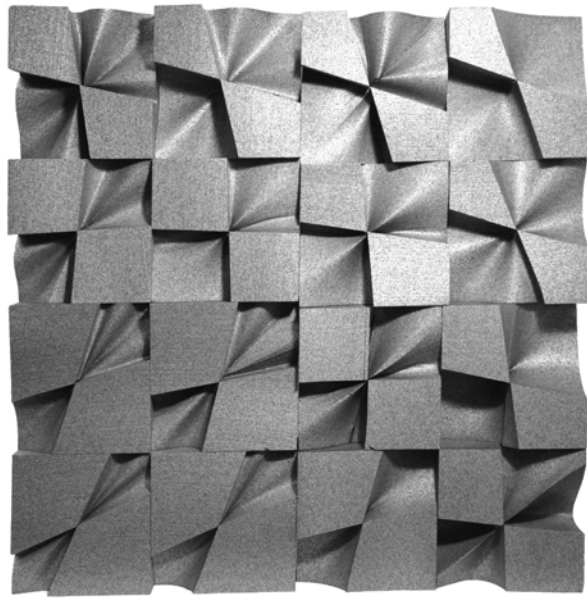
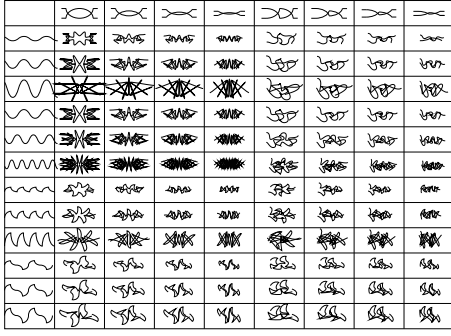


Fig. 4.3: Final prototype of Group 1: The element variations have been parametrically controlled (single element size: 300 x 300 x 300 mm)

#### 4.1.2 Group 2 - Movement patterns

This group explored the generation of patterns on the surface by applying repetitive movements to enhance and visualise the deformation of the curved cutting medium (see Fig. 4.5). With the *SWC* procedure, expressive double-curved surfaces can only be cut when one wire end changes its moving direction contrary to the other<sup>25</sup>, or, as examined in the next group, change the general moving direction radically, forcing the wire curve to leave its two-dimensional residing plane and step towards utilizing its three-dimensional behaviour. To extract this behaviour and fully profit from the potential of this curved cutting medium, this group spared no effort to test a multitude of different paths (symmetric and asymmetric) (see Fig. 4.4). For the final prototype they applied variations of transformations such as mirror, rotation, scale and translation to the path-curves and used both positive and negative parts of the cut, which resulted into a highly articulated aggregation (see Fig. 4.6), which could directly be employed for formwork purposes.



the group applied another cut in the longitudinal direction and flipped the parts (see Fig. 4.8). Thus, the critical edge was transferred to the center and the inner edge, which exhibited less discrepancies, moved outwards, resolving the continuity issues. Further to mention is that, at that time, the feedback-based fabrication procedure exhibited oscillation problems (see Section 3.1.7), which, although considered as lack of control, was intentionally forced by the students since it created small deviances on the surface, that reflected the wire's traces (see Fig. 4.9). The assembled panels differed in size and overlapped vertically.

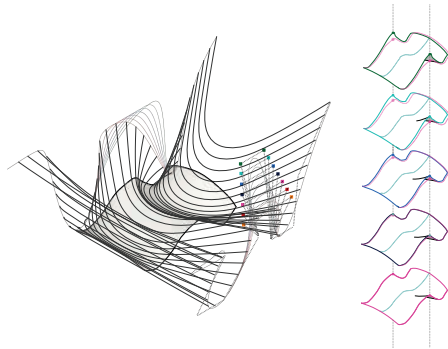


Fig. 4.7: Subtle variation of the path-curves' peak, generating slightly differing surfaces

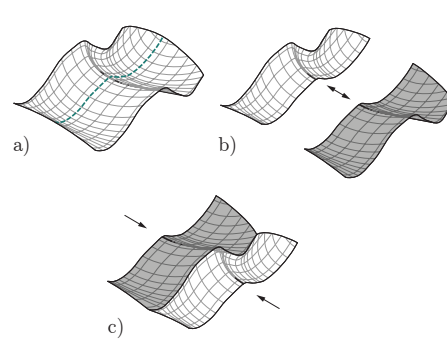


Fig. 4.8: a), b) Cutting the panel in the longitudinal direction and c) flipping the parts



Fig. 4.9: Final prototype of Group 3: The panels with varying element size overlapped vertically.

#### 4.1.4 Groups 4 and 5 - Ruled surfaces

The two other groups focused on the assembly of panels with ruled surfaces. One team produced multiple equal hyperbolic paraboloid panels which aggregated into, in contrast to the other prototypes, a more space filling structure (see Fig. 4.10). Although the connection of the panels has to be considered further, the group cleverly circumvented the problem of the aforementioned critical edge through joining just the controlled (entry- and exit-) edges. The resulting aggregation, which may not necessarily need to consist of equal panels, could eventually be used for dividing walls and have structural qualities through the double-curved panels. The other team generated differentiated ruled surface panels to investigate variable shadow conditions (see Fig. 4.11) and thereby extended the design brief of investigating also a functional façade system.



Fig. 4.10: Final prototype of Group 4:  
Hyperbolic paraboloid panels

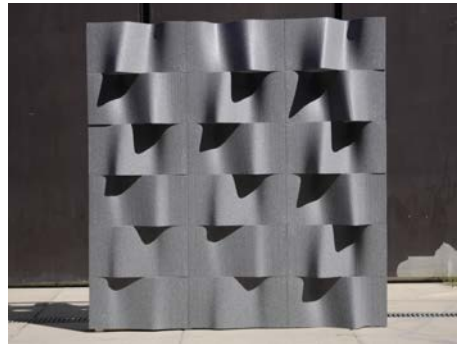


Fig. 4.11: Final prototype of Group 5:  
Variable shadow conditions

#### 4.1.5 Results

The elective course pushed the development of the research project in virtually all aspects and allowed for a large number of iterative tests and form explorations. However, the design set-up with the path-curves as input, led to a lot of error-prone results in the simulation, for which reason the students had to intensively rework the path-curves. Additionally, the feedback-based robotic control produced oscillating movements in the fabrication procedure.



This combined premature technology was quite a challenge for the students, since they had to come up with design solutions that cover the imprecise fabrication, which may have been the reason why two groups switched to using just ruled surfaces. Following this experiences, the next goal, was to enhance the design set-up to provide more intuitive handling and to improve the adaptive control. Summing up, the elective course has led to valuable findings for the preparation of the following summer school, as documented next.

## 4.2 **Swisspearl<sup>®</sup> Summerschool 2015**

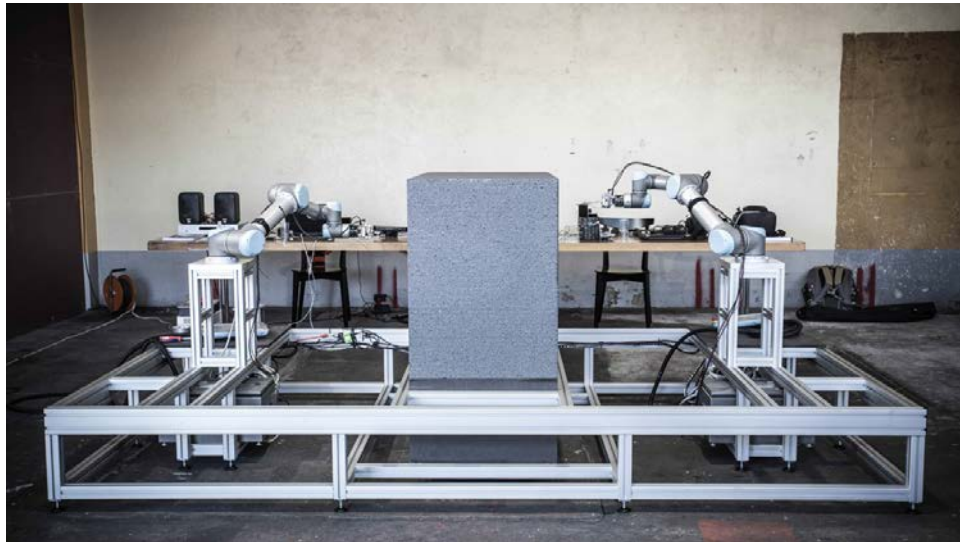


*Fig. 4.12: Employed robotic set-up in the Swisspearl<sup>®</sup> Summerschool 2015*

On the basis of the experiences from the elective course, the design- and simulation framework was improved to use the edge-curves as input (see Section 3.3.5) and the adaptive control was extended to feedback-feedforward control (see Section 3.1.7), however the simulation did not yet incorporate the force-distribution equation (see Section 3.3.3) and therefore the calculation of the speed trajectories as fabrication input was rather a rough estimation [12].

To validate the second iteration of the design- and simulation framework a

two-week Swisspearl® Summerschool 2015 [121] was conducted. Furthermore, this workshop focused on expanding the *SWC* technology towards the application at an architectural scale by developing façade typologies (see Fig. 4.12, the up-scaled robotic set-up). Within the design and conceptual phase of the workshop, the 14 students started exploring the technique through a series of manual tests, using a hand-held hot-wire cutting device and foam blocks of 300 x 400 x 600 mm (see Fig. 4.14) to develop an intuitive understanding of the *SWC* process<sup>26</sup>.

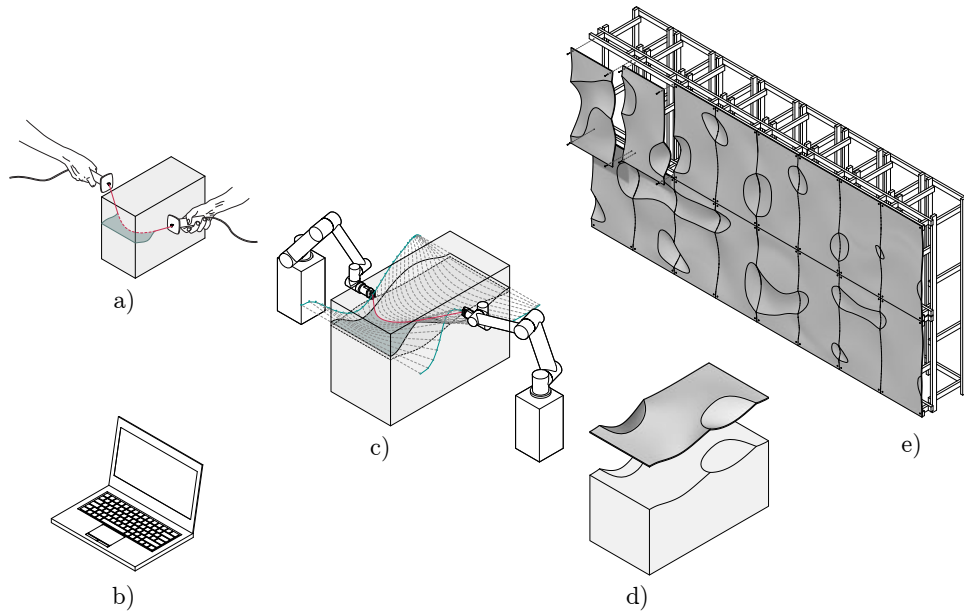


Fig. 4.13: Workflow: a) manual testing b) computational design c) robotic fabrication, d) manual lamination e) assembly



Fig. 4.14: Manual testing



Fig. 4.15: Lamination process

Subsequently, based on the findings of the manual tests, these concepts were translated into the computational simulation framework to elaborate an overall design concept and parametric model for the aggregation of façades composed of custom panel sizes of 1200 x 600 mm. With the given design setup,

the focus was on the control and the modulation of three planar curves: the two edge curves of the panel and another curve that defined the amount of wire length in the foam (see Section 3.3.5). The parametric control of the edge curves facilitated the design of the façade system, as same edge curves allowed for continuity between the panels.

The simulated surfaces of the parametric model contained already the fabrication instructions, which were directly sent to the adaptive control software, applying the combined feedforward-feedback control. After robotically cutting, the elements were used as moulds for the lamination<sup>27</sup> with the fibre-cement composite Swisspearl® (also known conventionally as Eternit), a well-established manufacturing procedure (see Fig. 4.15). After the 24 hours dry-out phase, the panels were mounted on a wooden sub-structure.

The challenge of this unique combination of automated cutting and manual lamination was to find the synthesis between two very different material systems: each one with his specifically constraint design space. Four student groups developed four different design concepts, which were materialized as full scale prototypes.

#### **4.2.1 Group 1 - Double cuts**

The first group concentrated on a procedure consisting of two sequential cuts on the same foam block and as such created intersections between the two resulting surfaces (see Figs. 4.16, 4.17). These intersections, or crest lines, which appeared as patterns on the final prototype (see Fig. 4.18), were parametrically controlled by the edge curves through varying heights and positions of the control points. Since the behaviour of the composite material in respect to double-curvature was quite unknown and due to the limited time-frame of production, these panels were partially realised very flat, which, in hindsight, may not have been necessary. However, the resulting three-dimensional curves of intersection led to an interesting composition and additionally stiffened the panels.

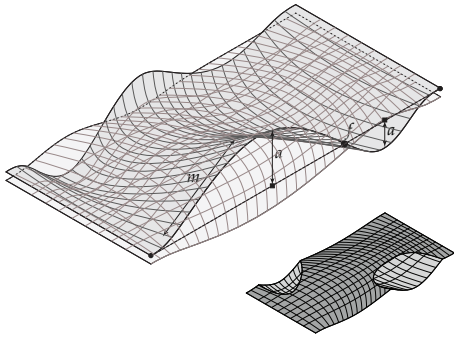


Fig. 4.16: Conceptual drawing: Two intersecting surfaces



Fig. 4.17: Photo of manual tests

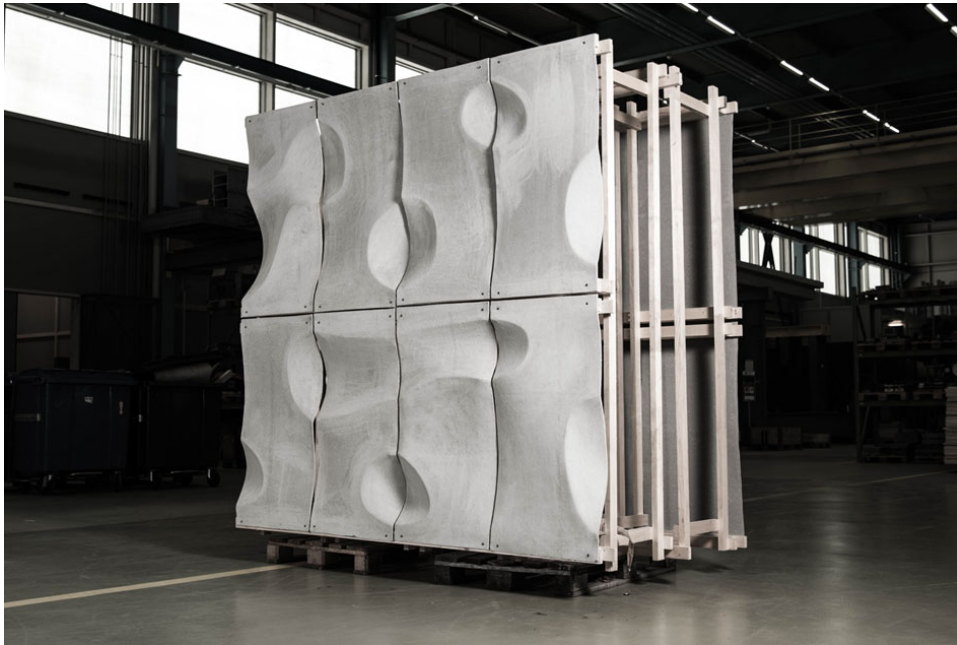


Fig. 4.18: Final prototype of Group 1: Double Cuts

#### 4.2.2 Group 2 - Flipping peaks and valleys

The second group explored a parametric differentiation of the edge curves with alternating combination of sharp peaks and valleys. Similarly to the *Movement Patterns* (see Section 4.1.2) the wire's movement and the uniqueness of the process was demonstrated expressively in the fabricated surfaces. To establish a certain surface continuity, every second panel was flipped for altering the direction of the hot-wire's movement (see Fig. 4.19).

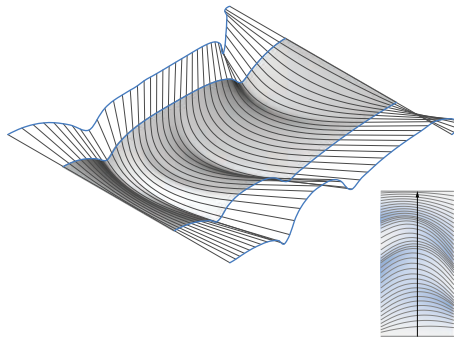


Fig. 4.19: Design concept: edge curves with peaks and valleys



Fig. 4.20: Photo of manual tests, flipping cutting direction



Fig. 4.21: Final prototype of Group 2: Flipping peaks and valleys

### 4.2.3 Group 3 - Waves

The concept of the third group concentrated more on exhausting the composite material's limits. In developing a non-standard version of the company's well known corrugated sheet, they additionally hid the vertical connections between the panels by using *waves*. Through empirical testing the maximum range of surface stretch and compression of the cement composite was identified and used as a design constraint for the parametric control of the edge curves, thus pushing the boundaries of the material process. However, since

the path-curves exhibited high curvature, resulting in rapid speed variations, the developed panels were generated just with a slightly curved wire (see Fig. 4.22).

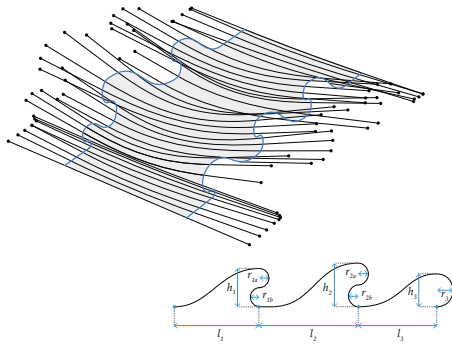


Fig. 4.22: Design concept: panel and edge curve parameters



Fig. 4.23: Photo of manual test



Fig. 4.24: Final prototype of Group 3: Waves – hiding vertical connection

#### 4.2.4 Group 4 - Subdivision

The fourth group's concept was to assemble six smaller fabricated pieces into one single mould for the lamination of larger panels. This system, combined with the controlled changing of edge curves to generate almost ruled, but still



partly double-curved, surfaces, explored subdivision as strategy to widen the spectrum of possible surfaces.

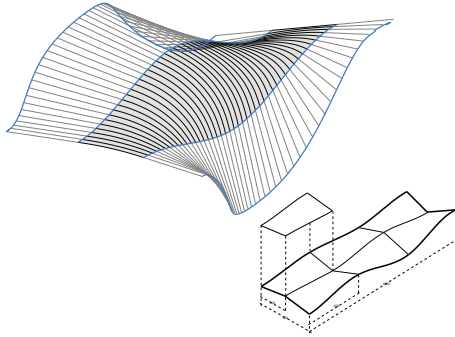


Fig. 4.25: Conceptual drawing and design concept



Fig. 4.26: Manual test for hyperbolic surfaces



Fig. 4.27: Final prototype of Group 4: Subdivision

#### 4.2.5 Results

Overall, the pursued physical explorations within the framework of the Summerschool led to a variety of different results, promising interesting avenues for *SWC* to be used for 1:1 future constructive processes. The combined speediness and efficiency of the *SWC* process and the lamination process allowed for a large number of iterative physical tests and a comprehensive

empirical investigation of the architectural potentials of the technique. This has clearly evidenced the viability and application range of *SWC*. Through the integrated computational design and simulation framework and the adaptive robotic control, the students designed prototypes that were coherent with their materialisation and therefore confirming the success of the second iteration of the design- and simulation framework. Further, the up-scaling of the process, apart from some additional path-planning, worked without any problems. The *SWC* procedure creates a specific family of double curved surfaces linked with the related machining limitations. Thus, the solution space is constrained, but it is exactly this particularity that challenges the design scope and generates architectural diversity.



*Fig. 4.28: Overview, various final prototypes*

## Notes

<sup>24</sup> Self-intersections through ruled surfaces are documented and exhibited as models for example in the Institute Henri Poincaré [122, p. 39].

<sup>25</sup> With the *SWC* procedure, expressive double-curved surfaces can only be cut when one wire end changes its moving direction contrary to the other, likewise in the creation of the hyperbolic paraboloid.



<sup>26</sup> The hand-held device was already provided in the *SWC* elective course, however not fully accepted by the students.

<sup>27</sup> For the lamination it was not necessary to coat the polystyrene moulds: they were directly used without preparation.



## 5 Conclusion and outlook

### 5.1 Summary and discussion

The goal of this thesis was to develop techniques and methods for the multi-robotic hot-wire cutting procedure *Spatial Wire Cutting* and investigate its architectural potential in the design and production of geometrically complex formwork components. Over the course of development, fundamental knowledge was gained about the process, its characteristics and limitations, which have been successively integrated in the custom software framework and periphery. Besides, the process' predictability and control was continuously improved, validating the applied methodology. Thus, existing hot-wire cutting techniques have been extended with a new geometric capability, a particular vocabulary of double-curved sweep surfaces. Hereinafter each of the core topics of investigation is shortly summarized and discussed.

#### 5.1.1 Adaptive robotic control system

In regards to the experimental set-up (see Section 3.1.2), suitable synchronisation and control strategies have been developed that allowed to successfully control the *SWC* process. Through several physical experiments the requirements for a custom end-effector were identified, which, equipped with sensors, permitted to track the relevant physical variables. These were utilized in the online control as feedback and additionally stored for later analysis, enabling to acquire information from the process. One of the most relevant developmental steps was the extension of the feedback control with feedforward control, which stabilised the robots' movements and improved the repeatability of the fabrication process, as successfully demonstrated by

the comparative studies (see Section 3.4.2.2). This advancement however, was just possible with a proper speed estimation for the feedforward control, which required first a comprehensive investigation into the process variables and their integration in the simulation.

The biggest challenge in the control of the process was to keep the hot-wire constantly in an appropriate tension, which was identified to range between 1 to 3 N, targeting the optimal tension force  $T_{opt}$  in the experimental set-up. This range is sensitive, as through synchronisation issues or joint acceleration problems the tension drops immediately, through which a correct speed estimation was indispensable. However, for the calculation of the speed trajectories, robotic simulation was intentionally not integrated to not computationally overload the design tool. As a consequence, on multiple occasions  $T_{opt}$  could not be successful reached, the wire melted the material and led to insufficient surface qualities. With hindsight, it would have been advantageous to integrate robotic motion planning, so that erroneous results would be omitted in the first place. Moreover, the end-effector was intentionally implemented passive, interfering as little as possible in the process and keeping all actions performed by the robotic arms. In regard to possible improvements of the robotic control, this could eventually be modified to solve other problems, such as the avoidance of joint acceleration limits (see Section 5.3.1). Reconsideration for further development would also concern the three-step position synchronization (see Section 3.1.5.5). While it worked acceptable within the scope of research, it could be improved through a master-slave control system.

### 5.1.2 Analysis and modelling of material behaviour

The prevailing physical entities of *SWC* may differ very little to standard hot-wire cutting, yet by curving the wire, cutting mechanics change and the solution space expands drastically as all interacting variables are exploiting their respective operating ranges simultaneously. Successive tests and

process studies allowed to accumulate a body of knowledge about the procedure, understanding the relationships between heat-input, speed, cutting- and tension forces, etc., and allowing the development of an abstracted digital counterpart. One of the biggest challenges within this research was that with the chosen set-up it was not possible to track the process inside the foam-block, in this case the curvature of the wire at a given moment in time. This required to make assumptions, estimations and models describing the interior. For example, rather than simulating the variable temperature along the wire, the force distribution equation was developed, based on measured quantities. It was successively integrated in the simulation and proved to allow for a good estimation of process variables. However, it has to be noted that this constitutes also just a first approximation, as it is based on the cutting force model that gives an estimate of cutting force under steady-state conditions. These are conditions, in which the temperature of the wire inside the foam is constant. Since in transition states (entry phase or exit phase, see Section 3.3.2) the temperature along the wire in the foam distributes gradually, this is very likely not to match.

### 5.1.3 Design and simulation framework

A design and simulation framework has been developed that served as mediator between design intent and producibility of *SWC* surfaces. The simulation was based on the empirical relationships gained from the material studies and therefore emulated the geometrical articulation together with its respective process variables, serving as fabrication input. Over the course of development, the estimation of process variables was improved and lead to an enhancement of both the geometric predictability and the control of the robotic fabrication system.

The challenge was to provide a design tool as accurate as possible while not loosing performance, in order to provide direct feedback on design decisions. The framework has been evaluated through workshops with students and successively adjusted to allow for an intuitive design process. A big step in the

development was the transition from designing edge curves instead of path curves, which resulted from the design task of developing façade systems, as same edge curves allowed for continuity between façade panels: Designing and modulating three planar curves instead of two three-dimensional curves facilitated the control over the resulting surface and omitted erroneous input curves in the first place. Further reconsiderations regarding the input parameters for the simulation framework should include the preceding division of path/edge curves into discrete synchronized robot positions: the framework should rather search for optimal positions along the curves.

The comparison between simulated surface and actual fabricated object revealed high tolerances. Thus, the simulation framework cannot predict the resulting physical surface with absolute precision. It has to be noted that the simulation model in the current state of development has still a high degree of simplification and abstraction of the physical process: Not all factors were integrated and small inaccuracies sum up along the process, as revealed by the comparative studies (see Section 3.4.2). Moreover, if considering these tolerances not only for a single element, but in context with the overall assembly in respect to scale and relation between the elements, certain tolerances even out or become acceptable. For example, in the case of façade systems (see Section 4.2), the deviations on the surface become less of an issue, if continuity at the edges between adjacent panels can be guaranteed. Although not accurate, the curvature of the surface in general is anticipated through the simulation framework and therefore it can be employed to digitally investigate, explore the geometrical particularities of the *SWC* process and develop design strategies therefrom.

#### 5.1.4 Application and validation

The developed techniques, such as adaptive control and simulation, were continuously validated with physical artefacts from model- to full scale prototypes and proved promising avenues for *SWC* in 1:1 future construction processes. This integrative methodology pushed the development forward

and allowed to develop an in-depth understanding of the specific limitations and possibilities of the procedure. The combined design and simulation framework and the process' applicability for architectural purposes was validated with the help of architectural students, who accepted the challenge of designing within a very specific design space. Although it was non-trivial to come up with design solutions in respect to the process' boundaries, their examination and discourse allowed to reveal its inherent particular geometry. This geometry would have stayed hidden, if the constraints of materialisation would not have been pre-rationalized, but a software would have been available for post-processing arbitrary designed geometry. It is the purpose of fabrication-aware design to make the relations and constraints of material processes explicit and available to the designing architect in order to examine and exploit the process' full potential. While the investigation into the process' architectural application focused mainly on façade systems, the process offers several further application scenarios, which are mentioned in Section 5.3.3.

## 5.2 Contributions

The thesis has demonstrated that the integration of digital design and simulation techniques with adaptive control strategies can foster the creation of unique and differentiated formal vocabularies in the design and production of architectural formwork components. Over the course of development, several topics have been investigated that are generally relevant for fabrication-aware design methods and digital fabrication processes with non-linear material behaviour. The following section highlights the contributions of the research.

### 5.2.1 Integrated design and fabrication techniques

The integrated design and fabrication approach allowed to tackle the research project's complex problem of anticipation and control holistically. Issues arising from within the individual research directions could not be treated fully

encapsulated, as discoveries, advancement and changes affected the development in others. These dependencies and relationships however, allowed to tune the parameters and find the balance in the project's development. For example, the simulation calculates an estimation of fabrication parameters, that don't need to be exact, as the fabrication control can cover inaccuracies within a certain range autonomously, but still requires the estimation of input parameters as basis to work properly. Hence, the computational anticipation of the process and its controlled realisation, the digital model and its physical pendant, act complementary.

Defining this threshold of techniques is especially important within the field of digital fabrication in architecture, as it is not mandatory to implement a perfect digital model, but only the abstraction of a process to the extent in which an acceptable precision and a coherency between designed artefact and its fabrication can be provided. The question of how much technology is necessary to achieve a high degree of simulation accuracy, is not only a question of available resources, it is rather a question of how to define the respective soft- and hardware interfaces of the whole design- and fabrication system.

### 5.2.2 Formal peculiarity

*Spatial Wire Cutting* has brought forward a new geometric capability to robotic hot-wire cutting, a particular language of double-curved sweep surface geometry, exemplified through a multitude of cutting samples and façade prototypes. This peculiar geometry would have hardly been discovered within a purely digital design environment and therefore demonstrates the discovery of process inherent form that is possible through digital fabrication technologies.

While a mathematical description and classification of surfaces created by the technique was not the goal of the thesis, an appropriate representation was achieved through the simulation and the force-magnitude/speed colouring on



the simulated surface. This allowed to visualise the physical variables present in the process responsible for the geometrical extension to hot-wire cutting.

### 5.2.3 Material process driven design methods

In the traditional sense of processing methods, it is the tool that modifies and shapes the material. In the *Spatial Wire Cutting* procedure however, tool and material, hot-wire and polystyrene foam, are both being shaped and modified through the interaction with each other and therefore merge the concept of processed material and processing tool.

Contrary to projects with materials that exhibit complex material behaviour by themselves, such as materials with lower viscosity like concrete [17] or clay [123, 124], for *Spatial Wire Cutting* it is the material's processing method that brings forward the complex behaviour of the hot-wire. Within this context, the scope of possible shapes is mostly broader than the range in which the procedure is controllable through digital fabrication technology. Thus, digital fabrication opens up new and complex design spaces that do not possess clearly defined boundaries and need to be explored empirically. For example, during initial material studies some cutting tests were identified as erroneous results (see Fig. 3.28), since the optimal tension force could not be targeted. With increased fabrication control however, these effects could also be used as quality in architectural design.

The thesis contributes to the investigation of material process driven design methods as it presents a method of how process variables can be abstracted and implemented in a design tool that serves both for pre-rationalisation and discovery of form. It limits the design scope to the extent in which fabrication control can be ensured and shifts the focus from the design of form to the geometrical modelling of input parameters (curves). On this basis the simulation calculates the representation of the resulting surface, through which aesthetic qualities and design aspects can be the main concern. Material process driven design methods are methods, which do not necessarily

describe exact geometry but constraints and rules that create geometry. Ultimately, this thesis has demonstrated that non-linear material behaviour and its mastering with digital fabrication technology can enhance architectural design and become a constituent driver for it.

### 5.3 Future work

The presented research investigated the potential of the robotic hot-wire cutting process *Spatial Wire Cutting* and has outlined some of the architectural implications of an integrated design, simulation and fabrication approach. Within the scope of this thesis, several arising questions and problems could be identified that yield potential for further investigation. One of the main challenges for future development is reducing the deviation between digitally simulated surface and physically fabricated artefact. There are multiple, also combinable, approaches to tackle this problem, which are identified below.

#### 5.3.1 Robotic setup and adaptive control

The experimental setup with two off-the-shelf robotic arms equipped with customized end-effectors served well for the scope of this research. However, it has to be noted that this setup implies some restrictions and creates problems that eventually could be reduced. For example, the shape of the hot-wire and the engaged wire length is, amongst others, influenced by the distance between the two end-effectors attached to the robotic arms. The length of the heated hot-wire throughout the cutting procedure is constant and has a little leeway through the fixed physical spring, which reduces or expands its length according to the acting force. Additionally, the required constant tension force throughout the procedure is difficult to maintain if the path curves exhibit high-curvature, leading to joint acceleration problems. This could be avoided through pre-rationalisation in the design tool, but it would constrain the design space. Another option would comprise an end-effector with a force-sensitive spool that winds and unwinds the hot-wire

according to the measured force. This would replace the physical spring, increase the design space, as the hot-wire length could vary within the process, and would bridge critical high curvature sections of the path curves. Another idea worth investigating could also be a dynamic, but stationary tool, coupled with the movement of the foam-block, as applied for example in the in FFTLOM project (see Section 2.1.2.2) and likewise in the BladeRunner project (see Section 2.1.3.2).

As mentioned in Section 3.2.4, mainly to constrain the scope of investigation, it was decided to keep the heat input constant. With respect to further research into cutting mechanics, the analysis and integration into design logics of a combined dynamic modulation of both the heat input and the cutting speed could be beneficial as it would also increase the design space and would solve joint acceleration issues. Heat input control has for example been investigated by Brooks [39, p. 111] to maintain a constant temperature at the entry situation and consequently constant kerf width and surface quality.

The reduction of the deviation between digitally simulated surface and physically fabricated artefact has to be approached from multiple directions. A first step could be the extension of the fabrication control towards adaptively adjusting the path curves in order to fulfil the estimated tangent vectors alongside the speed modulation. This wouldn't solve the deviations on the inner surface, but the deviations of the common edges of adjacent building elements. The current control setup with the implemented piecewise sending of path information would actually already allow for this, but has been not tested within the scope of the thesis. Another option to reduce tolerances would be to feedback the captured data into the algorithmic design framework, which recomputes and updates the fabrication parameters for the successive cutting procedures. With increased performance of the simulation, this concept could also be applied online within the cutting procedure, constantly re-simulating and adjusting the path curves, in order to respond to the inevitable accumulation of deviations.

### 5.3.2 Modelling of physical behaviour

In this thesis stochastic data modelling was used to learn from the captured data of the physical process: Based on several cutting iterations with different parameter settings, a material dependent model of relationships between heat input, speed and resulting cutting force was developed; analogous to Bain (see Section 3.2.3). This model was integrated in an equation describing the force distribution for a curved hot-wire, which was evaluated (see Section 3.4.1) and laid the basis for the simulation. As previously mentioned, the cutting force model is an approximation and may fit best for steady-state conditions with constant temperature along the wire in the foam. The *SWC* process is based on a sweeping motion, a continuous interaction with the material, the anticipation of which must be accurate since small inaccuracies sum up along the process. It is therefore necessary, to tackle the problem of harmonizing digital model and physical artefact either in the actual fabrication, as mentioned before, or, improve the underlying model of the simulation. Another approach to learn from data is machine learning, which comprises algorithms that learn from data without relying on rule-based programming. With increasing data set, the data model becomes more accurate [125] and could possibly cover the complexity of the process in a more comprehensive way. However, for the algorithmic model to work properly, not only sufficient learning data would be necessary, but a method that would capture the shape of the wire within the material in real-time. As such, the relation between process data and geometry creation would be more direct and would not only support the simulation, but could be used as online feedback in the fabrication. Furthermore, this method could also serve to produce new data sets automatically, for example to learn the hot-wire's behaviour of cutting a polystyrene foam with different material properties and to successively calibrate the design- and fabrication system thereon.

### 5.3.3 Surface classification, design tool and application

Central design focus throughout the realised student workshops and the elective course was the exploration of the individual cut elements' typology, from which a design logic for larger assemblies was developed. While this bottom-up design logic allowed to identify the particularity of the *SWC* process in an explorative manner, in view of further development the implementation of a design rationalising software could be targeted, in which arbitrary surfaces could be optimally approximated into *SWC* feasible geometries. One prerequisite for this implementation would be the analytic representation of the *SWC* curve, which creates the sweep surface through its continuous motion and alternation. This would also serve as the basis for a mathematical classification of surfaces created by the technique. In order to rationalize an arbitrary CAD surface it must be segmented into patches by finding curves on the surface that can be fitted to *SWC* curves. This would probably be the biggest challenge of such an implementation since the *SWC* curve is not planar and therefore strategies, as documented for example in [56] and [126], could not be directly transferred. However, once found, new surfaces could be obtained by interpolating the control parameters of these curves.

Such a design rationalising software would allow the designer to go back and forth between design intent and feasibility. Generally, the design tool could be improved through increased performance, enhanced intuitive handling and the visualisation of relevant fabrication data. Moreover, surface analysis and investigations of how to reach continuity between *SWC* surfaces are necessary, for example through flipping the cutting direction, as investigated by one group in the Summerschool (see Section 4.2.2).

Departing from the formal explorations into architectural elements such as façade systems (see Section 4.2), future applications could address the fabrication of volumetric, interlocking components which are three-dimensionally hold in place during assembly (see Section 2.1.3). Furthermore, obvious

applications would comprise formwork for concrete structures and lost formwork for composite elements. With a bigger robotic setup, the size of these elements can also be increased, since the upscaling of the process in the Summerschool (see Section 4.2) was performed without any problems. Additionally, the use of other polystyrene foams or hot-wire materials is certainly possible, substantiated through Bain's investigation of different foams and cutting tools [41, p. 177]. Besides the architectural application, the transferability of the process' cutting concept towards other material systems, such as wire cutting of clay, could also be investigated in further stages of development.

Hence, the potential of the *Spatial Wire Cutting* procedure is far from being exploited, many of the described open-ended concepts could be investigated and pursued. The procedure is one of potentially numerous digital fabrication techniques that reasonably combine production efficiency and formal discovery by giving materiality a leading role in the design- and fabrication process. Inherent to these digital fabrication processes is an optimised correlation between action and re-action, between material, machine and designed form, and it is exactly there, where the potential of the integrated digital and physical manipulation unfolds.

# List of Figures

1.1	Illustration of the <i>SWC</i> cutting procedure: Two robotic arms are modulating the curvature of the hot-wire, which adopts itself against the resistance of the processed material. Source: [12]	3
1.2	Diagram visualizing the applied methodology. Source: Author.	5
2.1	Developable ruled surfaces. Source: Author.	11
2.2	String surface model of a hyperbolic paraboloid. Source: [23]	11
2.3	Cagliari Contemporary Arts Center, Zaha Hadid Architects, Cagliari, Italy, 2006 [28]. Source: Zaha Hadid Architects	13
2.4	Fondation Louis Vuitton, Gehry Technologies, Paris, France, 2014. Source: [29], Image was cropped, licence: <a href="https://creativecommons.org/licenses/by/2.0/">https://creativecommons.org/licenses/by/2.0/</a>	13
2.5	Manual fabrication (left) and photo of the installation <i>EPS grotto</i> (right) from artist Kwangho Lee in collaboration with NAMELESS Architecture, 2013. Source: [30].	14
2.6	Variable Lamination Manufacturing. Source: [32].	15
2.7	Freeform Thick Layered Object Manufacturing (FFTLOM). Source: [36].	16
2.8	Freeform Automated Sculpting Technology (FAST). Source: [40].	17
2.9	Set-up used for fabricating <i>Persicope</i> by Matter Design Studio [42]. Source: Matter Design Studio	18
2.10	Set-up at RMIT Architectural Robotics Lab, workshop by Robots in Architecture [43]. Source: Association for Robots in Architecture	18
2.11	RDM vault, TU Delft, Netherlands, 2012 [44]. Source: TU Delft	19
2.12	The Catenary Pavilion, Gramazio Kohler Research, Langenthal, 2010. Source: Gramazio Kohler Research, ETH Zurich.	19
2.13	Project Opticut: Formwork (left) and casted prototype (right). Source: [49].	20
2.14	Robotic arm cutting large scale moulds at Odico Formworks Robotics [54]. Source: Odico Formworks Robotics	20
2.15	Project Bladerunner: Tri-robot hot-blade cutting configuration (left) and fabricated prototype (right). Source: [56].	21
2.16	Cutting samples fabricated in the feasibility study. Source: Gramazio Kohler Research, ETH Zurich.	22
2.17	Minimal surface of revolution. Source: [74]	25
2.18	Catenoid creation. Source: Author.	25
3.1	The experimental set-up. Source: Gramazio Kohler Research, ETH Zurich	31
3.2	Prototypical tool with linear potentiometer. Source: Author.	33

3.3	a) Prototypical tool with the ATI Nano17 force/torque sensor and b) deflection $\alpha$ from the tool's z-axis calculated with the sensor's measurements. Source: Author. . . . .	34
3.4	Measured tension force and deflection $\alpha$ along one cut. Source: Author. . . . .	35
3.5	Data plot from ten repeated cutting tests, linear potentiometer data in black, ATI Nano17 tool coloured. Source: Author. . . . .	35
3.6	Visualisation of the tool's operating ranges in axes $A$ and $B$ . Source: Author. . . . .	37
3.7	Exploded view of the cardan-joint end-effector. Source: Author. . . . .	38
3.8	Robot example path, specified through poses $\mathbf{P}_{a1}$ to $\mathbf{P}_{a5}$ and respec- tive blend radii $r_2$ to $r_4$ . Source: Author. . . . .	39
3.9	The traffic within the <i>SWC</i> control system. Source: Author. . . . .	40
3.10	Overview of the <i>Control Core</i> 's structure. Source: Author. . . . .	42
3.11	Robot buffer explanation. Source: Author. . . . .	45
3.12	Pose synchronisation with velocity calculation. Source: Author. . . . .	46
3.13	This (pseudo-)synchronization process in the <i>Control Core</i> is called if one of the robots enters the <code>READY_TO_RECEIVE</code> state.. Source: Author. . . . .	46
3.14	Handshake over digital I/Os: Robot $a$ = master, robot $b$ = slave. Source: Author. . . . .	47
3.15	UR program flowchart, focusing on the sub-processes <code>read</code> and <code>move</code> . Source: Author. . . . .	48
3.16	Fabrication process flowchart. Source: Author. . . . .	50
3.17	Feedback control. Source: Author. . . . .	52
3.18	Process data 151213_03B15: In phases with constant speed, such as time stamp 66 to 88, the PID controller works fine, however the out- put is oscillating in phases in which the speed is decreasing. Source: Author. . . . .	52
3.19	Combined feedback and feedforward control. Source: Author. . . . .	53
3.20	Process data 160304_B2140: The feedback-feedforward control starts approximately at time stamp 22. After a balancing phase, which ap- proximately lasts till time stamp 40, the force measurements stay in a range of $\pm 1$ N to the set-point and the speed measurements follow the simulated speed trajectory with no apparent oscillations.. Source: Author. . . . .	53
3.21	Graphic of the hot-wire moving through in the foam block. Source: Author. . . . .	55
3.22	Calculation of the tension force vector $\mathbf{t}_a$ from the tool's measure- ments and calculation of the resulting cutting force $F_{res}$ from tension force vectors $\mathbf{t}_a$ and $\mathbf{t}_b$ (from robot tool $b$ ). Source: Author. . . . .	56
3.23	Process data 150803_D179F: Characteristic cutting force and cutting stages. Source: Author. . . . .	58
3.24	Relationship between tool temperature and cutting force, cp. Brooks figure 1.18. [39]. Source: Author. . . . .	59
3.25	Process data 150803_D179F: From recorded tension forces and an- gles $\alpha$ , the resulting cutting forces $F_{res}$ were calculated and registered in the steady state. Source: Author. . . . .	60
3.26	Model of relation between $Q_{eff}$ and the tension force $T$ in the steady state for an engaged wire length of 400 mm.. Source: Author. . . . .	61



3.27	Model of relation between $Q_{eff}$ and the cutting force $F$ in the steady state per unit of engaged wire length. Source: Author. . . . .	61
3.28	Cutting example with inadequate relation between left and right path-positions in the beginning: high force on left (top in picture) side controls the speed, while the wire at the right (bottom in picture) side melts the foam, since it is moving too slow. Additionally oscillation errors occur (see Section 3.4.1). Source: Author. . . . .	63
3.29	Cutting tests, in which the tension was not at a constant level, leading the material to melt. The resulting surface pattern clearly exhibits the wire's traces, however is hardly controllable. Source: Author. . .	63
3.30	Cutting example in which through joint acceleration limits the tension force could not successfully be targeted resulting into melted material. Source: Author. . . . .	63
3.31	Path curves, synchronized positions on the curves and foam block [12]. Source: Author. . . . .	64
3.32	Simulated hot-wire curves and lofted surface thereof [12]. Source: Author. . . . .	64
3.33	Computational wire representation. Source: Author. . . . .	65
3.34	Photos from the cut surface. The wire's traces cannot be scanned, however are visible with inclined light incidence. Source: Author. . .	67
3.35	Topview of symmetric and asymmetric path curves with phases a) to e). Source: Author. . . . .	68
3.36	1. Defined mapping curves for the force distribution, 2. overlay of wire shape and surface picture, 3. overlay of recorded tension force vector and wire shape. Source: Author. . . . .	69
3.37	Schematic of the simulation algorithm for one iteration step [109]. Source: Author. . . . .	72
3.38	Results from the simulation a) NURBS curves, force vectors at nodes and estimated deflection angles below, b) force magnitude color mapping onto the surface, c) speed value color mapping and speed trajectories below. Source: Author. . . . .	73
3.39	Force magnitudes and speed values of the nodes mapped to color value and displayed on the surface. Source: Author. . . . .	74
3.40	Preliminary simulation: overlapping curves in the entry phase. Source: Author. . . . .	75
3.41	Curve division a) by length, b) by curvature, or c) by arbitrary mapping. Source: Author. . . . .	75
3.42	a) Edge curves, distribution of positions and wire length extension function, b) simulated curves and lofted surface thereof, c) tangential extension of curve to calculate path curves [109]. Source: Author. . .	76
3.43	Multiple simulated surfaces, with randomly created edge-curve pairs as inputs (curves differing in amplitude, frequency, rotation). Source: Author. . . . .	76
3.44	Measured and simulated (dotted) process data (speed and deflection angle) from five cutting tests with different heat inputs $Q_l$ , but the same symmetric path curves. Phases a), b) and c) are indicated. Source: Author. . . . .	78

3.45	Measured and simulated process data (speed and deflection angle) from five cutting tests with different heat input $Q_l$ , but the same asymmetric path curves. Phases d) and e) are indicated. Source: Author. . . . .	79
3.46	Overlay of simulated curves and picture, measured tension force vector at its respective position for process data 151213_FA2A6 and path-curves. Source: Author. . . . .	80
3.47	Details from the overlay between simulated curves and surface picture, from a) entry, b) steady and c) exit phases, see Figure 3.46. Source: Author. . . . .	80
3.48	Overlay of simulated curves and picture, measured tension force vector at its respective position for process data 151214_8BAF4 and path-curves. Source: Author. . . . .	81
3.49	Details from the overlay between simulated curves and surface picture, from phases d) and e) with asymmetric force distribution, see Figure 3.48. Source: Author. . . . .	81
3.50	Input curves for the six simulated surfaces: a), b) edge-curves, c) wire length extension curve and d) resulting engaged wire length. Source: Author. . . . .	83
3.51	Six simulated surfaces with varying edge-curves as inputs, see Figure 3.50 and generated path-curves thereof. Source: Author. . . . .	83
3.52	Force magnitudes of the calculated nodes mapped as color values and visualized on the simulated surfaces. Source: Author. . . . .	84
3.53	Photos from the fabricated objects, 400 x 900 mm (width x length). Source: Author. . . . .	84
3.54	Gaussian curvature analysis on the reconstructed meshes from the 3D-scanned point clouds. Source: Author. . . . .	85
3.55	Process data comparison of 160304_B2140, surface 1). Source: Author.	86
3.56	Point cloud data from the scanning process and simulated surfaces with fabrication deviance mapping. The colours on the surfaces indicate the closest distance to the reconstructed mesh from the point cloud. Source: Author. . . . .	86
3.57	Process data comparison of 160304_F208D and 160304_C9874, surface 2). More comparisons can be found in Appendix B.3.2. Source: Author. . . . .	87
3.58	Comparison between two cuts of the reconstructed meshes from the point clouds. Distances mapped to color and visualized on the surface. Below: histogram of the distances. Source: Author. . . . .	88
3.59	Surface details of cut objects. Source: Gramazio Kohler Research, ETH Zurich. . . . .	89
4.1	Crossed cutting movement, resulting into a slight sigmoid curve. Source: Gramazio Kohler Research, ETH Zurich. . . . .	92
4.2	Variation possibilities on one element: angle, depth and path-curves. Source: Gramazio Kohler Research, ETH Zurich. . . . .	92
4.3	Final prototype of Group 1: The element variations have been parametrically controlled (single element size: 300 x 300 x 300 mm). Source: Gramazio Kohler Research, ETH Zurich . . . . .	93

4.4	Table of path generation: different patterns and path correspondence. Source: Gramazio Kohler Research, ETH Zurich. . . . .	94
4.5	Fabricated objects with three different pattern movements. Source: Gramazio Kohler Research, ETH Zurich. . . . .	94
4.6	Final prototype of Group 2: Assembly of multiple objects fabricated with different pattern movements (element size: 600 x 300 x 200 mm). Source: Gramazio Kohler Research, ETH Zurich . . . . .	94
4.7	Subtle variation of the path-curves' peak, generating slightly differing surfaces. Source: Gramazio Kohler Research, ETH Zurich. . . . .	95
4.8	a), b) Cutting the panel in the longitudinal direction and c) flipping the parts. Source: Gramazio Kohler Research, ETH Zurich. . . . .	95
4.9	Final prototype of Group 3: The panels with varying element size overlapped vertically.. Source: Gramazio Kohler Research, ETH Zurich	95
4.10	Final prototype of Group 4: Hyperbolic paraboloid panels. Source: Gramazio Kohler Research, ETH Zurich. . . . .	96
4.11	Final prototype of Group 5: Variable shadow conditions. Source: Gramazio Kohler Research, ETH Zurich. . . . .	96
4.12	Employed robotic set-up in the Swisspearl® Summerschool 2015. Source: Gramazio Kohler Research, ETH Zurich . . . . .	97
4.13	Workflow: a) manual testing b) computational design c) robotic fabrication, d) manual lamination e) assembly. Source: Gramazio Kohler Research, ETH Zurich . . . . .	98
4.14	Manual testing. Source: Gramazio Kohler Research, ETH Zurich. . .	98
4.15	Lamination process. Source: Gramazio Kohler Research, ETH Zurich.	98
4.16	Conceptual drawing: Two intersecting surfaces. Source: Gramazio Kohler Research, ETH Zurich. . . . .	100
4.17	Photo of manual tests. Source: Gramazio Kohler Research, ETH Zurich. . . . .	100
4.18	Final prototype of Group 1: Double Cuts. Source: Gramazio Kohler Research, ETH Zurich . . . . .	100
4.19	Design concept: edge curves with peaks and valleys. Source: Gra- mazio Kohler Research, ETH Zurich. . . . .	101
4.20	Photo of manual tests, flipping cutting direction. Source: Gramazio Kohler Research, ETH Zurich. . . . .	101
4.21	Final prototype of Group 2: Flipping peaks and valleys. Source: Gramazio Kohler Research, ETH Zurich . . . . .	101
4.22	Design concept: panel and edge curve parameters. Source: Gramazio Kohler Research, ETH Zurich. . . . .	102
4.23	Photo of manual test. Source: Gramazio Kohler Research, ETH Zurich.	102
4.24	Final prototype of Group 3: Waves – hiding vertical connection. Source: Gramazio Kohler Research, ETH Zurich . . . . .	102
4.25	Conceptual drawing and design concept. Source: Gramazio Kohler Research, ETH Zurich. . . . .	103
4.26	Manual test for hyperbolic surfaces. Source: Gramazio Kohler Re- search, ETH Zurich. . . . .	103
4.27	Final prototype of Group 4: Subdivision. Source: Gramazio Kohler Research, ETH Zurich . . . . .	103

4.28 Overview, various final prototypes. Source: Gramazio Kohler Research, ETH Zurich . . . . .	104
A.1 AAG workshop: Manual tests and impressions. Source: Gramazio Kohler Research, ETH Zurich. . . . .	142
A.2 Final column of Group 1: The elements were produced by applying the same path curve on each of the four sides of the element. Source: Gramazio Kohler Research, ETH Zurich . . . . .	143
A.3 Final column of Group 2: The elements were produced by applying the same path curve on each of the four sides of the element. Source: Gramazio Kohler Research, ETH Zurich . . . . .	143
A.4 Final column of Group 3: The elements were produced by cutting twice on each of the four sides of the column, creating surface intersections. Source: Gramazio Kohler Research, ETH Zurich . . . . .	144
A.5 Final column of Group 4: The elements were cut along the transverse direction of the column through a single cut. Source: Gramazio Kohler Research, ETH Zurich . . . . .	144
B.1 Model of relation between $Q_{eff}$ and tension force $T$ in the steady state for engaged wire lengths of 400 (left) and 500 mm (right).. Source: Author. . . . .	145
B.2 Model of relation between $Q_{eff}$ and cutting force $F$ in the steady state per unit of engaged wire length $l_f$ . Tests with $l_f = 400$ in grey, $l_f = 500$ in black.. Source: Author. . . . .	146
B.3 Measured and simulated process data (speed and deflection angle) from symmetric cutting test 151209_36769 with $Q_l$ 68.79, deflection 0.48. Phases a) to c) are indicated. Source: Author. . . . .	148
B.4 Measured and simulated process data (speed and deflection angle) from symmetric cutting test 151209_BF986 with $Q_l$ 67.97 and deflection 0.58. Phases a) to c) are indicated. Source: Author. . . . .	148
B.5 Measured and simulated process data (speed and deflection angle) from symmetric cutting test 151209_BF986 with $Q_l$ 71.69 and deflection 0.68. Phases a) to c) are indicated. Source: Author. . . . .	149
B.6 Measured and simulated process data (speed and deflection angle) from symmetric cutting test 151213_7E043 with $Q_l$ 66.42 and deflection 0.48. Phases a) to c) are indicated. Source: Author. . . . .	149
B.7 Measured and simulated process data (speed and deflection angle) from five cutting tests with different heat inputs $Q_l$ , but the same asymmetric path curves with deflection 0.48. Phases d) and e) are indicated. Source: Author. . . . .	150
B.8 Measured and simulated process data (speed and deflection angle) from five cutting tests with different heat inputs $Q_l$ , but the same asymmetric path curves with deflection 0.58. Phases d) and e) are indicated. Source: Author. . . . .	151
B.9 Measured and simulated process data (speed and deflection angle) from five cutting tests with different heat inputs $Q_l$ , but the same asymmetric path curves with deflection 0.68. Phases d) and e) are indicated. Source: Author. . . . .	152

B.10 Overlay of simulated curves and picture, measured tension force vector at its respective position for process data 151213_78891 and path-curves (deflection 0.58). Source: Author. . . . .	153
B.11 Overlay of simulated curves and picture, measured tension force vector at its respective position for process data 151213_4D92E and path-curves (deflection 0.78). Source: Author. . . . .	153
B.12 Overlay of simulated curves and picture, measured tension force vector at its respective position for process data 151209_36769 and path-curves (deflection 0.48). Source: Author. . . . .	154
B.13 Overlay of simulated curves and picture, measured tension force vector at its respective position for process data 151211_AB87E and path-curves (deflection 0.68). Source: Author. . . . .	154
B.14 Comparison between process data of 160304_B2140 and simulated values, surface 1). Source: Author. . . . .	155
B.15 Comparison between process data of 160313_5017B and simulated values, surface 2). Source: Author. . . . .	155
B.16 Comparison between process data of 160304_C9874 and simulated values, surface 3). Source: Author. . . . .	156
B.17 Comparison between process data of 160304_369E5 and simulated values, surface 4). Source: Author. . . . .	156
B.18 Comparison between process data of 160313_03E5B and simulated values, surface 5). Source: Author. . . . .	157
B.19 Comparison between process data of 160306_CEE87 and simulated values, surface 6). Source: Author. . . . .	157
B.20 Process data comparison of cuts 160304_17295 and 160304_B2140, surface 1). Source: Author. . . . .	158
B.21 Process data comparison of cuts 160313_7C529 and 160313_5017B, surface 2). Source: Author. . . . .	158
B.22 Process data comparison of cuts 160304_C9874 and 160313_C2CEF, surface 3). Source: Author. . . . .	159
B.23 Process data comparison of cuts 160304_4C58B and 160304_680DB, surface 4). Source: Author. . . . .	159
B.24 Process data comparison of cuts 160305_314D1 and 160313_03E5B, surface 5). Source: Author. . . . .	160
B.25 Process data comparison of cuts 160306_CEE87 and 160306_BC582, surface 6). Source: Author. . . . .	160



# List of Tables

3.1	Input parameter values for developing the cutting force model . . . .	60
3.2	Input parameter values for the symmetric path curves . . . . .	68
3.3	NRMSD of speeds $v_a$ , $v_b$ and angles $\alpha_a$ , $\beta_a$ , $\alpha_b$ , $\beta_b$ . . . . .	85
B.1	Results of the computed steady state for measured angles $\alpha$ , tension forces $T$ , resulting cutting forces $F_{res}$ for an engaged wire length of 400 mm and cutting force $F$ per unit of engaged wire length. . . . .	145
B.2	Results of the computed steady state for measured angles $\alpha$ , tension forces $T$ , resulting cutting forces $F_{res}$ for an engaged wire length of 500 mm and cutting force $F$ per unit of engaged wire length. . . . .	146
B.3	Tests with symmetric path curves, NRMSD calculation in phases b) and c) of speed $v$ and angle $\alpha$ . . . . .	147
B.4	Tests with asymmetric path curves (400 mm foam block width), NRMSD calculation in phase e) of speeds $v_a$ , $v_b$ and angles $\alpha_a$ , $\alpha_b$ . .	147





# List of Symbols

## Process description

$I$	electric current
$R$	electric resistance
$V$	voltage
$Q$	heat input, $Q = I^2 R$
$l$	length of hot-wire [m]
$l_f$	engaged wire length [mm]
$v$	speed [mm/s], resp. $v_a, v_b$ for robots $a$ and $b$
$\mathbf{v}$	velocity, resp. $\mathbf{v}_a, \mathbf{v}_b$
$Q_l$	heat input per unit length of hot-wire, $Q_l = \frac{Q}{l}$ , [W/m]
$Q_{eff}$	effective heat input (area specific), $Q_{eff} = \frac{Q_l}{0.001v}$ , [J/m <sup>2</sup> ]
$T_{opt}$	optimal tension force [N]
$T$	tension force [N], resp. $T_a, T_b$ for robots $a$ and $b$
$\mathbf{t}$	tension force vector, resp. $\mathbf{t}_a, \mathbf{t}_b$ for robots $a$ and $b$
$F$	cutting force per unit of engaged wire length [N/mm]
$F_{res}$	resulting cutting force [N] acting on the whole wire length
$\mathbf{P}$	path positions, resp. $\mathbf{P}_a, \mathbf{P}_b$ for robots $a$ and $b$
$\alpha$	angle about Cardan joint axis $A$ , resp. $\alpha_a, \alpha_b$ for robots $a$ and $b$
$\beta$	angle about Cardan joint axis $B$ , resp. $\beta_a, \beta_b$ for robots $a$ and $b$

## Wire shape calculation

$n$	number of nodes
$n_u$	number for free nodes ( $= n - 2$ )
$n_f$	number for fixed nodes ( $= 2$ )
$m$	number of edges ( $= n - 1$ )
$\mathbf{C}_u$	$[m \times n_u]$ , connectivity matrix of $n_u$ free nodes
$\mathbf{C}_f$	$[m \times n_f]$ , connectivity matrix of $n_f$ fixed nodes
$\mathbf{X}_u$	$[n_u \times 3]$ , coordinate matrices of free nodes
$\mathbf{X}_f$	$[n_f \times 3]$ , coordinate matrices of fixed nodes
$\mathbf{Q}_k$	$[m \times m]$ , diagonal matrix of $\mathbf{q}_k$ at iteration index $k$
$\mathbf{S}^{-1}$	$[m \times m]$ , inverted diagonal matrix of the target edge lengths

**Force distribution**

$n$	number of nodes
$i$	node index
$s$	edge length between the nodes, $s = s_i$ , [mm]
$\hat{\mathbf{t}}_i$	unit tangent vector for node $i$
$\hat{\mathbf{f}}_i$	unit force direction for node $i$
$v_i$	speed for node $i$ , [mm/s]

# Bibliography

- [1] A. Picon. “Architecture and the Sciences: Scientific Accuracy or Productive Misunderstanding?” In: *Precisions: Architektur zwischen Wissenschaft und Kunst / Architecture between Sciences and the Arts*. Berlin: Á. Moravánszky and O. W. Fischer, 2008, pp. 48–81. URL: <http://nrs.harvard.edu/urn-3:HUL.InstRepos:4133141>.
- [2] George Legendre. “Mathematics of Space”. In: ed. by George Legendre. Vol. 81. Architectural Design 4. John Wiley & Sons, 2011. Chap. The Mathematics of Sensible Things, pp. 9–17.
- [3] M. Carpo. *The Alphabet and the Algorithm*. Writing Architecture. The MIT Press, 2011.
- [4] A. Mirjan et al. “Designing Behaviour: Materializing Architecture with Flying Machines”. In: *GAM.10, Intuition and the Machine*. Ed. by Technische Universität Graz. Graz Architecture Magazine (GAM). Ambra Verlag, 2014, pp. 236–247. URL: <http://www.gramaziokohler.com/data/publikationen/1063.pdf>.
- [5] F. Gramazio and M. Kohler. *Digital Materiality in Architecture*. Baden: Lars Müller Publishers, 2008.
- [6] M. Carpo. “Revolutions: Some New Technologies in Search of an Author”. In: *Log: Observations on architecture and the contemporary city*. Vol. 15. New York: Anyone Corporation, 2009.
- [7] C. R. Jepsen, M. K. Kristensen, and P. H. Kirkegaard. “Dynamic Double Curvature Mould System”. In: *Computational Design Modeling : Proceedings of the Design Modeling Symposium, Berlin 2011*. Ed. by C. Gengnagel et al. Berlin: Springer, Berlin, Heidelberg, 2011, pp. 291–300. DOI: 10.1007/978-3-642-23435-4\_33. URL: [http://link.springer.com/chapter/10.1007/978-3-642-23435-4\\_33](http://link.springer.com/chapter/10.1007/978-3-642-23435-4_33).
- [8] F. Gramazio et al. “Zero Waste Free-Form Formwork”. In: *Proceedings of the Second International Conference on Flexible Formwork*. Bath, United Kingdom: BRE CICM, University of Bath, 2012, pp. 258–267. URL: [http://fabwiki.fabric-formedconcrete.com/lib/exe/fetch.php?media=switzerland:zero\\_waste\\_free-form\\_formwork.pdf](http://fabwiki.fabric-formedconcrete.com/lib/exe/fetch.php?media=switzerland:zero_waste_free-form_formwork.pdf).
- [9] R. Schipper et al. “Optimization of the flexible mould process for the production of double-curved concrete elements”. In: *Program and Book of Abstracts for the 1st Concrete Innovation Conference (CIC), Oslo 11th-13th of June*. Ed. by Harald Justnes. 2014, p. 88. URL: [http://homepage.tudelft.nl/6w3a0/documents/Schipper2014\\_000.pdf](http://homepage.tudelft.nl/6w3a0/documents/Schipper2014_000.pdf).
- [10] B. Khoshnevis. “Automated construction by contour crafting – related robotics and information technologies”. In: *Automation in Construction* 13.1 (Jan.

- 2004), pp. 5–19. URL: <http://dx.doi.org/10.1016/j.autcon.2003.08.012>.
- [11] Loughborough University. *3D Concrete Printing: an innovative construction process*. Accessed online 05.12.2016. URL: <http://www.freeformconstruction.com/>.
- [12] R. Rust et al. “Spatial Wire Cutting - Cooperative robotic cutting of non-ruled surface geometries for bespoke building components”. In: *Living Systems and Micro-Utopias: Towards Continuous Designing, Proceedings of the 21st International Conference of the Association for Computer-Aided Architectural Design Research in Asia (CAADRIA 2016)*. Ed. by S. Chien et al. Vol. 21. Hong Kong: The Association for Computer-Aided Architectural Design Research in Asia (CAADRIA), Apr. 2016, pp. 529–538. URL: [http://papers.cumincad.org/data/works/att/caadria2016\\_529.pdf](http://papers.cumincad.org/data/works/att/caadria2016_529.pdf).
- [13] A. Kilian. “Design innovation through constraint modeling”. In: *International Journal of Architectural Computing* 4.1 (2006), pp. 87–105.
- [14] G. Semper. *Der Stil in den technischen und tektonischen Künsten oder praktische Ästhetik: ein Handbuch für Techniker, Künstler und Kunstfreunde*. Vol. 1. München F. Bruckmann, 1878. URL: <https://archive.org/details/derstilindentech01sempuoft>.
- [15] F. Otto and B. Rasch. *Finding Form: Towards an Architecture of the Minimal*. Edition Axel Menges; 3rd edition, 1996.
- [16] D. Veenendaal, M. West, and P. Block. “History and overview of fabric formwork: using fabrics for concrete casting”. In: *Structural Concrete - Journal of the fib* 12.3 (2011), pp. 164–177. DOI: 10.1002/suco.201100014.
- [17] E. Lloret et al. “Complex concrete structures: Merging existing techniques with digital fabrication”. In: *Computer-Aided Design* 60 (Mar. 2015), pp. 40–49. URL: <http://dx.doi.org/10.1016/j.cad.2014.02.011>.
- [18] N. Hack and W. V. Lauer. “Mesh-Mould: Robotically Fabricated Spatial Meshes as Reinforced Concrete Formwork”. In: *Made by Robots: Challenging Architecture at a Larger Scale*. Vol. 84. Architectural Design (AD) 3. 2014, pp. 44–53. DOI: 10.1002/ad.1753.
- [19] D. Pigram and W. McGee. “Formation Embedded Design: A methodology for the integration of fabrication constraints into architectural design”. In: *Proceedings of the 31st Annual Conference of the Association for Computer Aided Design in Architecture (ACADIA)*. 2011, pp. 122–131.
- [20] M. Rippmann and P. Block. “New Design and Fabrication Methods for Freeform Stone Vaults Based on Ruled Surfaces”. In: *Computational Design Modeling - Proceedings of Design Modeling Symposium Berlin 2011*. Ed. by C. Gengnagel et al. Springer, Berlin: Springer Berlin Heidelberg, Oct. 2011, pp. 181–189. DOI: 10.1007/978-3-642-23435-4\_21.
- [21] M. Rippmann and P. Block. “Digital Stereotomy: Voussoir geometry for freeform masonry-like vaults informed by structural and fabrication constraints”. In: *Proceedings of the IABSE-IASS Symposium 2011*. London, UK, Sept. 2011.
- [22] W. McGee, J. Feringa, and A. Søndergaard. “Processes for an Architecture of Volume”. In: *Robotic Fabrication in Architecture, Art and Design*. Ed. by J. Braumann S. Brell-Cokcan. Springer, Wien New York, 2012, pp. 62–71.

- [23] *Hyperbolic Paraboloid*. Accessed online 16.05.2018. URL: <http://www.polthier.info/articles/venice/onlineExps/figures/HyperbolicParaboloidFischer.html>.
- [24] M. Burry. “Digital Tectonics”. In: ed. by N. Leach, D. Turnbull, and C. Williams. Wiley-Academy, 2004. Chap. Virtually Gaudí, pp. 23–33.
- [25] J. Burry and M. Burry. “Gaudí and CAD”. In: *ITcon* 11 (2006), pp. 437–446.
- [26] S. Flöry and H. Pottmann. “Ruled Surfaces for Rationalization and Design in Architecture”. In: *Proceedings of ACADIA 2010*. New York: The Cooper Union, 2010, pp. 103–109.
- [27] *Fondation Louis Vuitton Museum*. Accessed online 02.09.2016. URL: <http://www.gehrytech.com/en/projects/4/>.
- [28] *Nuragic and Contemporary Art Museum*. Accessed online 16.05.2018. URL: <http://www.zaha-hadid.com/architecture/nuragic-and-contemporary-art-museum/>.
- [29] *La Fondation Louis Vuitton*. Accessed online 01.03.2017. URL: <https://www.flickr.com/photos/129231073@N06/23087276119/>.
- [30] *EPS grotto*. Accessed online 01.03.2017. 2013. URL: <http://www.kwangholee.com>.
- [31] D.G. Ahn, S.H. Lee, and D.Y. Yang. “Development of transfer type variable lamination manufacturing (VLM-st) process”. In: *International Journal of Machine Tools & Manufacture* 42.14 (2002), pp. 1577–1587. DOI: doi:10.1016/S0890-6955(02)00054-8.
- [32] D.G. Ahn, S.H. Lee, and D.Y. Yang. “A study on the influence of the sloped cutting angle on kerfwidth and part quality in the hotwire cutting of EPS foam for the VLM-s rapid prototyping process”. In: *International Journal of Machine Tools & Manufacture* 43 (2003), pp. 1447–1464. DOI: 10.1016/S0890-6955(03)00170-6.
- [33] B. De Smit, J. J. Broek, and I. Horvath. “Experimental Investigation of Factors Influential for the Flexible Blade Based Prototyping Process”. In: *Proceedings of the 1999 ASME Design Engineering Technical Conference*. Vol. 4. New York, N.Y: American Society of Mechanical Engineers, 1999, pp. 181–192.
- [34] J.J. Broek et al. “Free-form thick layer object manufacturing technology for large-sized physical models”. In: *Automation in Construction* 11.3 (2002), pp. 335–347. DOI: doi:10.1016/S0926-5805(00)00108-4.
- [35] H. Broek, I. Horváth, and B. de Smit. “Exploration of influential parameters for speed control of the flexible blade cutting process”. In: *Tools and Methods of Competitive Engineering (TMCE) 2002*. Ed. by I. Horvath, P. Li, and J.S.M. Vergeest. Huazhong University of Science and Technology (HUST), Wuhan, China: HUST Press, 2002, pp. 783–794.
- [36] B. De Smit et al. “Developing a Tool for the Direct Cutting of Freeform Surfaces out of Extruded Polystyrene Foam”. In: *Euro-u Rapid 2002 Conference*. 2002. URL: <http://citeseerx.ist.psu.edu/viewdoc/summary?doi=10.1.1.59.1593>.

- [37] B. De Smit et al. "Validating algorithms for calculation of the shape of a flexible blade". In: *International Journal of Machine Tools & Manufacture* 46.7-8 (2006), pp. 890–900. DOI: [10.1016/j.jmpt.2006.05.003](https://doi.org/10.1016/j.jmpt.2006.05.003).
- [38] D. Aitchison et al. "An investigation into the prediction of the optimal machining conditions for polystyrene form cut with a taut hot-wire". In: *The annals of "Dunarea de Jos" University of Galati, Fascicle V, Technologies in Machine Building* (2006), pp. 19–24.
- [39] H. Brooks. "Plastic Foam Cutting Mechanics for Rapid Prototyping and Manufacturing Purposes". PhD thesis. Christchurch, New Zealand: University of Canterbury, 2009.
- [40] H. L. Brooks and D. R. Aitchison. "Force feedback temperature control for hot-tool plastic foam cutting". In: *Proceedings of the Institution of Mechanical Engineers, Part B: Journal of Engineering Manufacture*. 2010, pp. 709–719. DOI: [10.1243/09544054JEM1717](https://doi.org/10.1243/09544054JEM1717).
- [41] J. Bain. "Thermomechanical Hot Tool Cutting and Surface Quality in Robotic Foam Sculpting". PhD thesis. Christchurch, New Zealand: University of Canterbury, 2011.
- [42] Matter Design Studio. *Periscope: Foam Tower*. Accessed online 01.03.2017. URL: <http://www.matterdesignstudio.com/periscope/>.
- [43] *RMIT Architectural Robotics Lab*. Accessed online 01.03.2017. URL: <http://architecturalrobotics.org/post/104455795522/hotwire-foam-cutting-stack-it-workshop-with-robots>.
- [44] *RhinoVAULT and fabrication based design workshop*. Accessed online 16.05.2018. 2012. URL: <http://www.rok-office.com/projects/dragon-skin-vault-1017>.
- [45] P. F. Yuan, H. Meng, and P. Devadass. "Performative Tectonics - Robotic Fabrication Methodology Towards Complexity". In: *Robotic Fabrication in Architecture, Art and Design 2014*. Ed. by W. McGee and M. Ponce de Leon. Springer International Publishing, 2014. DOI: [10.1007/978-3-319-04663-1\\_12](https://doi.org/10.1007/978-3-319-04663-1_12).
- [46] T. Schwartz. *Automated FoamDome #2*. Accessed online 23.12.2016. URL: [http://thibaultschwartz.com/?g1\\_work=automated-foamdome-2synthetic-2012](http://thibaultschwartz.com/?g1_work=automated-foamdome-2synthetic-2012).
- [47] W. McGee and B. Clifford. "Periscope: Foam Tower". In: *FABRICATE: Making Digital Architecture*. Ed. by R. Glynn and B. Sheil. Riverside Architectural Press, 2011, pp. 76–79.
- [48] F. Gramazio, M. Kohler, and J. Willmann. *The Robotic Touch - How Robots Change Architecture*. Park Books, 2013.
- [49] J. Feringa and A. Søndergaard. "Fabricating Architectural Volume - Stereotomic Investigations in Robotic Craft". In: *Fabricate: Negotiating Design and Making*. Ed. by F. Gramazio, M. Kohler, and S. Langenberg. Zurich, Switzerland: gta-Verlag, 2014, pp. 76–83.
- [50] P. F. Martins et al. "Expanding the Material Possibilities of Lightweight Prefabrication in Concrete Through Robotic Hot-Wire Cutting". In: *Real Time - Proceedings of the 33rd eCAADe (Education and research in Computer Aided Architectural Design in Europe) Conference - Volume 2*. Ed. by

- B. Martens et al. Vol. 2. Vienna University of Technology, Vienna, Austria, Sept. 2015, pp. 341–351.
- [51] M. Stavric and M. Kaftan. “Robotic Fabrication of Modular Formwork for Non-Standard Concrete Structures”. In: *Digital physicality – Proceedings of the 30th eCAADe conference*. Ed. by H. Achten et al. Vol. 2. 2012, pp. 431–437.
- [52] M. Kaftan and M. Stavric. “Robotic Fabrication of Modular Formwork - An innovative approach to formwork fabrication for non-standard concrete structures”. In: *Open Systems: Proceedings of the 18th International Conference on Computer-Aided Architectural Design Research in Asia (CAADRIA 2013)*. Ed. by R. Stouffs et al. The Association for Computer-Aided Architectural Design Research in Asia (CAADRIA), Hong Kong, and Center for Advanced Studies in Architecture (CASA), Department of Architecture-NUS, Singapore., 2013, pp. 75–84.
- [53] B. Clifford et al. “Variable Carving Volume Casting - A Method for Mass-Customized Mold Making”. In: *Robotic Fabrication in Architecture, Art and Design 2014*. Ed. by W. McGee and M. Ponce de Leon. Springer International Publishing, 2014, pp. 3–15. URL: [https://www.researchgate.net/publication/262637613\\_Variable-Carving-Volume-Casting\\_A-Method\\_for\\_Mass-Customized\\_Mold\\_Making](https://www.researchgate.net/publication/262637613_Variable-Carving-Volume-Casting_A-Method_for_Mass-Customized_Mold_Making).
- [54] Odico. *Odico Technologies*. Accessed online 01.03.2017. URL: <https://odico.dk/technologies>.
- [55] *Odico Formwork Robotics*. Accessed online 02.02.2017. URL: <http://odico.dk>.
- [56] A. Søndergaard et al. “Robotic Hot-Blade Cutting - An Industrial Approach to Cost-Effective Production of Double Curved Concrete Structures”. In: ed. by Dagmar Reinhardt, Rob Saunders, and Jane Burry. *Robotic Fabrication in Architecture, Art and Design 2016*. Sydney: Springer International Publishing, 2016, pp. 151–163. DOI: 10.1007/978-3-319-26378-6\_11. URL: [https://doi.org/10.1007/978-3-319-26378-6\\_11](https://doi.org/10.1007/978-3-319-26378-6_11).
- [57] *Bladerunner*. Accessed online 05.12.2016. URL: <http://gxn.3xn.com/projects/by-name/213-bladerunner>.
- [58] D. Brander et al. “Designing for Hot-Blade Cutting: Geometric Approaches for High-Speed Manufacturing of Doubly-Curved Architectural Surfaces”. In: *Advances in Architectural Geometry 2016*. Ed. by S. Adriaenssens et al. vdf Hochschulverlag AG an der ETH Zürich, 2016, pp. 306–327. DOI: 10.3218/3778-4\_21. URL: <http://vdf.ch/advances-in-architectural-geometry-2016.html>.
- [59] D. Brander et al. “Hot Blade Cuttings for the Building Industries”. In: *Preprint* (2016).
- [60] *Integrales Faserzement Verbund Element (IFVE)*. Accessed online 09.30.2016. URL: [http://www.deplazes.arch.ethz.ch/dplz\\_site/index.php?nav=forschung&id=1](http://www.deplazes.arch.ethz.ch/dplz_site/index.php?nav=forschung&id=1).
- [61] M. Hanak. “Forschungsprojekt: Integrales Faserzement-Verbundelement”. In: *Arch155 Bunt* (June 2010). Eternit (Schweiz) AG, 8867 Niederurnen, p. 34. URL: [http://www.swisspearl.ch/de/Medien/Werkzeitschriften/Arch\\_155\\_de.pdf](http://www.swisspearl.ch/de/Medien/Werkzeitschriften/Arch_155_de.pdf).

- [62] F. Gramazio, M. Kohler, and J. Willmann. *The Robotic Touch – How Robots Change Architecture*. Park Books, 2013, pp. 324–331.
- [63] *Rhinoceros*. Accessed online 02.12.2016. URL: <https://www.rhino3d.com/>.
- [64] V. Helm et al. “Mobile robotic fabrication on construction sites: DimRob”. In: *2012 IEEE/RSJ International Conference on Intelligent Robots and Systems*. Vilamoura, Algarve, Portugal, 2012, pp. 4335–4341.
- [65] K. Dierichs, T. Schwinn, and A. Menges A (2013). “Robotic pouring of aggregate structures: responsive motion planning strategies for online robot control of granular pouring processes with synthetic macro-scale particles”. In: *Robotic fabrication in architecture, art and design*. Ed. by S. Brell-Cokcan and J. Br. Springer Wien New York, 2013, pp. 196–205.
- [66] F. Raspall, F. Amsberg, and S. Peters. “Material Feedback in Robotic Production: Plastic and Elastic Formation of Materials for Reusable Mold-Making”. In: *Robotic Fabrication in Architecture, Art and Design 2014*. Ed. by W. McGee and M. Ponce de Leon. Springer International Publishing Switzerland 2014, 2014, pp. 333–345. DOI: 10.1007/978-3-319-04663-1\_23.
- [67] L. Vasey, I. Maxwell, and D. Pigram. “Adaptive Part Variation: A Near Real-Time Approach to Construction Tolerances”. In: *Robotic Fabrication in Architecture, Art and Design 2014*. Ed. by W. McGee and M. Ponce de Leon. Springer International Publishing Switzerland 2014, 2014, pp. 291–304. DOI: 10.1007/978-3-319-04663-1\_20.
- [68] K.D.D. Willis et al. “Interactive Fabrication: New Interfaces for Digital Fabrication”. In: *Proceedings of the Fifth International Conference on Tangible, Embedded, and Embodied Interaction*. TEI ’11. Funchal, Portugal: ACM New York, NY, USA, 2011, pp. 69–72. DOI: 10.1145/1935701.1935716. URL: <http://doi.acm.org/10.1145/1935701.1935716>.
- [69] K. Dörfler, F. Rist, and R. Rust. “Interlacing - An Experimental Approach of Integrating Digital and Physical Design Methods”. In: *Rob/Arch 2012 - Robotic Fabrication in Architecture, Art and Design*. Ed. by S. Brell-Cokcan and J. Braumann. Vienna: Springer-Verlag Wien, 2012, pp. 82–91. ISBN: 978-3-7091-1465-0. DOI: 10.1007/978-3-7091-1465-0\_7. URL: [http://dx.doi.org/10.1007/978-3-7091-1465-0\\_7](http://dx.doi.org/10.1007/978-3-7091-1465-0_7).
- [70] R. L. Johns. “Augmented Materiality: Modelling with Material Indeterminacy”. In: *Fabricate: Negotiating Design and Making*. Ed. by F. Gramazio, M. Kohler, and S. Langenberg. gta-Verlag, 2014.
- [71] *Procedural Landscapes, ETH Zurich, 2011*. Accessed online 15.12.2016. URL: <http://gramaziokohler.arch.ethz.ch/web/e/lehre/208.html>.
- [72] *Procedural Landscapes 2, ETH Zurich, 2011*. Accessed online 15.12.2016. URL: <http://gramaziokohler.arch.ethz.ch/web/e/lehre/211.html>.
- [73] D. Pigram, I. Maxwell, and W. McGee. “Towards Real-Time Adaptive Fabrication-Aware Form Finding in Architecture”. In: *Robotic Fabrication in Architecture, Art and Design 2016*. 2016, pp. 426–437. DOI: 10.1007/978-3-319-26378-6\_34.
- [74] *Minimal surface of revolution*. Accessed online 16.05.2018. URL: [https://en.wikipedia.org/wiki/Minimal\\_surface\\_of\\_revolution](https://en.wikipedia.org/wiki/Minimal_surface_of_revolution).
- [75] J. Burry and M. Burry. *The New Mathematics of Architecture*. London, United Kingdom: Thames & Hudson Ltd, 2010.



- [76] R. Mong. *The enigma of Robert Hooke*. Accessed online 26.07.2016. Aug. 2016. URL: <https://quantumfrontiers.com/2015/08/31/the-enigma-of-robert-hooke/>.
- [77] E.H. Lockwood. "A Book of Curves". In: Cambridge University Press, 1961. Chap. Chapter 13: The Tractrix and Catenary, pp. 119–124. URL: <http://www.aproged.pt/biblioteca/ABookofCurvesLockwood.pdf>.
- [78] W. H. Meeks III and J. Pérez. "The classical theory of minimal surfaces". In: *Bulletin (New Series) of the American Mathematical Society* 48.3 (2011), pp. 325–407. URL: <http://www.ams.org/journals/bull/2011-48-03/S0273-0979-2011-01334-9/S0273-0979-2011-01334-9.pdf>.
- [79] C. Truesdell. "The influence of elasticity on analysis: The classic heritage". In: *Bulletin (New Series) of the American Mathematical Society* 9.3 (1983), pp. 293–310. URL: <http://projecteuclid.org/euclid.bams/1183551289>.
- [80] W. A. Oldfather, C. A. Ellis, and D. M. Brown. "Leonhard Euler's Elastic Curves". In: *Isis* 20.1 (Nov. 1933), pp. 72–160. URL: <http://www.jstor.org/stable/224885>.
- [81] L. Spuybroek. "The Structure of Vagueness". In: *TEXTILE - The Journal of Cloth and Culture* 3.1 (2005), pp. 6–19. URL: <http://dx.doi.org/10.2752/147597505778052620>.
- [82] K. Linkwitz and H.-J. Schek. "Einige Bemerkungen zur Berechnung von vorgespannten Seilnetzkonstruktionen". In: *Archive of Applied Mechanics* 40.3 (May 1971), pp. 145–158. DOI: 10.1007/BF00532146.
- [83] H.-J. Schek. "The Force Density Method for Form Finding and Computation of General Networks". In: *Computer Methods in Applied Mechanics and Engineering* 3.1 (1974), pp. 115–134. DOI: 10.1016/0045-7825(74)90045-0.
- [84] P. Gallina, R. Mosca, and P. Pascutto. "Optimized Hotwire Cutting Robotic System for Expandable Polystyrene Foam". In: *AMST'05 Advanced Manufacturing Systems and Technology, Proceedings of the Seventh International Conference*. Ed. by E. Kuljanic. Springer Wien New York, 2005, pp. 377–386.
- [85] P. Gallina. "Delayed Reference Control for Hotwire Cutting of Expandable Polystyrene Foam". In: *Journal of Manufacturing Science and Engineering* 128 (Feb. 2006), pp. 360–365. DOI: 10.1115/1.2124990.
- [86] *Sanaa's EPFL Learning Center*. Accessed online 15.12.2016. URL: <http://www.archello.com/en/project/rolex-learning-center/2214240>.
- [87] *Toyo Ito's Meiso No Mori Municipal Funeral Hall*. Accessed online 15.12.2016. URL: <http://architizer.com/blog/architectural-details-toyo-ito/>.
- [88] *Amanda Levet Architects' Spencer Dock Bridge*. Accessed online 15.12.2016. URL: <http://www.nedcam.com/spencer-dock-bridge-dublin.htm>.
- [89] M. Eigensatz et al. "Case Studies in Cost-Optimized Paneling of Architectural Freeform Surfaces". In: *Advances in Architectural Geometry 2010*. Ed. by C. Ceccato et al. Springer Wien New York, 2010, pp. 49–72.
- [90] *Hotwire Direct*. Accessed online 02.02.2017. URL: <http://www.hotwiresystems.com/hot-wire-cnc-foam-cutting-machines-foam-base-arch-cutter/>.
- [91] *Mini CNC Foam Cutter*. Accessed online 15.12.2016. URL: <http://www.instructables.com/id/Mini-CNC-Foam-Cutter/>.

- [92] *Make a CNC Hot-Wire Foam Cutter*. Accessed online 15.12.2016. URL: <http://www.instructables.com/id/Make-a-CNC-Hot-Wire-Foam-Cutter-from-parts-availab/>.
- [93] *KUKA/prc*. Accessed online 07.12.2016. URL: <http://www.robotsinarchitecture.org/kuka-prc>.
- [94] *Robots.IO*. Accessed online 07.12.2016. URL: <https://robots.io>.
- [95] *HAL Robotics | Advanced Machine Simulation, Programming & Control – Innovative robotic systems for industry & construction*. Accessed online 02.08.2016. URL: <http://www.hal-robotics.com>.
- [96] A.S. Day. “An introduction to dynamic relaxation”. In: *The Engineer* 219.5688 (1965), pp. 218–221.
- [97] M. Deuss et al. “ShapeOp - A Robust and Extensible Geometric Modelling Paradigm”. In: *Design Modelling Symposium*. 2015.
- [98] R. Southern. *The force density method: A brief introduction*. Tech. rep. Poole, England: Bournemouth University, 2011. URL: <http://eprints.bournemouth.ac.uk/20650/1/fdm.pdf>.
- [99] K. Dörfler and R. Rust. “Nach vor und zurück. Verschränkung digitaler und physischer Gestaltungsprozesse”. MA thesis. Technische Universität Graz, 2012. URL: [http://archdiploma13.archlab.tuwien.ac.at/1/webmill.php?fx=d&filename=/modulor\\_data/Dokumente/2/00246261\\_m.pdf](http://archdiploma13.archlab.tuwien.ac.at/1/webmill.php?fx=d&filename=/modulor_data/Dokumente/2/00246261_m.pdf).
- [100] K. Dörfler, R. Rust, and F. Rist. “Moderation of Vagueness: Experiments on the Interconnection between Physical and Digital Processes of Form Generation”. In: *GAM.10, Intuition and the Machine*. Ed. by Technische Universität Graz. Graz Architecture Magazine. Ambra Verlag, 2014, pp. 196–205.
- [101] *ATI F/T Sensor: Nano17*. Accessed online 02.02.2017. URL: [http://www.ati-ia.com/products/ft/ft\\_models.aspx?id=Nano17](http://www.ati-ia.com/products/ft/ft_models.aspx?id=Nano17).
- [102] *UR5 Script manual for Software version 1.8*. Accessed online 02.11.2016. URL: [https://s3-eu-west-1.amazonaws.com/ur-support-site/17224/scriptmanual\\_en.pdf](https://s3-eu-west-1.amazonaws.com/ur-support-site/17224/scriptmanual_en.pdf).
- [103] *Axis-angle representation*. Accessed online 21.12.2016. URL: [https://en.wikipedia.org/wiki/Axis%E2%80%93angle\\_representation](https://en.wikipedia.org/wiki/Axis%E2%80%93angle_representation).
- [104] *Grasshopper*. Accessed online 02.02.2017. URL: <http://www.grasshopper3d.com/>.
- [105] *ROS message protocol*. Accessed online 21.12.2016. URL: [http://wiki.ros.org/simple\\_message](http://wiki.ros.org/simple_message).
- [106] A. K. Bondhus, K. Y. Pettersen, and H. Nijmeijer. “Master-Slave Synchronization of Robot Manipulators: Experimental Results”. In: *IFAC Proceedings Volumes*. Vol. 38. 1. 2005, pp. 367–372. URL: <http://dx.doi.org/10.3182/20050703-6-CZ-1902.01331>.
- [107] E. Cicek, J. Dasdemir, and E. Zengeroglu. “Coordinated synchronization of multiple robot manipulators with dynamical uncertainty”. In: *Transactions of the Institute of Measurement and Control* 37.5 (2015), pp. 672–683. DOI: 10.1177/0142331214550520. URL: <http://citeseerx.ist.psu.edu/viewdoc/download?doi=10.1.1.1024.7823&rep=rep1&type=pdf>.
- [108] *ROS industrial UR driver program*. Accessed online 02.02.2017. URL: [https://github.com/ros-industrial/universal\\_robot/blob/indigo-devel/ur\\_driver/prog](https://github.com/ros-industrial/universal_robot/blob/indigo-devel/ur_driver/prog).

- [109] R. Rust, F. Gramazio, and M. Kohler. “Force Adaptive Hot-Wire Cutting: Integrated Design, Simulation, and Fabrication of Double-Curved Surface Geometries”. In: *Advances in Architectural Geometry 2016*. Ed. by S. Adriaenssens et al. Sept. 2016, pp. 288–305. DOI: 10.3218/3778-4\_20.
- [110] D. Veenendaal and P. Block. “An overview and comparison of structural form finding methods for general networks”. In: *International Journal of Solids and Structures* 49.26 (2012), pp. 3741–3753.
- [111] *Leica Nova MS50*. Accessed online 05.12.2016. URL: [http://hds.leica-geosystems.com/en/Leica-Nova-MS50\\_103592.htm](http://hds.leica-geosystems.com/en/Leica-Nova-MS50_103592.htm).
- [112] *ROS wikipedia*. Accessed online 21.12.2016. URL: [https://en.wikipedia.org/wiki/Robot\\_Operating\\_System](https://en.wikipedia.org/wiki/Robot_Operating_System).
- [113] *swissporLAMBDA Vento*. Accessed online 02.02.2017. URL: <http://www.swisspor.ch/index.php?section=datasheet&cmd=productPage&id=61>.
- [114] *Programming guide PS 2000 B*. Accessed online 21.12.2016. URL: [http://www.elektroautomatik.de/files/eautomatik/treiber/ps2000b/programming\\_ps2000b.zip](http://www.elektroautomatik.de/files/eautomatik/treiber/ps2000b/programming_ps2000b.zip).
- [115] *ShapeOp*. Accessed online 20.12.2016. URL: <http://shapeop.org/>.
- [116] *SciPy*. Accessed online 21.12.2016. URL: <https://www.scipy.org/>.
- [117] *Canny Edge Detection in OpenCV*. Accessed online 02.02.2017. URL: [http://docs.opencv.org/trunk/da/d22/tutorial\\_py\\_canny.html](http://docs.opencv.org/trunk/da/d22/tutorial_py_canny.html).
- [118] *Meshlab*. Accessed online 20.12.2016. URL: <http://meshlab.sourceforge.net/>.
- [119] M. Kazhdan, M. Bolitho, and H. Hoppe. In: *Eurographics Symposium on Geometry Processing (2006)*. Ed. by K. Polthier and A. Sheffer. 2006. URL: <http://hhoppe.com/poissonrecon.pdf>.
- [120] *Spatial Wire Cutting, ETH Zurich, 2015, Elective Course*. Accessed online 02.11.2016. URL: <http://gramaziokohler.arch.ethz.ch/web/lehre/e/0/0/0/292.html>.
- [121] *Swisspearl® Summerschool*. Accessed online 21.12.2016. URL: <http://www.swisspearl.ch/de/services/helpdesk/summerschool>.
- [122] D. R. Shelden and A. J. Witt. “Continuity and Rupture”. In: *Mathematics of Space*. Ed. by G. Legendre. Vol. 81. Architectural Design (AD) 4. John Wiley & Sons, 2001, pp. 36–43.
- [123] K. Dörfler et al. “Remote Material Deposition: Exploration of Reciprocal Digital and Material Computational Capacities”. In: *What’s the Matter: Materiality and Materialism at the Age of Computation*. Ed. by M. Voyatzaki. Barcelona, Spain, 2014, pp. 361–377.
- [124] S. Mostafavi et al. “Informed Design to Robotic Production Systems: Developing Robotic 3D Printing System for Informed Material Deposition”. In: *eCAADe 2015: Real Time - Extending the Reach of Computation, Volume 2, Proceedings of the 33rd International Conference on Education and Research in Computer Aided Architectural Design in Europe*. Ed. by B. Martens et al. Vol. 2. 33. eCAADe (Education et al., Sept. 2015, pp. 287–296. URL: [http://papers.cumincad.org/data/works/att/ecaade2015\\_129.content.pdf](http://papers.cumincad.org/data/works/att/ecaade2015_129.content.pdf).
- [125] L. Breiman. “Statistical Modeling: The Two Cultures”. In: *Statistical Science* 16.3 (2001), pp. 199–231. URL: [http://projecteuclid.org/download/pdf\\_1/euclid.ss/1009213726](http://projecteuclid.org/download/pdf_1/euclid.ss/1009213726).

- [126] M. Bartoň, H. Pottmann, and J. Wallner. “Detection and Reconstruction of Freeform Sweeps”. In: *Computer Graphics Forum* 33.2 (May 2014), pp. 23–32. ISSN: 0167-7055. DOI: 10.1111/cgf.12287. URL: <http://dx.doi.org/10.1111/cgf.12287>.
- [127] *Workshop 6: Force-Adaptive Hot-Wire Cutting*. Accessed online 22.02.2017. URL: <http://www.aag2016.ch/workshop-6/>.

# Appendix

## A AAG Workshop 2016

The two-day workshop at the *Advances in Architectural Geometry (AAG)* conference in September 2016 focused on applying the *SWC* technique for the production of polystyrene columns [127].

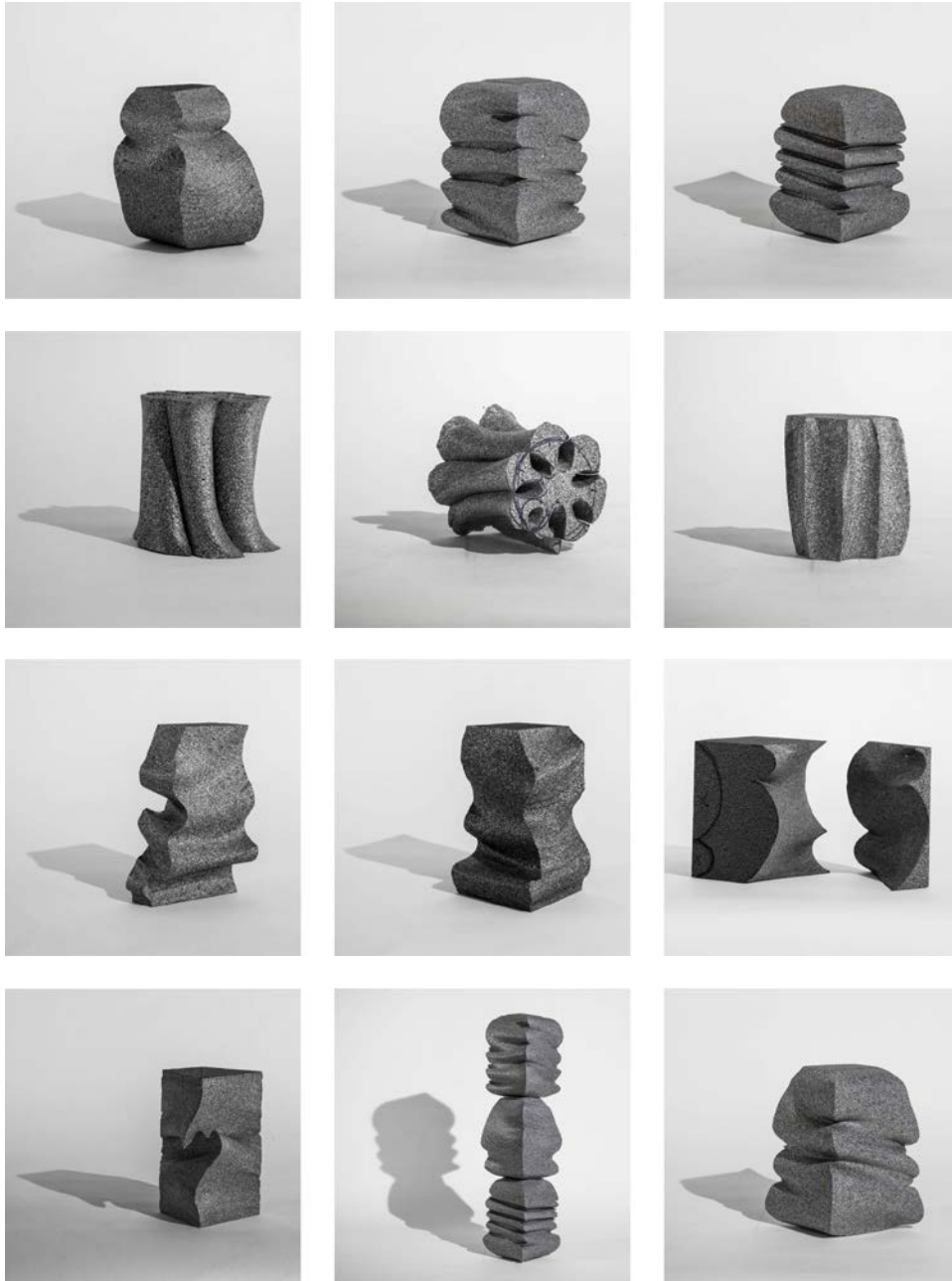
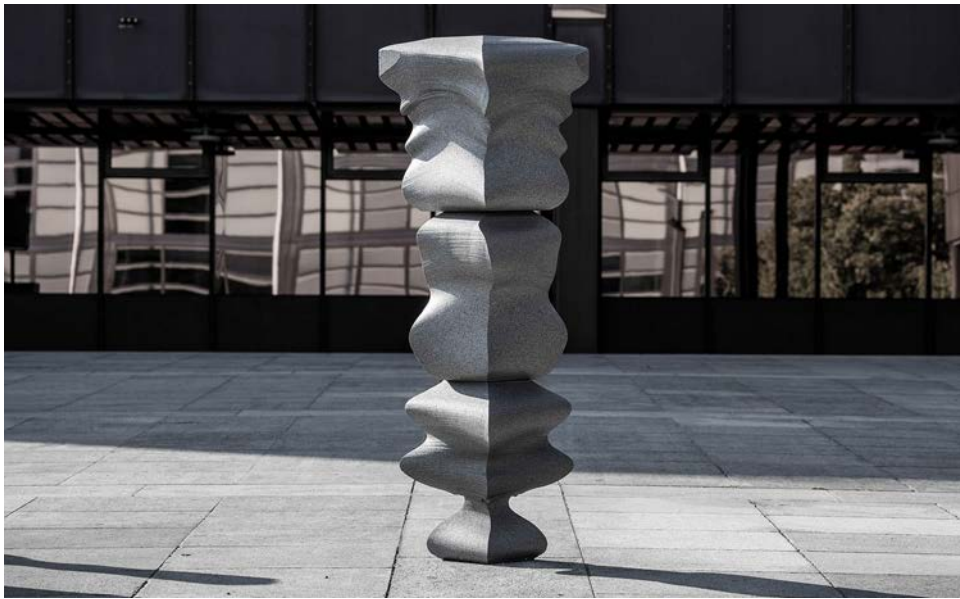


Fig. A.1: AAG workshop: Manual tests and impressions

Similar to the methodology applied in the Swisspearl® Summerschool 2015, the participants explored the technique first through a series of manual tests (see Fig. A.1), using the hand-held hot-wire cutting device. Later, they translated their

concepts into the computational design- and simulation framework to elaborate an overall design concept and parametric model for a stacked column consisting of three to four elements. These elements were hot-wire cut from foam blocks sizing 600 x 600 x 800 mm using the robotic setup from the Summerschool (see Fig. 4.12). Apart from one group, that cut the element along the transverse direction of the column (see Fig. A.5), the elements were produced by cutting on each of the four sides of the column along the longitudinal direction and rotating the foam block to process the successive side.



*Fig. A.2: Final column of Group 1: The elements were produced by applying the same path curve on each of the four sides of the element*

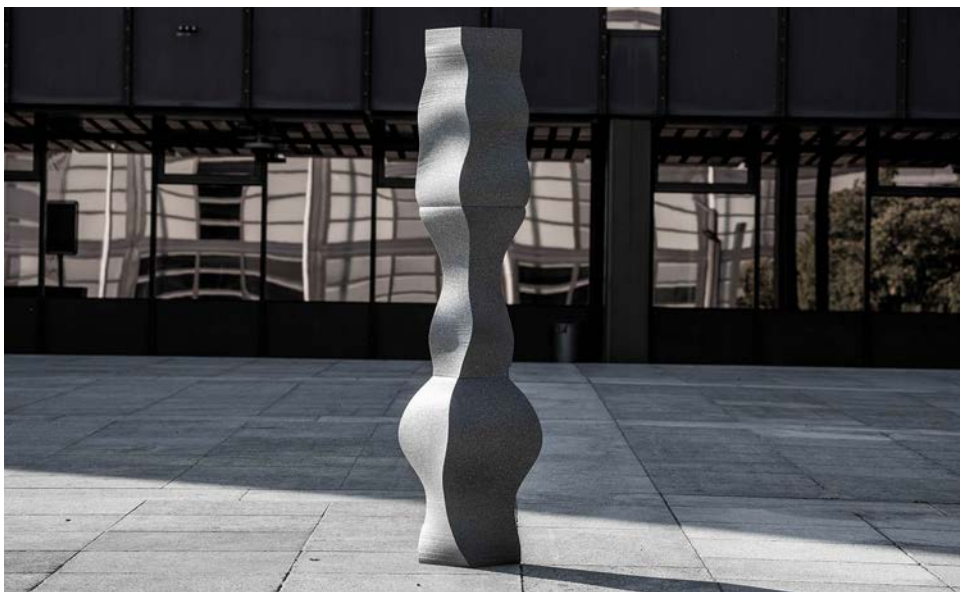


*Fig. A.3: Final column of Group 2: The elements were produced by applying the same path curve on each of the four sides of the element*



*Fig. A.4: Final column of Group 3: The elements were produced by cutting twice on each of the four sides of the column, creating surface intersections*



*Fig. A.5: Final column of Group 4: The elements were cut along the transverse direction of the column through a single cut*



## B Process data

### B.1 Cutting force model

datafile id	$Q_l$ [W/m]	$v$ [mm/s]	$Q_{eff}$ [J/m <sup>2</sup> ]	$\alpha$ [rad]	$T$ [N]	$F_{res}$ [N]	$F$ [mN/mm]
150803_DA293	66.0	15.0	4400	0.124	1.125	0.279	0.696
150803_BB69D	73.0	17.5	4169	0.156	1.827	0.567	1.417
150803_DF370	77.6	17.5	4433	0.126	1.216	0.305	0.763
150803_04DA6	86.5	20.0	4325	0.131	1.240	0.323	0.808
150803_989B6	97.2	20.0	4859	0.079	0.161	0.026	0.064
150803_460D7	95.7	20.0	4783	0.092	0.440	0.081	0.203
150803_6C08A	95.4	22.5	4239	0.178	1.883	0.666	1.666
150803_DF3AB	94.0	22.5	4179	0.194	2.292	0.882	2.204
150803_62413	106.9	22.5	4750	0.090	0.299	0.054	0.135
150803_156E1	104.9	22.5	4663	0.126	0.869	0.218	0.545
150804_6EEA6	63.2	12.5	5056	0.076	0.320	0.048	0.121
150804_8070A	63.8	12.5	5104	0.051	0.010	0.001	0.003
150804_E8956	63.4	12.5	5070	0.051	0.060	0.006	0.015
150804_26C0E	63.8	15.0	4253	0.149	1.986	0.590	1.474
150804_37BBE	63.3	15.0	4218	0.150	2.079	0.620	1.550
150804_471BF	66.7	15.0	4444	0.125	1.414	0.352	0.880
150804_0D8C6	67.4	15.0	4492	0.125	1.193	0.299	0.746
150804_B6E8E	98.0	20.0	4902	0.077	0.442	0.068	0.169
150804_816EC	97.8	20.0	4889	0.077	0.555	0.085	0.213
150804_F7B73	97.3	22.5	4325	0.154	1.543	0.472	1.180
150804_91840	108.7	22.5	4829	0.088	0.308	0.054	0.135
150804_1CF37	108.0	22.5	4799	0.101	0.560	0.113	0.282
150804_3A057	108.5	25.0	4338	0.138	1.339	0.369	0.924
150803_F8BB6	73.2	17.5	4180	0.154	0.868	0.266	0.664
150803_46370	87.1	20.0	4356	0.118	0.800	0.188	0.470
150803_B880C	106.4	25.0	4254	0.153	0.843	0.257	0.643
150803_0C818	104.8	25.0	4192	0.166	0.572	0.189	0.472

Table B.1: Results of the computed steady state for measured angles  $\alpha$ , tension forces  $T$ , resulting cutting forces  $F_{res}$  for an engaged wire length of 400 mm and cutting force  $F$  per unit of engaged wire length.

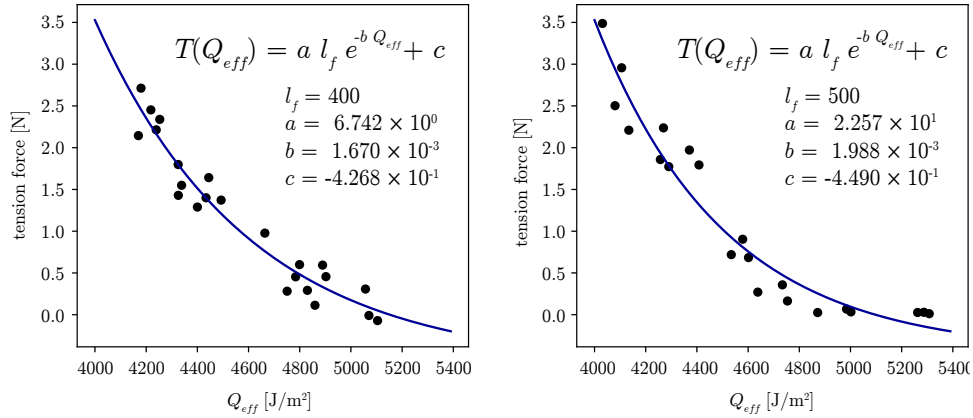


Fig. B.1: Model of relation between  $Q_{eff}$  and tension force  $T$  in the steady state for engaged wire lengths of 400 (left) and 500 mm (right).

datafile id	$Q_t$ [W/m]	$v$ [mm/s]	$Q_{eff}$ [J/m <sup>2</sup> ]	$\alpha$ [rad]	$T$ [N]	$F_{res}$ [N]	$F$ [mN/mm]
150803_745E7	66.1	12.5	5287	0.039	0.029	0.002	0.005
150803_B1437	66.3	12.5	5307	0.026	0.012	0.001	0.001
150803_9B018	66.1	15.0	4408	0.138	1.793	0.493	0.986
150803_7D0C0	65.6	15.0	4370	0.150	1.972	0.590	1.181
150803_DFA0E	74.8	15.0	4984	0.052	0.068	0.007	0.014
150803_E68A1	75.0	15.0	5001	0.052	0.034	0.004	0.007
150803_A28EC	75.1	17.5	4290	0.151	1.773	0.535	1.070
150803_6F18F	74.7	17.5	4269	0.175	2.237	0.779	1.558
150803_6B1D5	83.2	17.5	4753	0.077	0.164	0.025	0.051
150803_AFF71	82.8	17.5	4733	0.077	0.358	0.055	0.111
150803_EA2CD	82.7	20.0	4133	0.178	2.209	0.783	1.565
150803_CB229	82.1	20.0	4105	0.199	2.957	1.170	2.340
150803_D000D	92.1	17.5	5262	0.040	0.027	0.002	0.004
150803_A6750	92.8	20.0	4637	0.101	0.271	0.055	0.109
150803_F5B99	92.0	20.0	4601	0.065	0.684	0.089	0.178
150803_1BD1C	91.6	20.0	4578	0.000	0.904	0.001	0.002
150803_CCEC0	91.8	22.5	4080	0.176	2.503	0.874	1.749
150803_70206	102.0	22.5	4534	0.126	0.719	0.181	0.361
150804_DEF6F	80.6	20.0	4031	0.215	3.487	1.491	2.982
150804_AFC6C	85.3	17.5	4871	0.053	0.026	0.003	0.005
150804_130FD	85.1	20.0	4257	0.200	1.858	0.737	1.474
150803_F03C0	93.4	22.5	4151	0.115	1.203	0.275	0.550
150803_EA560	100.0	22.5	4443	0.169	1.748	0.587	1.175
150803_3B464	98.2	20.0	4909	0.138	0.795	0.219	0.438
150804_33A32	63.4	15.0	4226	0.201	3.554	1.418	2.836
150804_4D74A	63.4	15.0	4229	0.199	3.526	1.393	2.785
150804_7B262	80.9	17.5	4620	0.128	1.267	0.323	0.646
150804_F6ED3	81.1	17.5	4634	0.126	1.091	0.274	0.549
150804_91E7E	80.8	17.5	4618	0.125	1.238	0.309	0.619
150804_3040B	88.9	20.0	4447	0.165	1.796	0.590	1.180
150804_552FD	88.1	20.0	4404	0.191	2.437	0.924	1.848

Table B.2: Results of the computed steady state for measured angles  $\alpha$ , tension forces  $T$ , resulting cutting forces  $F_{res}$  for an engaged wire length of 500 mm and cutting force  $F$  per unit of engaged wire length.

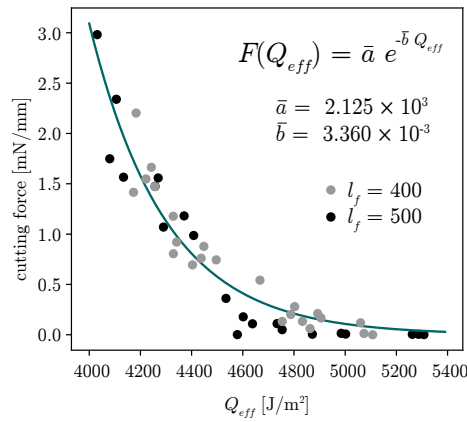


Fig. B.2: Model of relation between  $Q_{eff}$  and cutting force  $F$  in the steady state per unit of engaged wire length  $l_f$ . Tests with  $l_f = 400$  in grey,  $l_f = 500$  in black.

## B.2 Comparative studies N°1

### B.2.1 Process data comparison

datafile id	width	deflection $\alpha$	$Q_l$	NRMSD $v$	NRMSD $\alpha$
151213_BB526	300	0.48	67.1	0.078	0.070
151213_78891	300	0.58	60.2	0.067	0.096
151213_6C49D	300	0.68	68.2	0.053	0.073
151213_4D92E	300	0.78	68.8	0.054	0.056
151209_36769	400	0.48	68.8	0.161	0.139
151209_BF986	400	0.58	68.0	0.146	0.114
151211_AB87E	400	0.68	71.7	0.105	0.095
151211_8E058	400	0.78	68.8	0.069	0.066
151213_7E043	500	0.48	66.4	0.085	0.047
151213_635BC	500	0.58	66.7	0.082	0.046
151213_FA2A6	500	0.68	49.8	0.071	0.027
151213_EAE69	500	0.68	57.7	0.057	0.026
151213_249ED	500	0.68	66.3	0.053	0.027
151213_9850A	500	0.68	75.6	0.047	0.026
151213_A2770	500	0.68	84.3	0.043	0.027
151213_EDF0F	500	0.78	64.7	0.037	0.058
<b>average NRMSD</b>				0.076	0.062

Table B.3: Tests with symmetric path curves, NRMSD calculation in phases b) and c) of speed  $v$  and angle  $\alpha$ .

datafile id	deflection $\alpha$	$Q_l$	NRMSD $v_a$	NRMSD $v_b$	NRMSD $\alpha_a$	NRMSD $\alpha_b$
151214_FCBEF	0.48	52.6	0.048	0.071	0.238	0.233
151214_C131F	0.48	60.9	0.088	0.065	0.231	0.236
151214_CB9A7	0.48	69.4	0.031	0.054	0.223	0.245
151214_C546C	0.48	78.8	0.053	0.056	0.221	0.248
151214_079BA	0.48	88.4	0.041	0.047	0.196	0.244
151214_C0F83	0.58	52.3	0.130	0.064	0.349	0.184
151214_30BB0	0.58	60.4	0.133	0.052	0.335	0.200
151214_53AF7	0.58	68.8	0.143	0.053	0.348	0.199
151214_7CB57	0.58	78.4	0.097	0.069	0.332	0.195
151214_A7EB7	0.58	89.9	0.052	0.064	0.305	0.166
151214_B6849	0.68	53.1	0.130	0.085	0.477	0.129
151214_8BAF4	0.68	61.5	0.088	0.052	0.492	0.131
151214_CEF7B	0.68	69.9	0.087	0.048	0.489	0.135
151214_CD0DC	0.68	79.5	0.159	0.041	0.507	0.141
151214_CFB27	0.68	88.5	0.151	0.056	0.519	0.143
<b>average NRMSD</b>			0.095	0.058	0.351	0.189

Table B.4: Tests with asymmetric path curves (400 mm foam block width), NRMSD calculation in phase e) of speeds  $v_a$ ,  $v_b$  and angles  $\alpha_a$ ,  $\alpha_b$ .

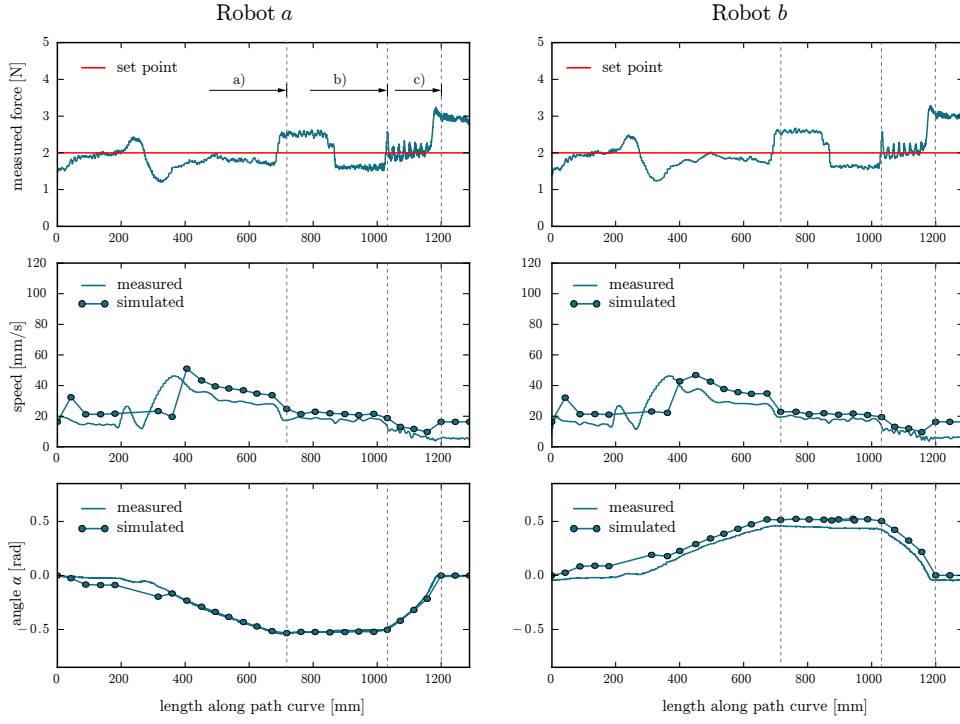


Fig. B.3: Measured and simulated process data (speed and deflection angle) from symmetric cutting test 151209\_36769 with  $Q_l$  68.79, deflection 0.48. Phases a) to c) are indicated

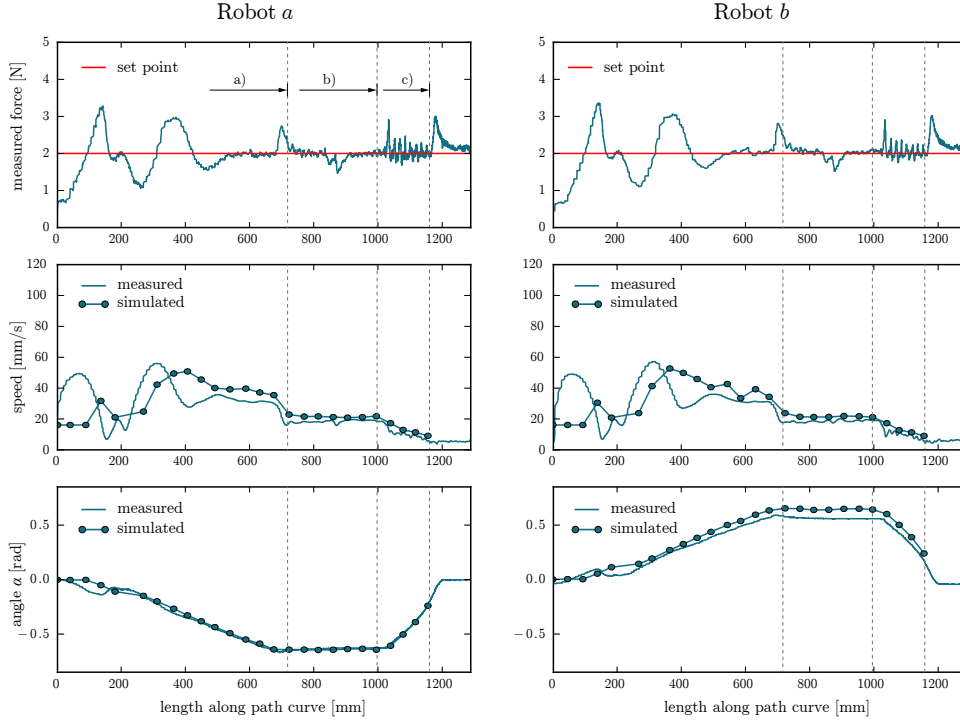


Fig. B.4: Measured and simulated process data (speed and deflection angle) from symmetric cutting test 151209\_BF986 with  $Q_l$  67.97 and deflection 0.58. Phases a) to c) are indicated

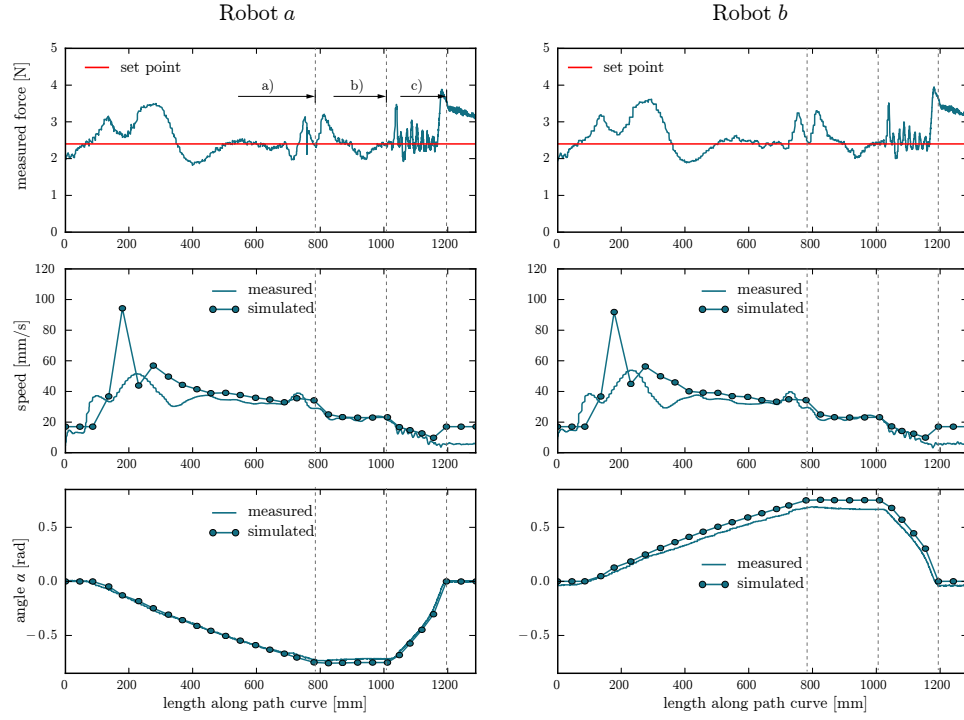


Fig. B.5: Measured and simulated process data (speed and deflection angle) from symmetric cutting test 151209\_BF986 with  $Q_t$  71.69 and deflection 0.68. Phases a) to c) are indicated

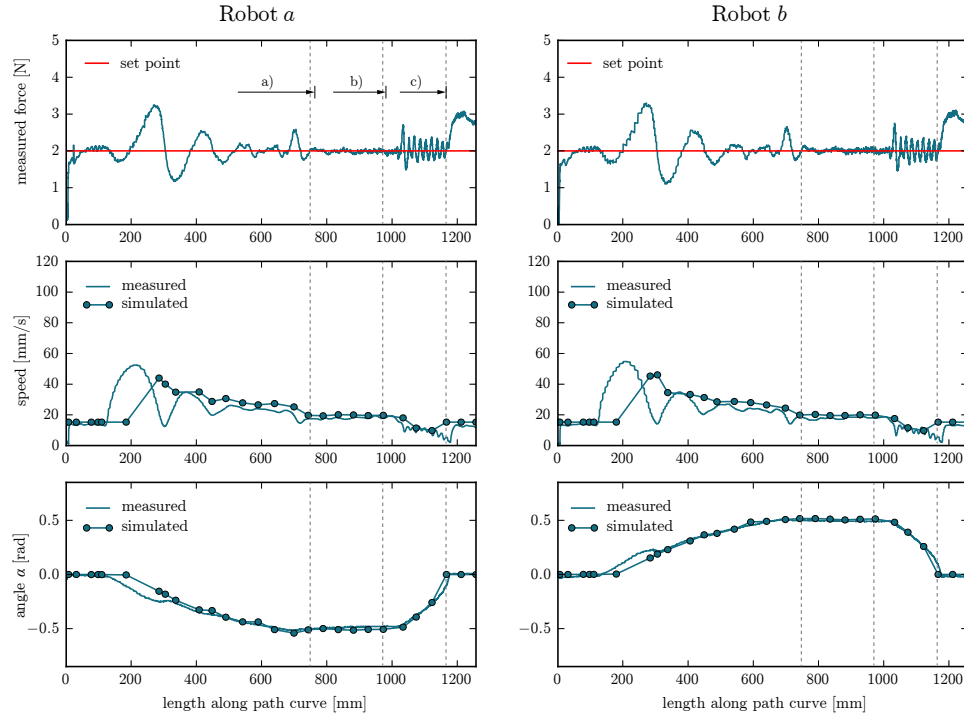


Fig. B.6: Measured and simulated process data (speed and deflection angle) from symmetric cutting test 151213\_7E043 with  $Q_t$  66.42 and deflection 0.48. Phases a) to c) are indicated

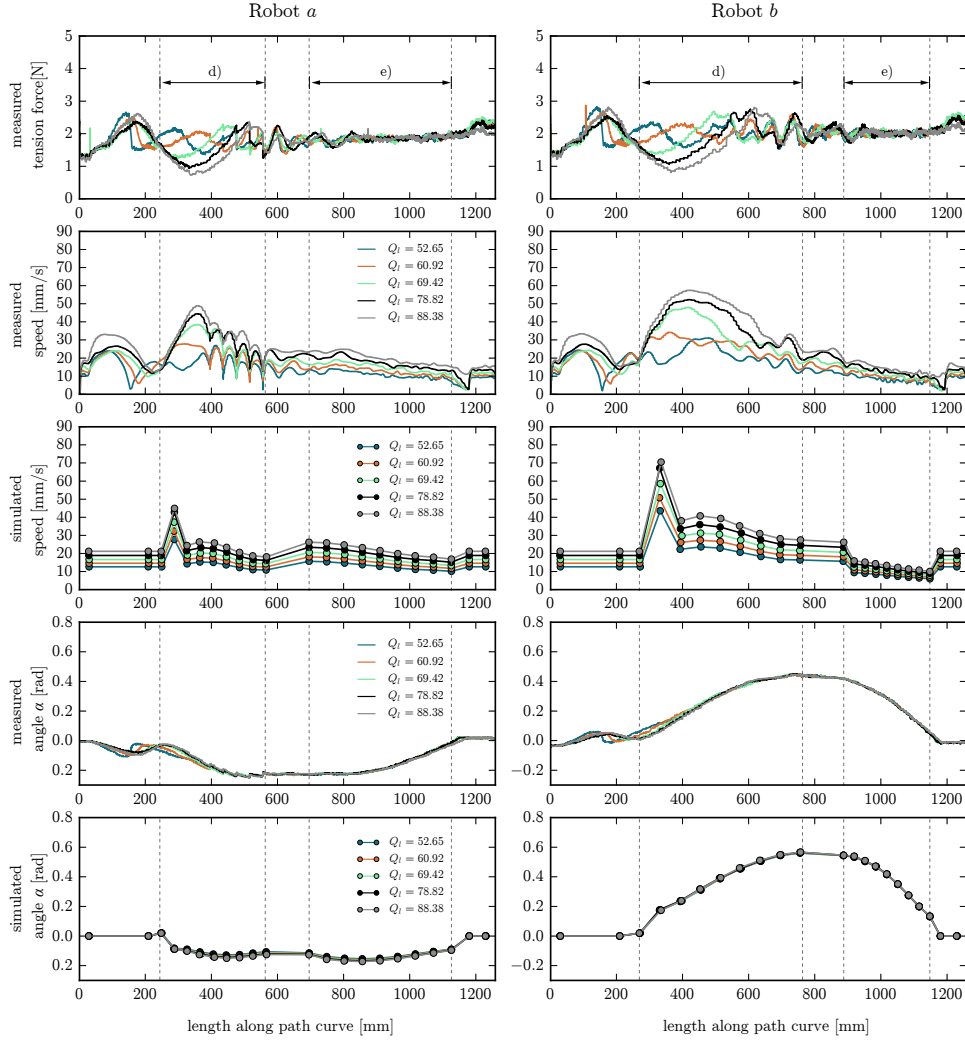


Fig. B.7: Measured and simulated process data (speed and deflection angle) from five cutting tests with different heat inputs  $Q_l$ , but the same asymmetric path curves with deflection 0.48. Phases d) and e) are indicated

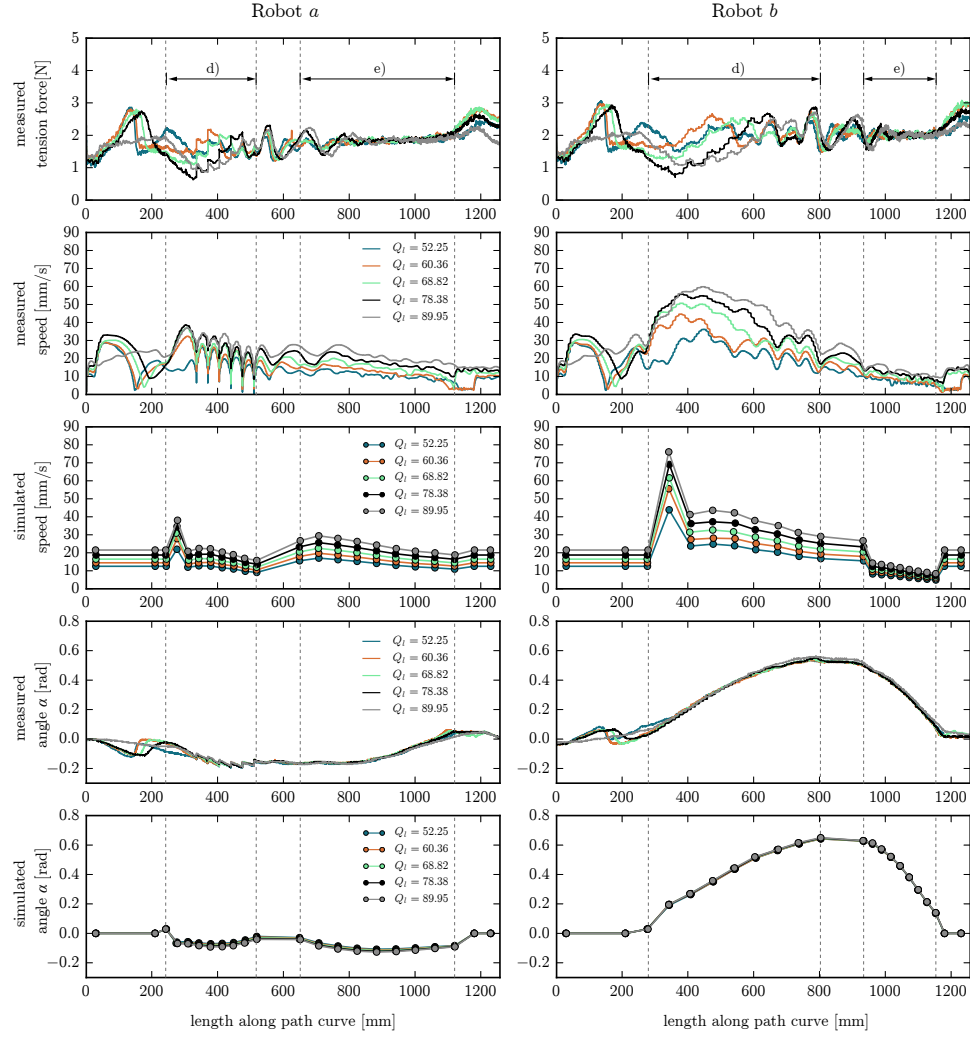


Fig. B.8: Measured and simulated process data (speed and deflection angle) from five cutting tests with different heat inputs  $Q_l$ , but the same asymmetric path curves with deflection 0.58. Phases d) and e) are indicated

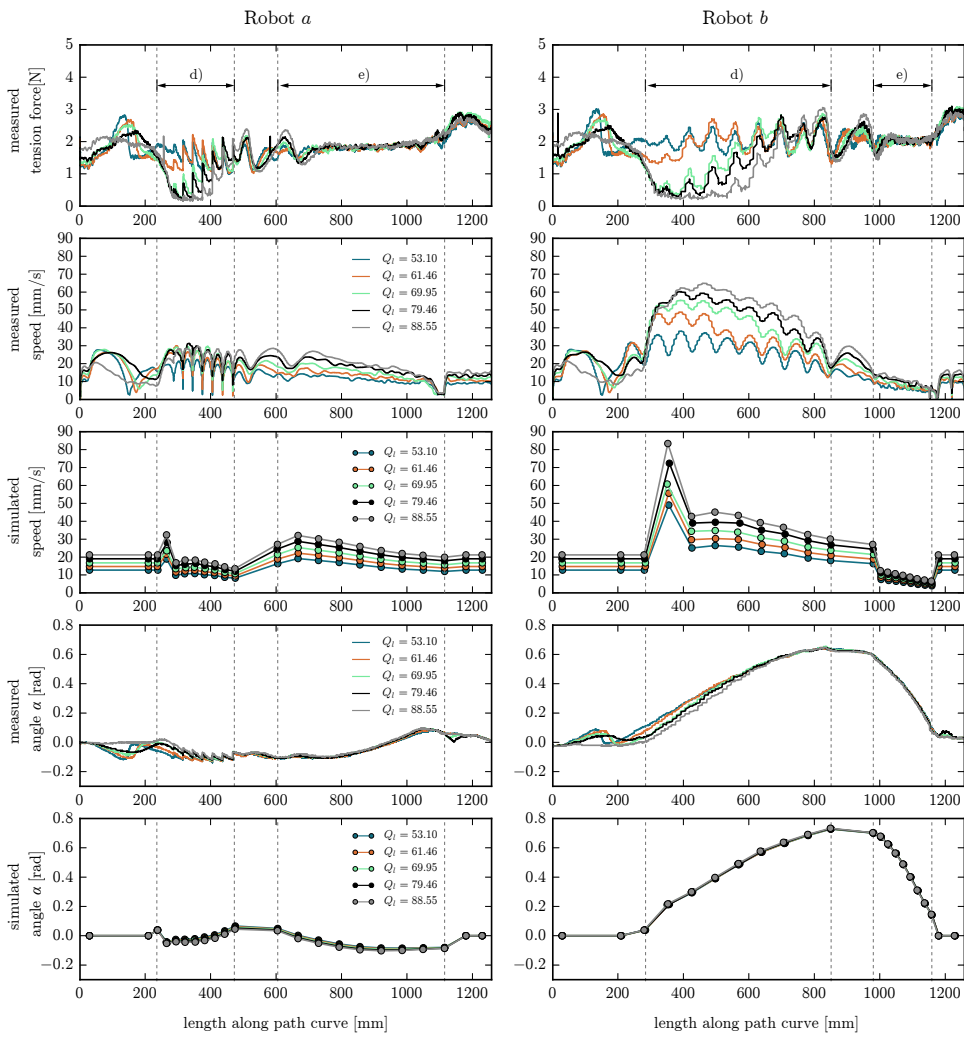


Fig. B.9: Measured and simulated process data (speed and deflection angle) from five cutting tests with different heat inputs  $Q_l$ , but the same asymmetric path curves with deflection 0.68. Phases d) and e) are indicated



### B.2.2 Shape comparison

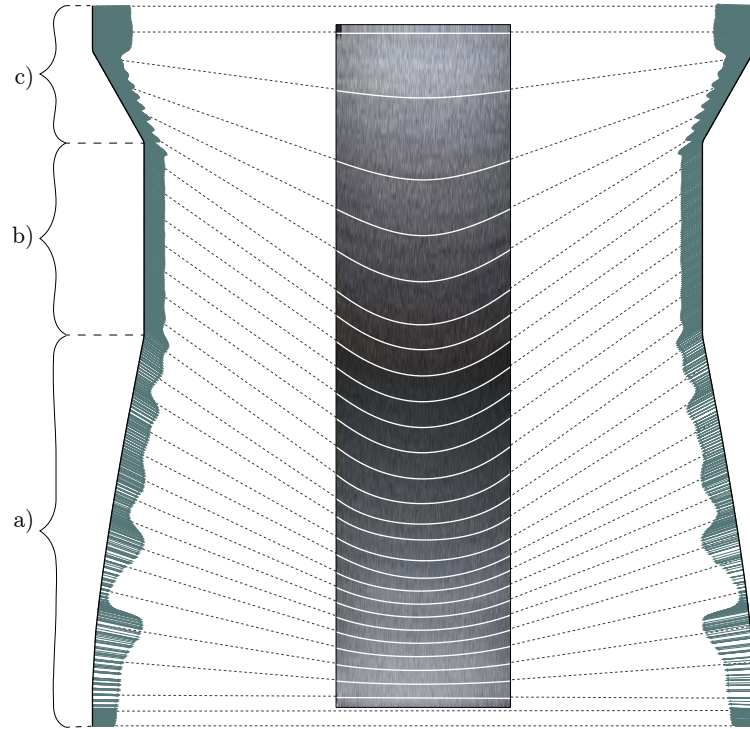


Fig. B.10: Overlay of simulated curves and picture, measured tension force vector at its respective position for process data 151213\_78891 and path-curves (deflection 0.58)

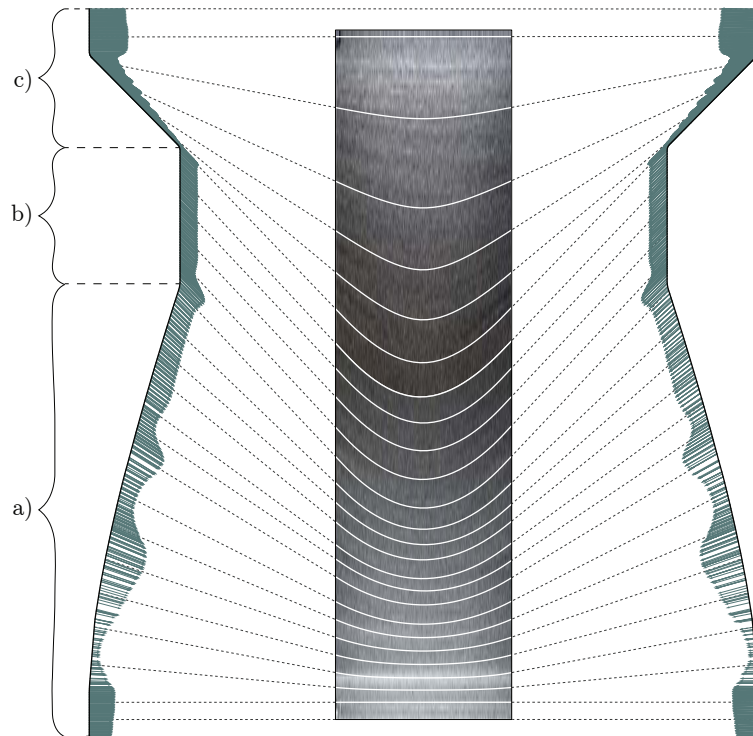


Fig. B.11: Overlay of simulated curves and picture, measured tension force vector at its respective position for process data 151213\_4D92E and path-curves (deflection 0.78)

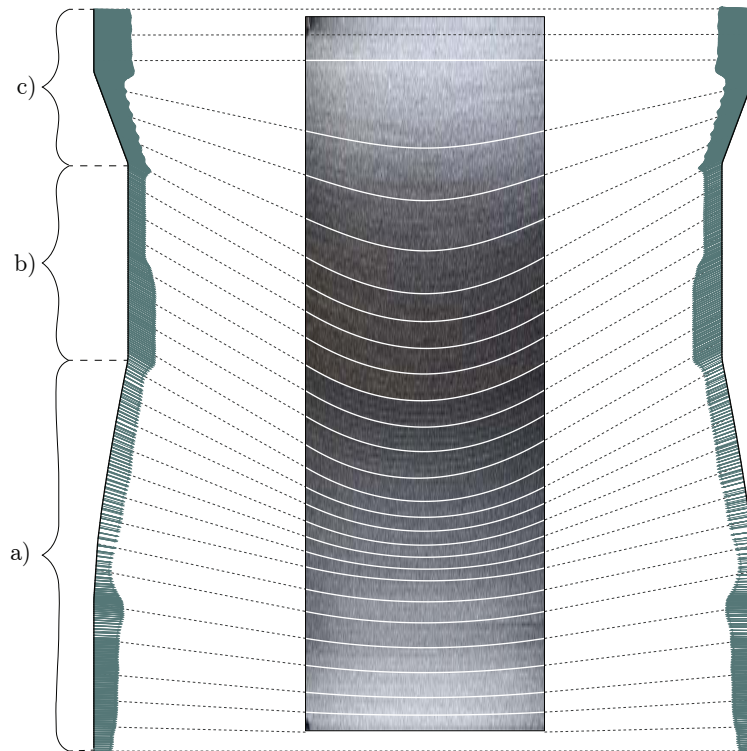


Fig. B.12: Overlay of simulated curves and picture, measured tension force vector at its respective position for process data 151209\_36769 and path-curves (deflection 0.48)

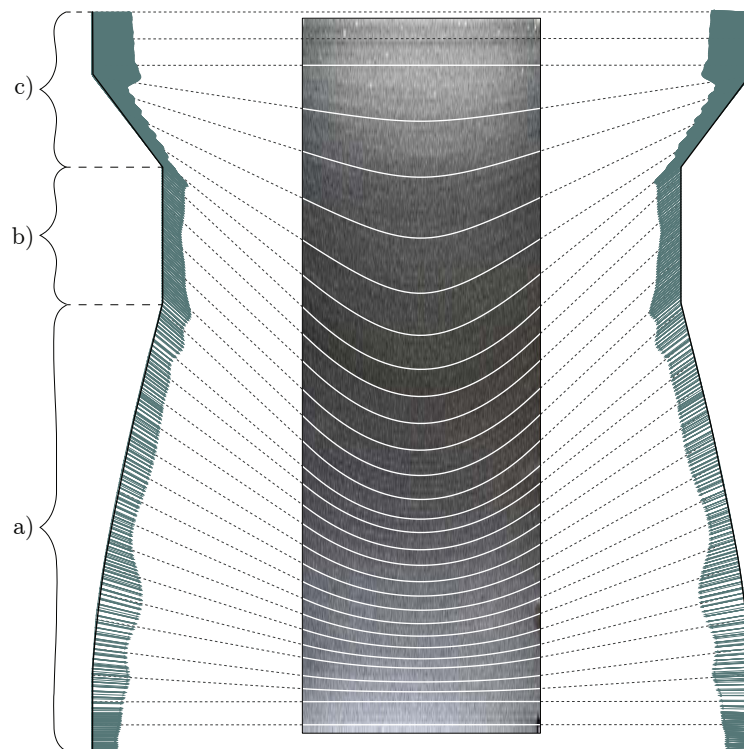


Fig. B.13: Overlay of simulated curves and picture, measured tension force vector at its respective position for process data 151211\_AB87E and path-curves (deflection 0.68)

### B.3 Comparative studies N°2

#### B.3.1 Predictability of the SWC process

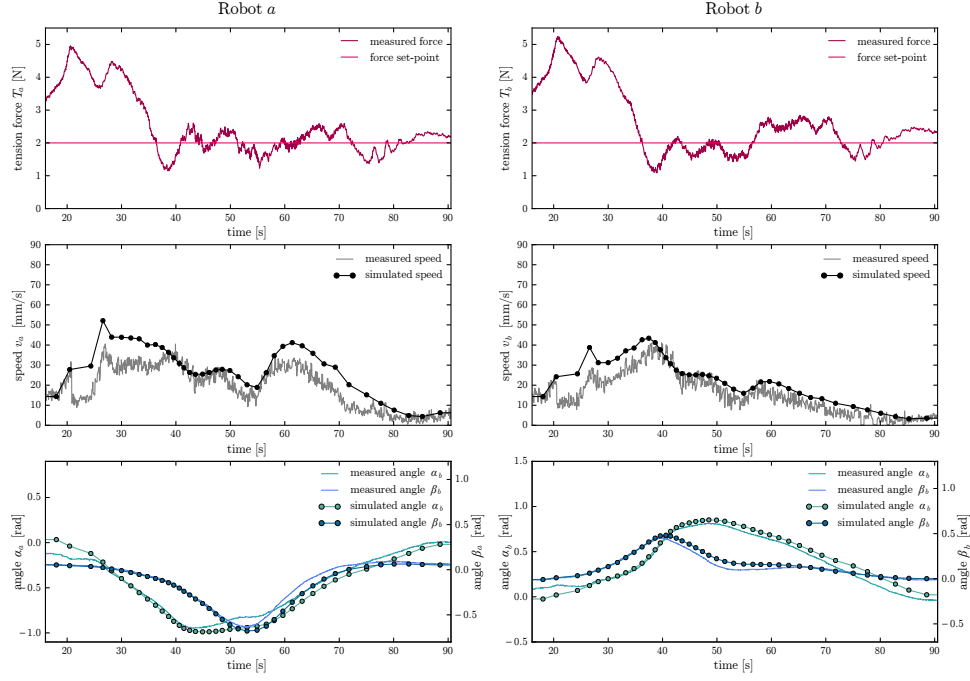


Fig. B.14: Comparison between process data of 160304\_B2140 and simulated values, surface 1)

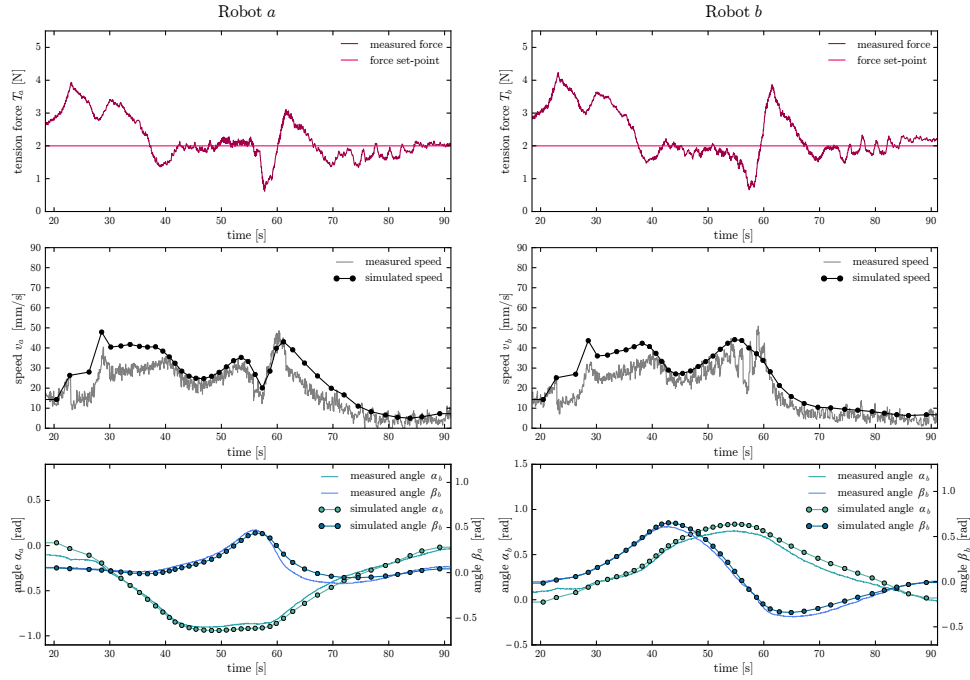


Fig. B.15: Comparison between process data of 160313\_5017B and simulated values, surface 2)

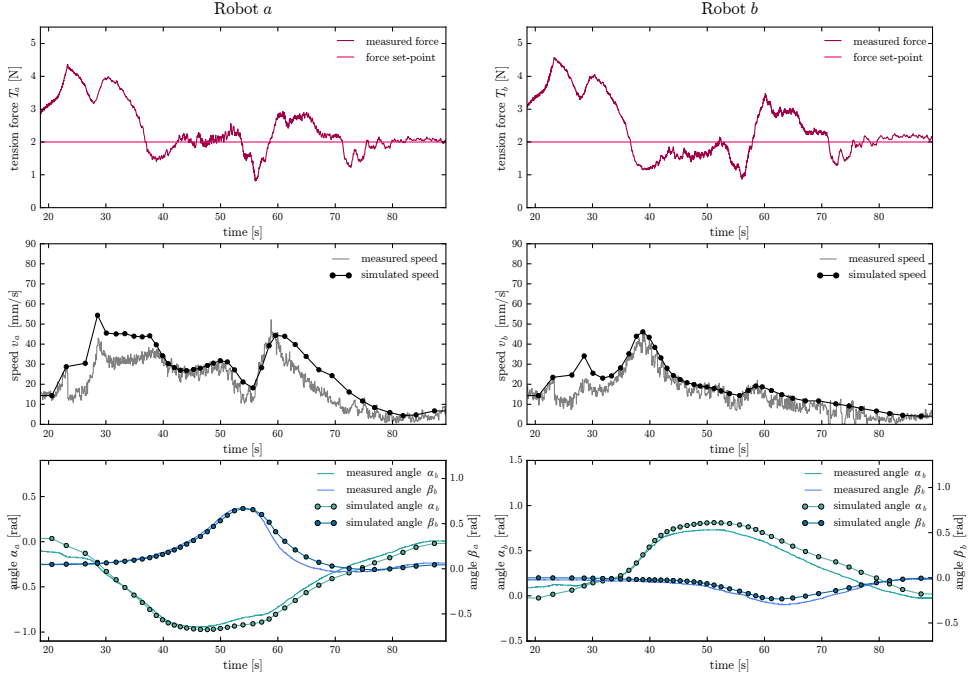


Fig. B.16: Comparison between process data of 160304\_C9874 and simulated values, surface 3)

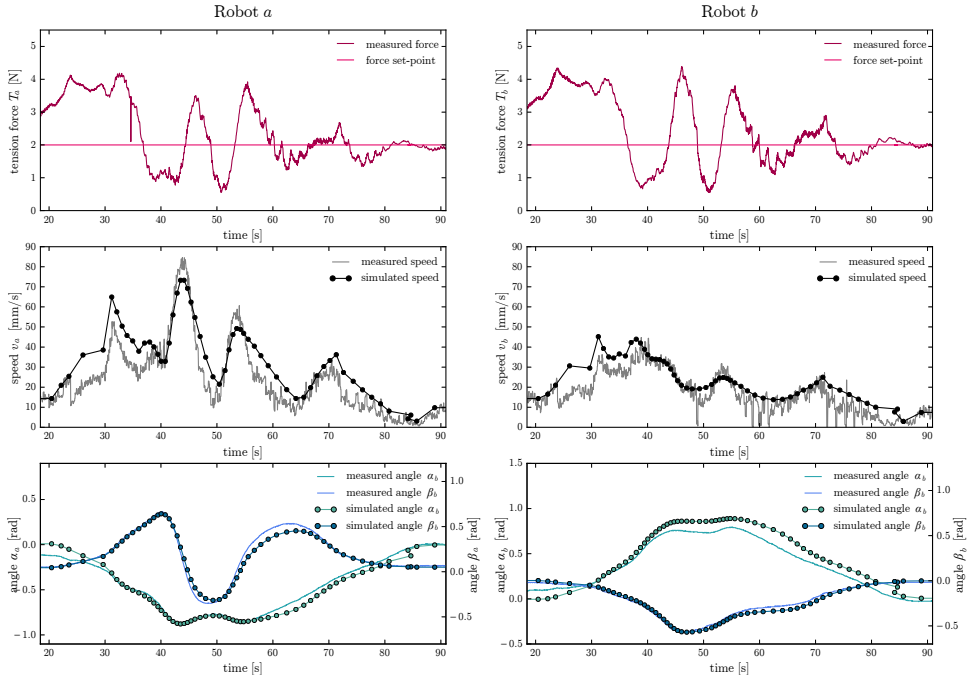


Fig. B.17: Comparison between process data of 160304\_369E5 and simulated values, surface 4)

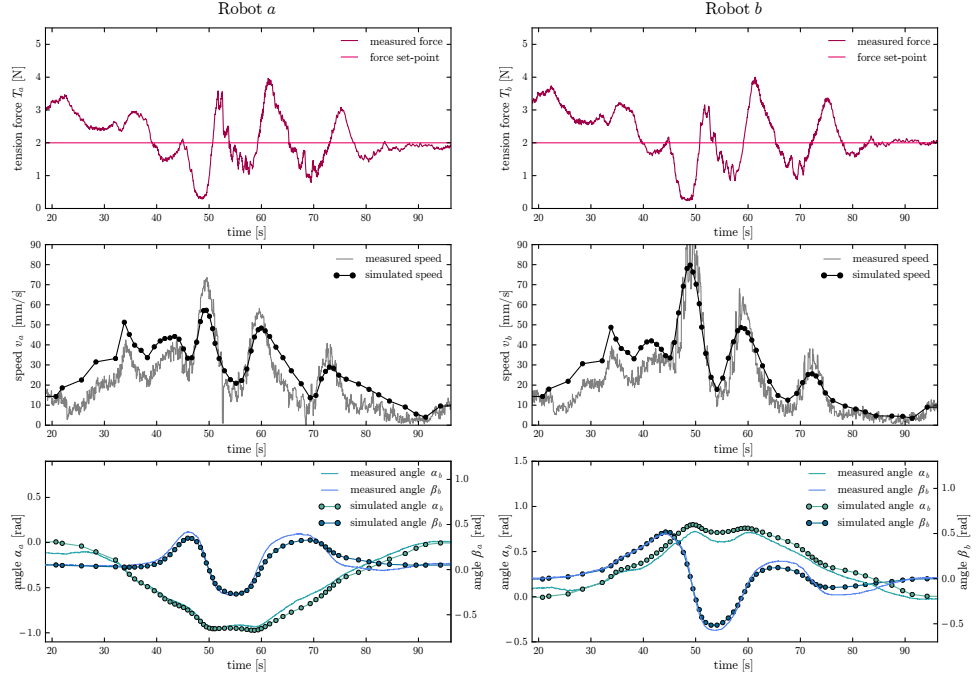


Fig. B.18: Comparison between process data of 160313\_03E5B and simulated values, surface 5)

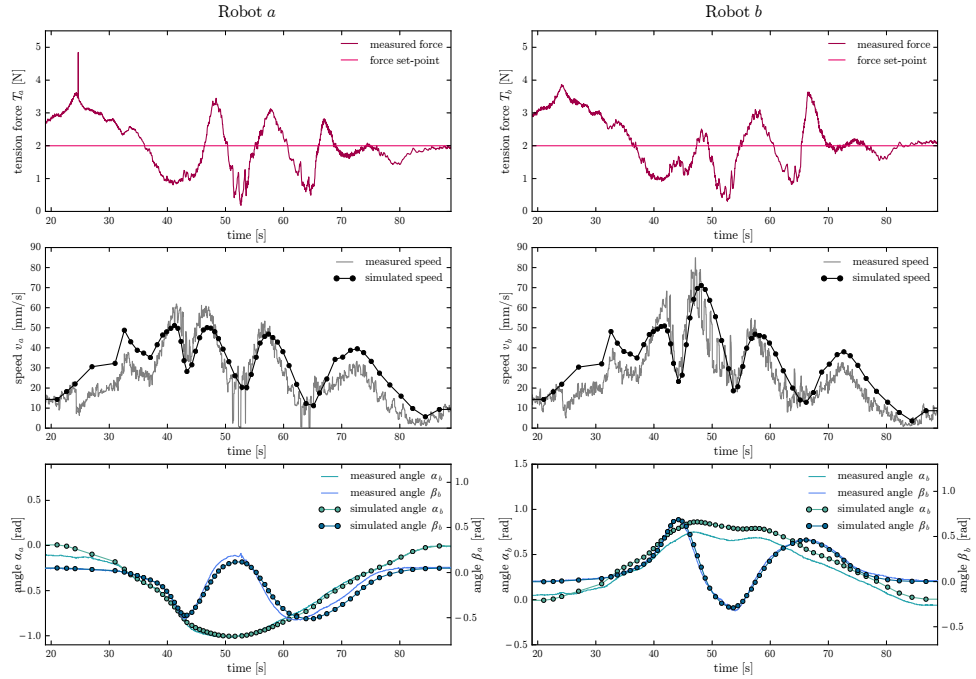


Fig. B.19: Comparison between process data of 160306\_CEE87 and simulated values, surface 6)

### B.3.2 Repeatability of the SWC process

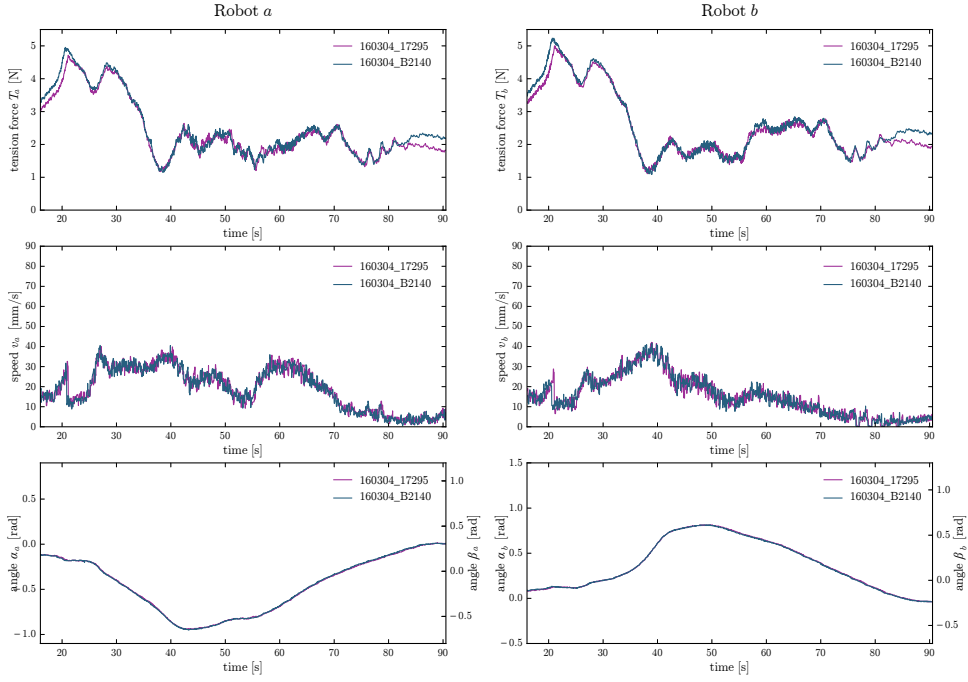


Fig. B.20: Process data comparison of cuts 160304\_17295 and 160304\_B2140, surface 1)

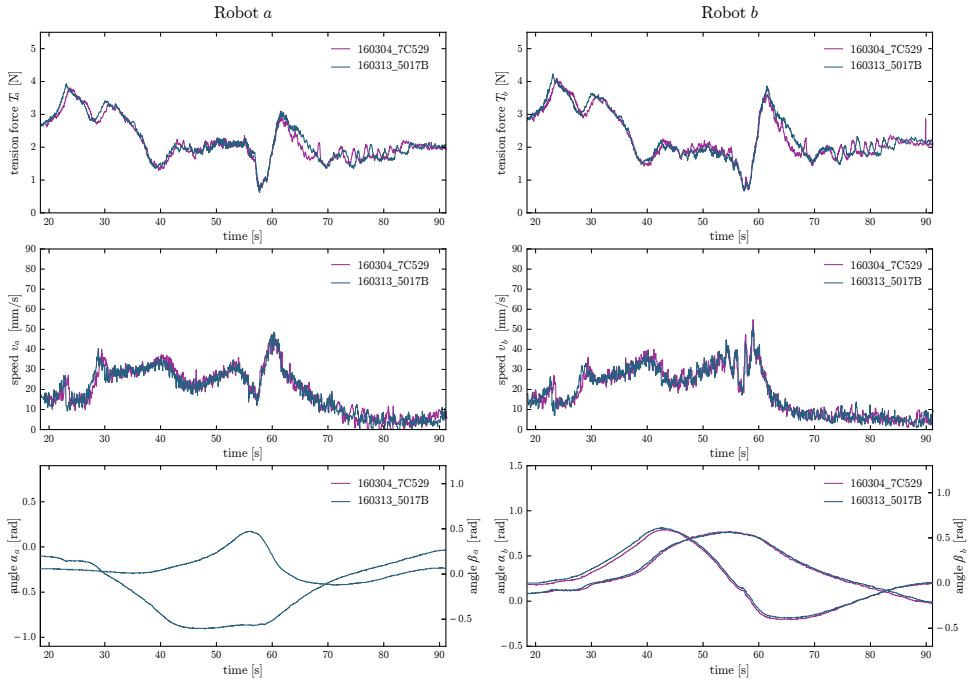


Fig. B.21: Process data comparison of cuts 160313\_7C529 and 160313\_5017B, surface 2)

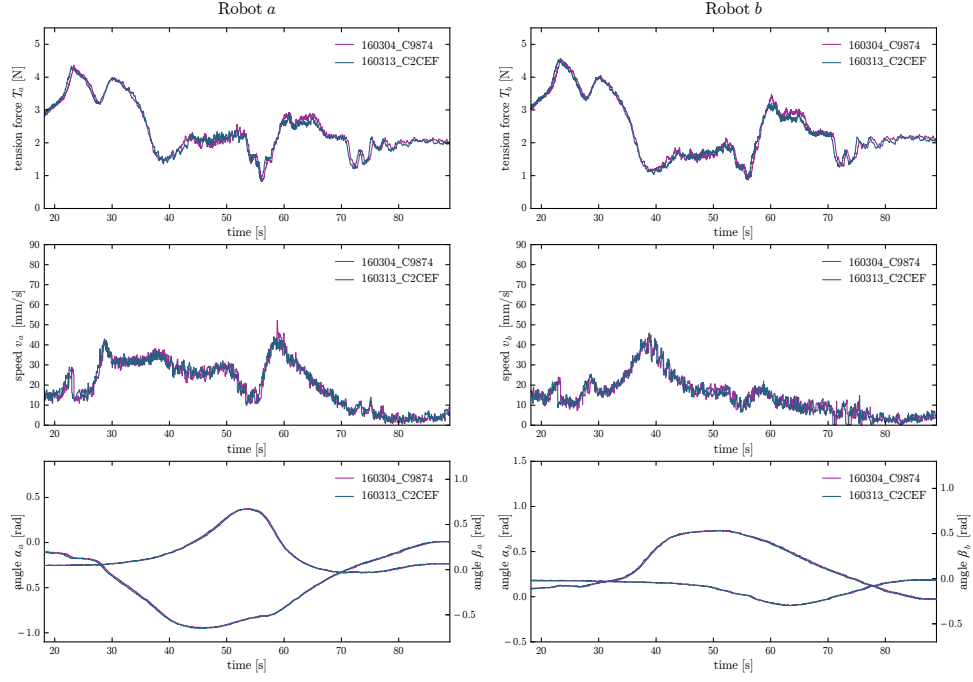


Fig. B.22: Process data comparison of cuts 160304\_C9874 and 160313\_C2CEF, surface 3)

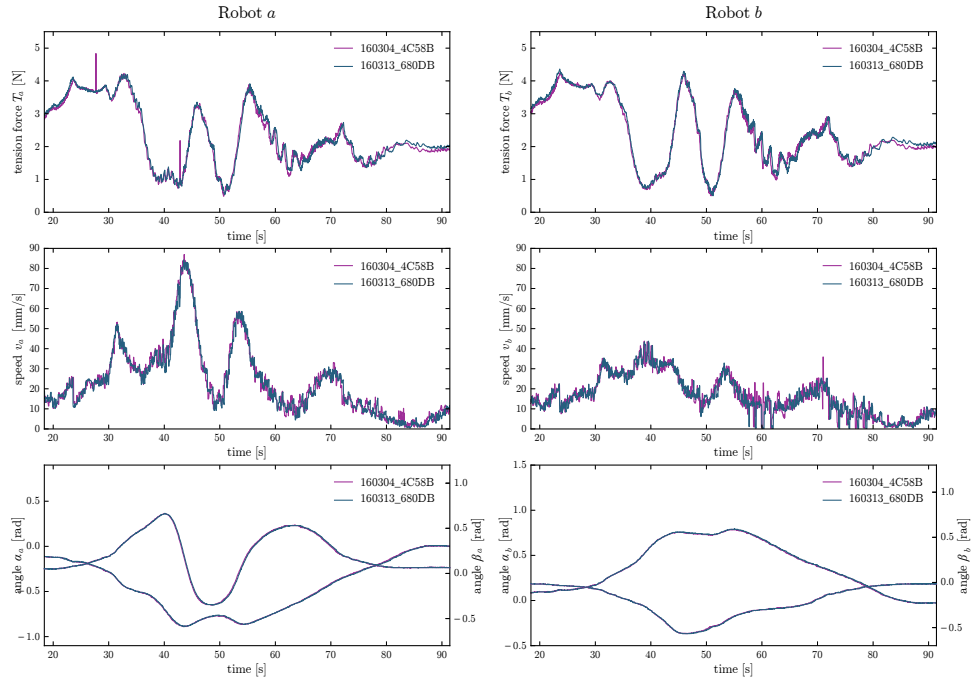


Fig. B.23: Process data comparison of cuts 160304\_4C58B and 160313\_680DB, surface 4)

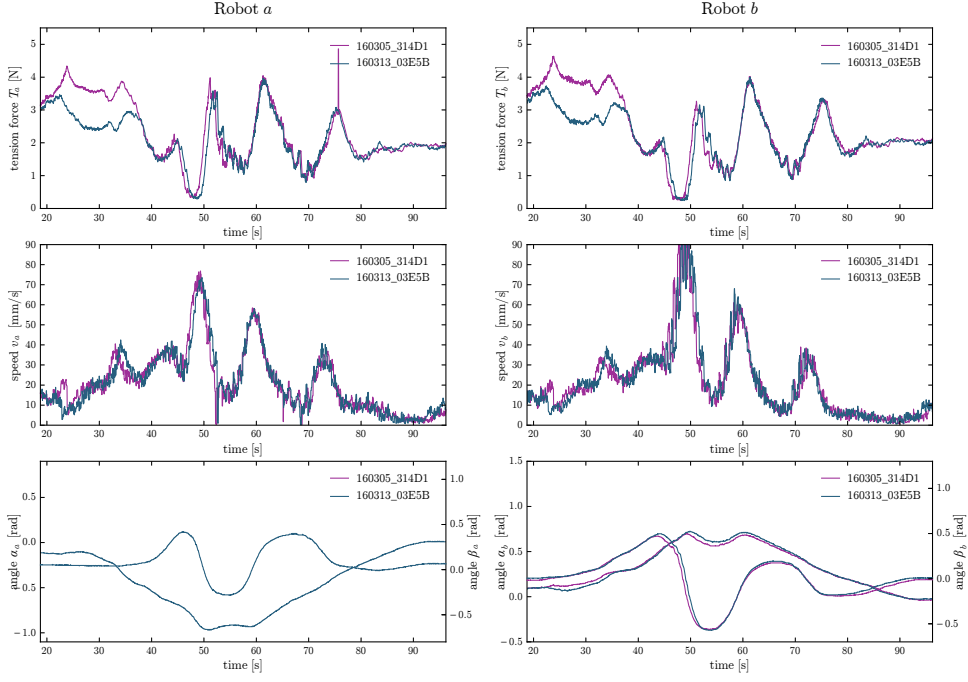


Fig. B.24: Process data comparison of cuts 160305\_314D1 and 160313\_03E5B, surface 5)

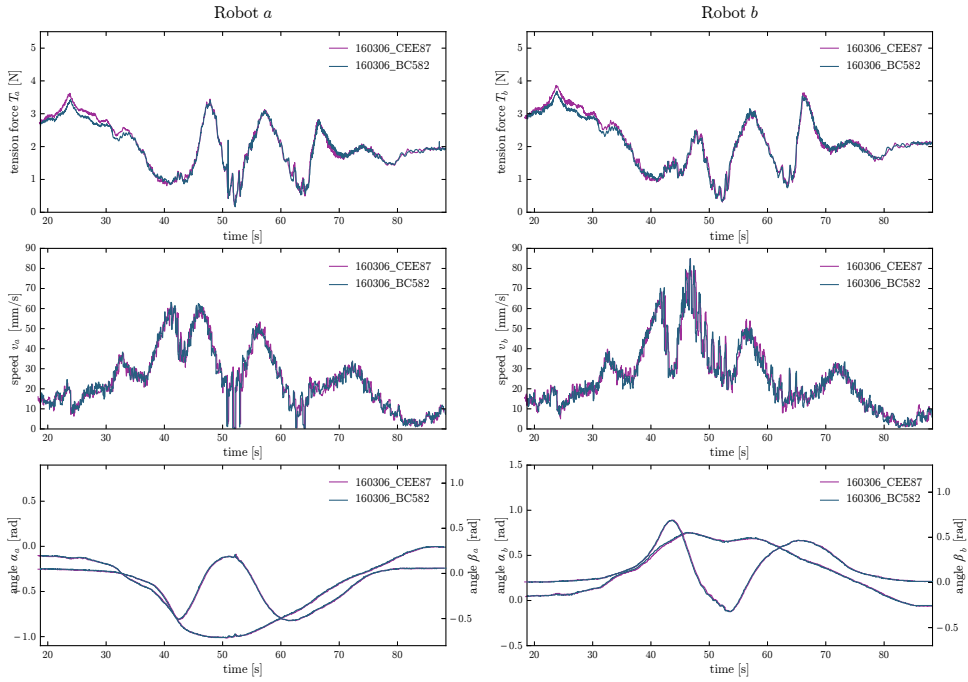


Fig. B.25: Process data comparison of cuts 160306\_CEE87 and 160306\_BC582, surface 6)



## C Project credits

This research is enabled by and funded through an Architecture & Technology PhD fellowship from the Institute of Technology in Architecture (ITA) of ETH Zurich.

Ryan Luke Johns conducted the three-month preliminary study at the Chair of Gramazio Kohler Research (see Section 2.1.4), providing a sound basis to start the thesis therefrom.

Florian Rist gave valuable advice and help in the development and realisation of the custom cardan joint end-effector (see Section 3.1.3.3).

Diederik Veenendaal suggested equation 3.6 and proofread Sections 2.1 – 2.4 in the paper *Force-Adaptive Hot-Wire Cutting* [109], which contents are also described in Sections 3.3.1, 3.3.3 and 3.3.4.

The Swisspearl® Summerschool 2015 and the following exhibition in the Architekturforum Zürich were supported by Eternit (Schweiz) AG. The Department of Architecture (D-ARCH) of ETH Zurich and swisspor AG co-supported the project. Many people from Eternit (Schweiz) AG contributed to the success of the Summerschool, especially Janine Löpfe, head of communication and Beat Brechtbühl, who, amongst many people working at the production facilities of Swisspearl® in Payerne, were extremely helpful with laminating the wire-cut moulds. The artist Marco Ganz contributed to the workshop with his precious discussions and his special sense for form and expression.

The elective course and the workshops discussed in this thesis have been conducted within the group of Gramazio Kohler Research at ETH Zurich, under the guidance of Professor Fabio Gramazio and Professor Matthias Kohler. Further credits belong to the whole team of Gramazio Kohler Research and the participants, listed below.

### C.1 *SWC* elective course 2015

Gramazio Kohler Research:

David Jenny (project lead), Romana Rust (research lead)

Students: Arash Adel, Jordan Berta, Stefan Caranovic, Alix Gasser, Kadivar Mohammad, Magdalena Osiniak, George Papamatthaiakis, Lukasz Pawlicki, Valerian Portokalis, See Hong Quek

## **C.2 Swisspearl<sup>®</sup> Summerschool 2015**

Gramazio Kohler Research:

David Jenny (project lead), Romana Rust (research lead)

Students: Grgurac Ana, Gheyselinck Aurèle, Sarah Barras, Li Bo, Marco Caprani, James Chenault, Stéphane de Weck, Ahmed Elshafei, Victoria Fard, Alix Gasser, Marco Palma, Julien Prudhomme, Ludwig Schilling, Stavroula Tsafou

## **C.3 AAG Workshop**

Gramazio Kohler Research:

Romana Rust (project and research lead), David Jenny (teaching lead)

Participants: Inés Ariza, Julien Beauchamp-Roy, Giulio Brugnaro, Christina Doumpti, Angelo Figliola, Nicholas Hoban, Marko Jovanovic, Lisa Keskinen, Riccardo La Magna, Josef Musil, Andrea Quartara, Inés J Pedras, Hsiao Wei Yu